REPORT DOCUMENTATION PAGE

Form Approved
OMB No. 0704-0188

1. AGENCY USE ONLY (Leave blank)	2. REPORT DATE	3. REPORT TYPE AND DATES COVERED
	31 May 1996	Final 01 Oct. 93 - 31 May 96

4. TITLE AND SUBTITLE

Laboratory And Field Scale Fracture Of Sea Ice

5. FUNDING NUMBERS

GN00014-93-1-0714

6. AUTHOR(S)

John P. Dempsey

7. PERFORMING ORGANIZATION NAME(S) AND ADDRESS(ES)

Clarkson University
P.O. Box 5710
Potsdam, NY 13699-5710
Tel: (315)268-6517
Fax: (315)268-7985

8. PERFORMING ORGANIZATION REPORT NUMBER

9. SPONSORING/MONITORING AGENCY NAME(S) AND ADDRESS(ES)

Office Of Naval Research
800 N. Quincy Street
Arlington, VA 22217-5660

10. SPONSORING/MONITORING AGENCY REPORT NUMBER

11. SUPPLEMENTARY NOTES

Approved For Public Release: Distribution Is Unlimited

12a. DISTRIBUTION/AVAILABILITY STATEMENT

12b. DISTRIBUTION CODE

13. ABSTRACT *(Maximum 200 words)*

This report contains details of laboratory and field scale studies carried out to study fracture of sea ice. The field scale studies were carried out in six field trips on in-situ arctic sea ice. Lab scale studies were carried out on the samples obtained from cores taken from the sea ice during the field trips. The details of the experimental method and protable loading system specifically designed for these tests are given. The first two field trips are analyzed to reveal the size effect on the fracture of S1 freshwater and S2 sea ice. The analysis is carried out using size effect laws. To analyze the creep-recovery and cyclic loading experiment, a model based on the nonlinear theory of viscoelasticity is proposed. It is shown that the model is capable of predicting the load-deformation paths under simple loading histories.

14. SUBJECT TERMS	15. NUMBER OF PAGES	16. PRICE CODE
	117	

17. SECURITY CLASSIFICATION OF REPORT	18. SECURITY CLASSIFICATION OF THIS PAGE	19. SECURITY CLASSIFICATION OF ABSTRACT	20. LIMITATION OF ABSTRACT
Unclassified	Unclassified	Unclassified	

FINAL REPORT

LABORATORY AND FIELD SCALE FRACTURE OF SEA ICE

PROJECT TITLE:	Laboratory and Field Scale Fracture of Sea Ice
PRINCIPAL INVESTIGATOR:	John P. Dempsey
INSTITUTION:	Clarkson University
ADDRESS:	Box 5710, Potsdam, NY 13699-5710
TELEPHONE (voice):	(315) 268-6517
TELEPHONE (fax):	(315) 268-7985
E-MAIL:	john@jpdnz.cee.clarkson.edu

GRANT/CONTRACT NO:	N00014-93-1-0714
R&T PROJECT CODE:	3324842
CONTRACT START,END DATES:	10/93–05/31/96

ABSTRACT

This report presents experimental and theoretical work completed as part of ONR grant titled 'Laboratory and Field Scale Fracture of Sea Ice', grant no. USNA N00014-93-1-0714. The goals of the program are to acquire knowledge of sea ice over a broad range of scales (0.1m to 10km) and subsequently develop a physically based (function of temperature, brine channels, spacing of channels, porosity, salinity) constitutive model capable of predicting behavior over the wide range. An abundance of lab scale investigations have been completed on sea ice as well as investigations above the 1km scale. The laboratory scale testing is typically completed under isothermal conditions with sizes less than 0.5m. Very little fracture and constitutive data exists for the scales between 0.1m and 1km. To link the scales, *in-situ* fracture and tensile experiments were completed, successfully spanning the range of 0.5m to 80m. Six field trips to the Arctic were made with the latter five investigating the large scale behavior of sea ice. Forty-six fracture and flexure tests spanning the above mentioned size range provided both fracture and constitutive data necessary for achieving the goals of the program. As a result, two important discoveries were made and are discussed in detail in this report.

First, analysis of the fracture results indicates that a scale effect on the nominal tensile strength of sea ice exists, consistent with results at both the lab and 1km scales. The strength decreases from a typical tensile strength of approximately 0.5 MPa at the lab scale to 50 kPa at the 80 meter size. The ability of two size effect laws developed for size effect behavior in concrete to predict this behavior is investigated.

Second, preliminary modelling efforts indicate that a linear viscoelastic model is not sufficient to predict the strain behavior of sea ice. A nonlinear stress dependence in the delayed elastic and viscous strain components was found to best fit the results. This nonlinear viscoelastic model is applied to the results of a fracture experiment completed as part of the SIMI program.

ACKNOWLEDGEMENTS

Phases I & II of this study were supported in part by a joint-industry-agency project (JIAP) initiated (Denis Blanchet) and managed (Kurt Kennedy) by Canadian Marine Drilling Limited (Canmar), a business unit of the Amoco Canada Petroleum Company specializing in arctic offshore drilling and marine activities. Funding for the JIAP was provided by Amoco, Canmar (Canada), Mobil, National Energy Board (Canada), Texaco (Phase I), Minerals Management Service and the Office of Naval Research (ONR). Peter Jess (Calgary) handled the logistics while Sandwell, Inc. (Calgary: Dan Masterson, Bill Graham, John Robertson and Paul Spencer) provided the loading system and handled many of the test aspects for Phases I & II. The Institute of Marine Dynamics, National Research Council of Canada provided logistical support (Phase I), data acquisition backup (Phase I), high speed video measurements (Phase II), and completed a small scale testing program (Phase II). In the latter instance, the author notes the support of Bruce Parsons (Phase I), Trent Slade and Michelle Johnston (Phases I & II), Mary Williams, Craig Kirby and Bob Gagnon (Phase II). Phases III, IV, V & VI were an integral part of ONR's Sea Ice Mechanics Accelerated Research Initiative [Grants N00014-90-J-1360 & N00014-93-1-0714]. Phases III, IV & VI were joint experiments at Barrow with David Cole (USACRREL), Victor Petrenko (Dartmouth), Lew Shapiro and Willy Weeks (University of Alaska at Fairbanks). Logistical support for Phases III, IV & VI were provided by Richard Glenn at NARL in Barrow; further support on site was provided by Carl Byers (Juneau). Phase V was part of the SIMI camp in the Beaufort Sea. Logistical and testing support was provided by Max Coon, Andy Heibig, Skip Echert, Stu Knoke and Bob Pritchard.

TABLE OF CONTENTS

LIST OF FIGURES

LIST OF TABLES

1 INTRODUCTION

The relevance of fracture mechanics to ice engineering is intuitively acceptable once one has witnessed ice impact on a structure, an ice jam, an icebreaker at work, or a bearing capacity failure. For instance, the indentation and penetration of an ice sheet by a structure is typically fracture-dominated. The different failure modes observed and studied are crushing, crushing with spalling, crushing with radial cracking, crushing with radial and circumferential cracking, and radial/circumferential cracking with buckling (Sodhi, 1986; Timco, 1987; Blanchet et al.,1989). The mechanism by which the above failure modes are established is tensile fracture. To reliably predict ice forces on structures, and to better understand the role of fracture, the dependencies of the opening mode (Mode I) fracture toughness on such factors as loading rate, loading direction, specimen geometry and sample size, as well as the ice properties need to be investigated.

Early investigations involving the fracture of ice (and other quasi-brittle materials such as concrete and rock) assumed the validity of linear-elastic fracture mechanics (LEFM) for the laboratory specimens employed, and LEFM toughness parameters such as K_{1c} were determined. However, parameters such as K_{1c} and G_{1c} obtained from normal laboratory sized specimens have been found to be dependent on the specimen size (Dempsey, 1991; Dempsey et al., 1992). There is reason to believe that much larger specimens are required to obtain the K_{1c} or G_{1c} values for ice. This necessitates the study of fracturing at larger scales.

Over the last 10 years, an abundance of small scale laboratory tests have been conducted on columnar saline ice at various tempertatures, rates and orientations (Table 1.1). The K_Q values were calculated assuming LEFM criteria. If the value obtained for the fracture toughness is to be regarded as a material property, then the stress intensity factor, K_1 at which a stationary macrocrack extends in a material

Author (Year)	Test Geometry	Length (|| to crack) (m)	d_{av} (cm)	Crack Length (m)	Orientation	Temp. °C	K_Q kPa$\sqrt{m}$
Vaudrey (1977)	4pt bend	0.05	1.0	0.013	??	-10	30-80
	4pt bend	0.05	1.0	0.013	??	-20	25-115
Urabe et al. (1980)	3pt bend	0.36	0.3	0.07	VV(top)	-2	50
	3pt bend	0.36	3.0	0.07	VV(bot)	-2	80
	3pt bend	0.33	2.0	0.07	VH	-2	60
Shapiro (1981)	4pt bend	0.05	2.0	0.012	HH	-20	120
Urabe et al (1981)	4pt bend	0.40	0.3	0.08	VV	-2	50
		0.40	2.2	0.08	VV	-2	75
		0.40	4.0	0.08	VV	-2	100
Timco and Frederking (1982)	4pt bend	0.065	1.5	0.012	HH	-20	100-140
Shen and Lin (1986)	3pt bend	0.16	??	0.08	VV	-20	80
Parsons et al. (1986)	DCB	0.4 - 1.0	5.0	0.25	VH	-10 - -20	67 - 281
			5.0		HH	-10 - -20	99 - 875
			5.0		VV	-10 - -20	56 - 307
Urabe et al (1986)	4pt bend	0.1	1-12	0.02	VH	-10	120
Tuhkuri (1987)	3pt bend in-situ	0.45	??	0.2	VH	-0.4	136,119
Parsons et al (1988)	Double torsion	1.0	5-10	0.25	VH		113±38
Bentley (1992)	3pt bend	0.2	0.5	0.06	VH	-13 - -20	50 - 90
DeFranco and Dempsey(1992)	3pt bend	0.15	1.0	0.045	VH	-25,-15,-5	60 - 150
		0.05	1.0	0.015	VH	-25,-15,-5	60 - 200
		0.017	1.0	0.005	VH	-25,-15,-5	60 - 200
Williams et al (1993)	3pt bend	0.1	1-2	0.05	VH	-15 - -20	76
	3pt bend	0.1	1-2	0.05	VV	-15 - -20	79
DeFranco et al (1994)	RTCLWL	0.254	1.5	0.105	VH	-15	90
Lazo (1994)	4pt bend	0.076	0.8	0.023	HH	-15	98
	4pt bend	0.076	0.8	0.023	VH	-15	56
LeClair et al (1996)	SCB	0.1	1-2	0.03	VH	-10	80-110
Adamson et al (1996)	SCB	0.1	1-2	0.03	VH	-12	35-70
	SCB	0.1	1-2	0.03	VH	-35	90-130

Table 1.1: Summary of Sea Ice Fracture Toughness Testing

must be independent of the size and shape of the test specimen and the method of loading. Due to the uncertainty in these parameters, K_Q was introduced (Dempsey, 1991) to represent the apparent fracture toughness at initiation. DeFranco et al (1992) found that lab scale experiments exemplify an increasing resistance to fracture until

a point at which unstable or catastrophic failure occurs. Considering this evidence, the fracture toughness parameter, K_{1c}, is not valid for characterizing the fracture behavior of ice.

Urabe et al (1980) and Parsons (1986) examined the anisotropy of sea ice through a set of tests at different orientations. Parsons (1986) introduced the notation of VV, VH, and HH to define the orientation of the crack plane and crack front and to standardize future fracture testing. Timco and Frederking (1982) studied the effects of depth in the ice sheet on the fracture toughness finding an increase in toughness at lower depths. They also applied the method of adding the sub-grain size to the crack length to arrive at a corrected notch length developed by Urabe et al (1981). This was proposed to make the small scale results comparable to larger tests. Shen and Lin (1986) varied the loading rate to investigate the effects on the fracture toughness, noting no noticeable trend for the rates of 10 to 400 $kPa\sqrt{m}/s$. Tuhkuri (1987) conducted a set of in-situ 3pt bend experiments, larger than any previous three-point-bend fracture tests in an effort to overcome any size effect. He varied the loading rate and found the toughness decreased with increased loading rate. In addition, he investigated notch acuity effects by sharpening some of the crack fronts, but saw no affect on the fracture toughness. DeFranco et al (1994) observed stable cracking (crack jumping) in experiments on the RTCLWL (reversed-taper crack-line wedge-loaded) geometry. An increasing resistance to fracture was seen in these experiments supporting the belief that K_{1c} at crack initiation is not a true measure of the fracture toughness. Considerable scatter in the fracture toughness results is evident in the tests to date. This can be attributed to ice type, crack length, loading rate, specimen size, temperature, specimen geometry, crack orientation and specimen preparation. On the average, small scale VH tests typically yielded values between 56 and 90 $kPa\sqrt{m}$. Smaller tests on the same ice (Williams et al, 1993) yielded values around 76 $kPa\sqrt{m}$. These results tend to show a size effect is present in the fracture toughness of sea ice.

Date Location...Phase	Ice Type	Ice Thickness h(m)	Test Geometries	Size L(m)	Scale	# Tests
1/15-29, 1992 Canmore, Alberta.....I	S1 fresh water ice	0.50	3pt[a] - FR[b] RT[c] - FR	0.50 0.34-28.64	1:81	4 9
4/17 - 5/7 1993 Resolute, N.W.T. II	FY[d] sea ice slightly aligned	1.8	3pt - FR SQ[e] - FR SQ - FL[f]	3.0 0.5-80 3.0	1:160	1 15 2
11/9-19, 1993 Barrow, Alaska[1]....III	FY[a] sea ice Strongly aligned	0.30	SQ[b] R[g] RT[d] CORE[h]	2.5 2.5 1.0 0.36		5 1 2 4
3/9-20, 1994 Barrow, Alaska[1]....IV	FY sea ice strongly aligned	1.5	SQ R SCB[i]	0.5-30 1.5-2.0 0.15	1:60	5 2 16
4/1-10, 1994 SIMI Floating Camp, Beaufort Sea[2]...V	FY sea ice slightly aligned	0.2-0.6 2<h<6	SQ MY Floe[j]	2-15 81	1:7.5	5 1
5/8-19,1994 Barrow Alaska[1]....VI	FY sea ice strongly aligned	1.7	SQ R	0.25-30 8	1:120 N/A	5 2

[1]Joint experiments with Cole, Petrenko, Shapiro and Weeks
[2]MY floe fracture experiment joint with Coon, Farmer, Pritchard and Xie
[a]3pt-Three point bend; [b]FR-Fracture; [c]RT-Reverse-tapered base-edge-cracked plates
[d]FY-First Year; [e]SQ-Square Plate (L×L); [f]FL-Flexure; [g]R-Rectangular Plate (L×2L)
[h]CORE - 0.2m diameter core, vertical, isothermal (small scale)
[i]SCB - Semi-Circular Bend Fracture/Flexure Geometry (small scale)
[j]MY Floe - Multi-Year floe

Table 1.2: Summary of Large-Scale Experiments

Presently, experimental information regarding the mechanical behavior of sea ice consists of both laboratory experiments and field scale measurements. The laboratory tests have been done on small sized samples where questions of heterogeneity are an issue and extrapolation to larger scale behavior is in question. The large scale behavior of events such as thermal fracturing and ridging is typically based on acoustical measurements and observations, lacking a sound mechanics background. A large

gap exists at the intermediate scale of 1 m to 1 km where very little information is available, prompting a thorough arctic field program designed to investigate test sizes from 0.1m to 100m. Six field trips were completed, testing freshwater and sea ice with varying thickness, temperature profile, c-axis alignment and size (Table 1.2). All of the large scale experiments were completed *in situ* retaining the inherent temperature, density and salinity of the sea ice. Cyclic and creep recovery sequences of loading were imposed on selected experiments to extract constitutive information necessary for the purposes of modeling. Rate effects were also investigated through a series of monotonic load ramps with varying rates. A final load or crack opening displacement controlled ramp was applied to fracture the sample. An extensive small scale program (in the field and in the laboratory) was also completed in an effort to link the full scale experiments with existing laboratory investigations. The extensive amount of information gathered from the field investigations provides the means necessary for validating existing models and size effect predictions.

The small scale program discussed above utilized the semi-circular-bend (SCB) geometry for both the fracture and flexure experiments related to Phases III, IV and VI. Chapter 2 of this dissertation presents a fracture mechanics analysis of the semi-circular (SC) and semi-circular-bend (SCB) fracture geometries. The weight function method is implemented to obtain wide ranging stress intensity factor (SIF) and crack opening displacement (COD) expressions. The special cases of the SC subject to a concentrated crack mouth loading and the SCB are analyzed in detail. The weight function for the SCB is fully developed, with an accurate expression for the SIF and and a numerical result for the crack mouth opening displacement (CMOD).

Chapter 3 presents the small scale SCB experiments carried out on the ice from the first two Barrow trips (Phases III & IV). These experiments were completed at the site while the large *in situ* tests were under way. Due to the strong c-axis alignment found in the sea ice, a study of the fracture properties parallel (hard-fail) and perpendicular (easy-fail) to the preferred c-axes orientation plane was completed. Effects on the

fracture toughness, elastic modulus and nominal strength are investigated.

Chapter 4 presents the large-scale experiments carried out during Phase I of the SIMI program. The primary goal of Phase I was to assess the feasibility of large-scale, full-thickness ice (freshwater and sea) fracture measurements. It was carried out on S1 large grained freshwater ice. Due to the overall success of the project an abundance of data for large scale fracture tests on freshwater ice was recorded. Progressively larger sizes were tested in an effort to transcend the macrocrystalline behavior and obtain the fracture behavior of the ice sheet. Unfortunately, due to the large grained ice encountered in this program and the limitations of the equipment, sizes at which the material properties and behavior were independent of size were not accomplished. Nevertheless, important information linking the small scale to the large scale was obtained.

Details of the large scale fracture test program (Phase II) on sea ice are presented in Chapter 5. The tests were conducted on columnar S2 sea ice spanning size ranges of 1:160 with the largest sample being 80m in length. These experiments cover a large enough size range to reveal the size effect present in the tensile strength. Size effects on the fracture toughness and elastic modulus are also investigated. A comparative small scale study on the same ice is included to show the transition in fracture behavior from the small to large scale.

During Phases III, IV, V and VI, the constitutive behavior of the ice as well as the fracture behavior was sought. To obtain this information, it was necessary to apply controlled loadings such as creep recovery and cyclic sequences. This required a loading system capable of closed loop control of the applied load. A computer controlled pneumatic loading system was designed and fabricated for these field trips. Chapter 6 discusses the design components of this system including some field results.

Chapter 7 investigates the application of non-linear viscoelastic modelling to the large scale behavior. The results of the creep recovery sequences are used to determine the various parameters of the model to best fit the data. The model is then applied

to the cyclic loadings as well as the monotonic ramps to failure.

2 FRACTURE ANALYSIS OF SEMI-CIRCULAR GEOMETRIES*

2.1 Introduction

There are several modes of fracture in quasi-brittle materials such as rock, concrete and ice: spalling, radial or circumferential cracking. These fracture modes represent independent cracking cases with variations in the crack plane and crack propagation direction relative to the texture (shape of the grains) and fabric (orientation of the grains) of the material. In order to investigate the influence of structural anisotropy, it is necessary to fabricate the specimens with precut crack planes aligned both horizontally and vertically. In the field, this is a difficult procedure. This has led directly to the development of methods using core-based fracture geometries such as the Chevron Edge Notch Round Bar in Bending (*CENRBB*), the Short Rod, and the Semi-Circular-Bend (*SCB*) specimen. The idea is to minimize the amount of handling and machining by using specimens that are readily fabricated from core pieces. The overall objective is to examine the influence of anisotropy on the fracture toughness using easily obtained cores of the material being studied.

The semi-circular (SC) and SCB geometries are ideal testing configurations due to minimal preparation required for each test. The SC geometry is ideal for field testing purposes as it is easily fabricated from cores removed from the testing material. It is important when field testing to conduct a set of small scale tests to correlate fracture properties with the large scale tests. In an effort to determine whether small scale studies can be extrapolated to large scale sea ice fracture events, four field trips to the Arctic were completed in 1993 and 1994. The SCB became the basis of the small scale field testing, prompting the detailed analysis presented in this paper. To compare large and small scale tests, it is essential to know the COD information as well as

*Accepted for publication in the *International Journal of Fracture* (Adamson, Dempsey and Mulmule, 1996)

the SIFs. The SCB test configuration has been advocated as a possible standard test method for rocks (Lim et al, 1993). For the case of Mode I loading (the edge crack being normal to the base), the SCB has been studied by Chong and Kuruppu (1984) and more recently by Lim et al (1993). In the work by Chong and Kuruppu (1984), limited numerical results are presented; Lim et al (1993) provide solutions over a wider range of crack lengths and spans and correlate the accuracy of the earlier solution. The latter paper bridges solutions by curve fitting. Although these papers provide a means of calculating the fracture toughness from experimental data, apparently no rigorous SIF results exist; moreover, there has been no information provided concerning the associated crack opening displacements.

2.2 The Weight Function Method

By applying the weight function method (Wu and Carlsson, 1991) to the semi-circular (SC) geometry (Fig. 2.1), the stress intensity factors (SIF's) and crack opening displacements (COD's) can be obtained for any arbitrary loading, including the SCB. Knowledge of a two-dimensional elastic crack solution (reference solution) as a function of crack length A for any loading $\Sigma_{XX}(0,Y)$, which will now be referred to simply as $\Sigma(Y)$, enables one to determine the stress intensity factor for the same geometry subject to any other loading:

$$K(A) = \frac{E'}{K_r(A)} \int_0^A \Sigma(Y) \frac{\partial U_r}{\partial A}(A,Y) dY \tag{2.1}$$

where $E' = E$ for plane stress and $E' = E/(1-\nu^2)$ for plane strain; $K_r(A)$ is the known or reference stress intensity factor and $U_r(A,Y)$ represents the known or reference crack face displacement.

Here it is convenient to introduce the non-dimensional notation (Fig. 1b)

$$y = \frac{Y}{R},\ a = \frac{A}{R},\ u_r(a,y) = \frac{U_r(A,Y)}{R},\ \sigma(y) = \Sigma_{XX}(0,Y) \tag{2.2}$$

Further,

$$V_r(a) = \frac{E'}{\sigma A} U_r(A,0)\,,\ \delta_r(A) = 2U_r(A,0), \tag{2.3}$$

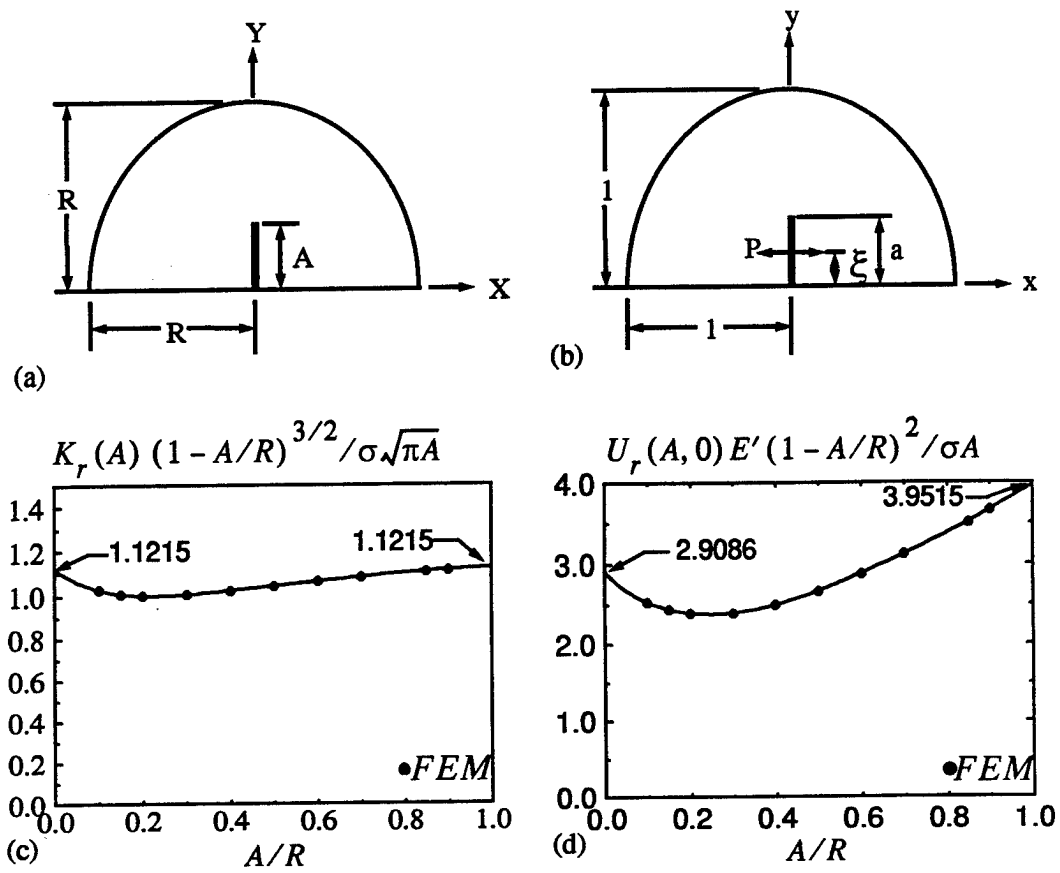

Figure 2.1: A single edge crack in the SC disk: (a) geometry and coordinates; (b) non-dimensional coordinates and concentrated crack face loading; (c) Reference SC SIF function; (d) Reference SC CMOD function

and

$$f_r(a) = K_r(A) \,/\, (\sigma\sqrt{\pi A})\,. \tag{2.4}$$

where the crack-mouth-opening-displacement of the reference problem is denoted here by $\delta_r(A)$; σ is the uniform crack face loading associated with the reference problem. Then

$$K(A)/\sqrt{R} = k(a) = \int_0^a \sigma(y) h_r(a,y)dy, \tag{2.5}$$

$$E'u(a,y) = \int_{a_0}^a k(s) h_r(s,y)ds. \tag{2.6}$$

Note that a_0 in (2.6) is problem specific, depending on the type and location of crack

face loading applied. The weight function is expressed as (Dempsey et al, 1995):

$$h_r(a,y) = \frac{1}{\sqrt{2\pi a}} \sum_{i=1}^{5} \mathcal{G}_i(a) \left(1 - \frac{y}{a}\right)^{i-\frac{3}{2}}, \quad y \leq a. \tag{2.7}$$

The $\mathcal{G}_i(a)$ functions are written in a form that explicitly reveals the singular behavior as $a \rightarrow 1$ in Dempsey et al (1995).

2.3 SC Reference Solution

Uniform crack face pressure is chosen as the reference load case for the single edge crack in the SC geometry where

$$f_r(a) = \frac{F(a)}{(1-a)^{\frac{3}{2}}}, \qquad V_r(a) = \frac{V(a)}{(1-a)^2}, \tag{2.8}$$

and

$$F(s) = \sum_{i=0}^{7} \alpha_i s^i, \qquad V(s) = \sum_{i=0}^{7} \gamma_i s^i, \tag{2.9}$$

The coefficients α_i and γ_i $(i = 0, 1, ..., 7)$ in (3.2) consecutively are given by:

$$\alpha_i : 1.1215, -1.4546, 6.0511, -10.8305, 8.8586, -0.7291, -3.3844, 1.4889.$$

$$\gamma_i : 2.9086, -5.8029, 25.5079, -71.1746, 153.6445, -201.6816, 138.8509, -38.3013 \tag{2.10}$$

These curve fit expressions were obtained by the same procedure as described in Dempsey et al (1995). The functions $F(a)$ and $V(a)$ in (2.8) are plotted in Fig. 2.1c and Fig. 2.1d.

The SIF solution for a concentrated load at the crack mouth in terms of the reference SIF and CMOD solutions is then immediately available, as found in Dempsey et al (1995):

$$K_P(A)B\sqrt{\pi A}/P = (aV_r(a))'/f_r(a). \tag{2.11}$$

The crack opening area for the concentrated load case can be derived explicitly by applying Betti's reciprocity theorem to the uniform and concentrated load cases giving

$$\mathcal{COA}_P(A)BE'/PA = 2V_r(a) \tag{2.12}$$

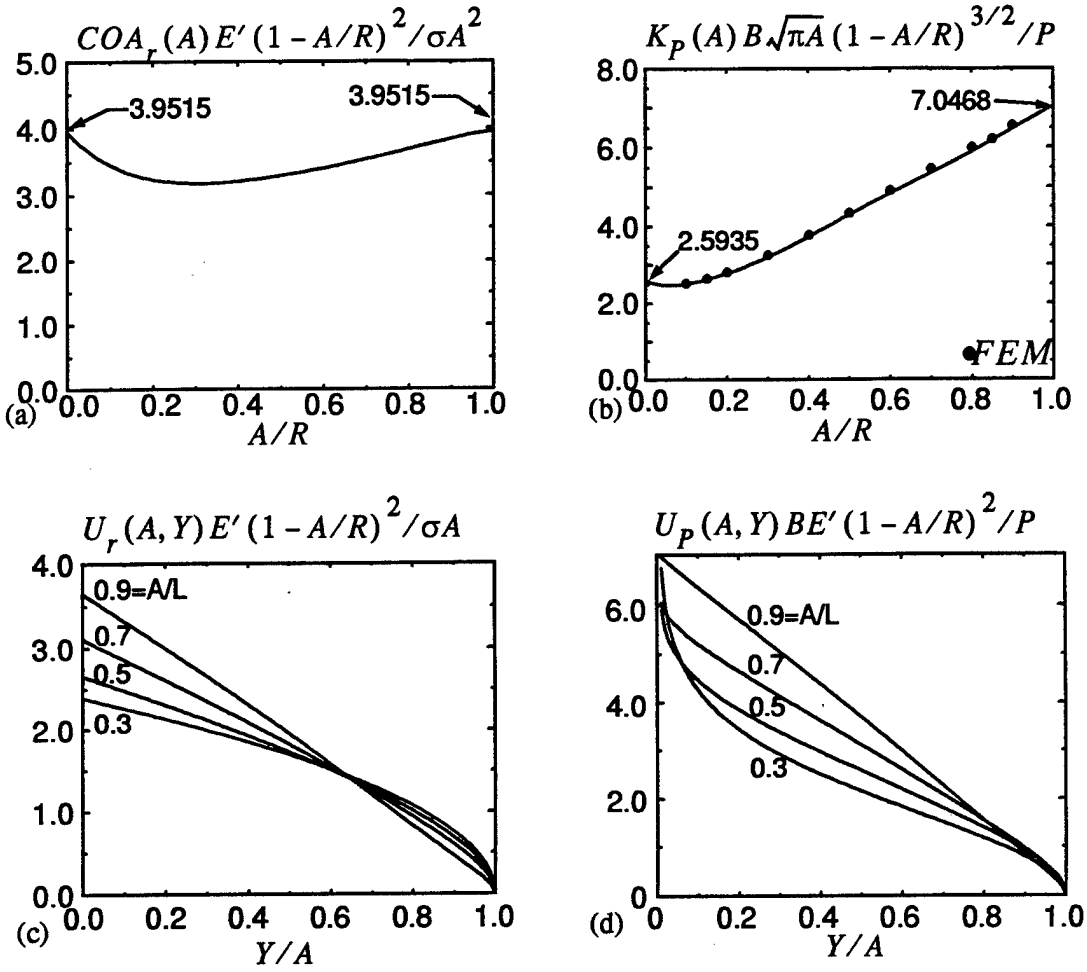

Figure 2.2: (a) SC reference crack opening area; (b) SIF for the concentrated loading at the SC crack mouth; (c) SC COD's for the uniform crack face pressure; (d) SC COD's for concentrated loading at the crack mouth

The above expressions actually apply to any geometry subject to concentrated loading at the crack mouth that is treated as outlined in Dempsey et al (1995).

The crack opening area for the reference solution is readily given by

$$\mathcal{COA}_r(A) = 2\pi\sigma A^2\phi(a)/E' \tag{2.13}$$

where

$$a^2\phi(a) = \int_0^a s\,[f_r(s)]^2 ds\,. \tag{2.14}$$

The expression for $\phi(a)$ stated in (2.14), given the form for $f_r(a)$ stated in $(2.8)_1$, has

been derived analytically for any arbitrary $f_r(a)$ and $V_r(a)$ by Dempsey et al (1995) for the RT geometry. A curve was fit to the expression to simplify the presentation here without compromising accuracy. The final result is given here by

$$\phi(a) = \frac{\Phi(a)}{(1-a)^2}, \qquad \Phi(s) = \sum_{i=0}^{7} \kappa_i s^i \tag{2.15}$$

where the coefficients κ_i ($i = 0, 1, ..., 7$ consecutively) are

$$\kappa_i : 0.6289, -1.081, 3.5188, -5.8425, -6.6906, -5.6382, -3.3323, -0.9800. \tag{2.16}$$

In other words, $\phi(a)$ in (2.14) is physically a normalized reference crack opening area. The reference crack opening area is plotted in Fig. 2.2a. The stress intensity factor for concentrated loading at the crack mouth, expressed via (2.11), is plotted in Fig. 2.2b with the FEM results for comparison. The reference crack opening profiles, $U_r(A, Y)$, are plotted in Fig. 2.2c and the CODs for concentrated loading at the crack mouth are plotted in Fig. 2.2d.

2.4 SCB Flexure

A rigorous analysis of the SIF and COD expressions for the SCB geometry is presented in this paper. To obtain the correct bending stress distribution along the prospective crack path, and thereby the associated SIF's and COD's, the method of superposition is employed. First, the solution for a circular disc of radius R subject to diametrically opposed compressive point loads is used as shown in Fig. 2.3a. The stress distributions along the X-axis and Y-axis passing through the center of the disc have been established (Frocht, 1948) and are as follows (using $x = X/R$):

$$\Sigma_{XX}(0, Y) = \frac{P}{\pi BR}, \qquad \Sigma_{YY}(X, 0) = -\frac{P}{\pi BR}\left(\frac{4}{(1+x^2)^2} - 1\right) \tag{2.17}$$

For future reference, P/BR will be defined as σ_{SCB}. The second expression in (2.17) is plotted in 2.3b. Consider now the uncracked SCB geometry shown in Fig. 2.3c with the major span defined as S. In Fig. 2.3d, the concentrated loads $P/2$ acting on $Y = 0$ at $X = \pm S/2$ are shown counterbalanced by the negative of $\Sigma_{YY}(X, 0)$

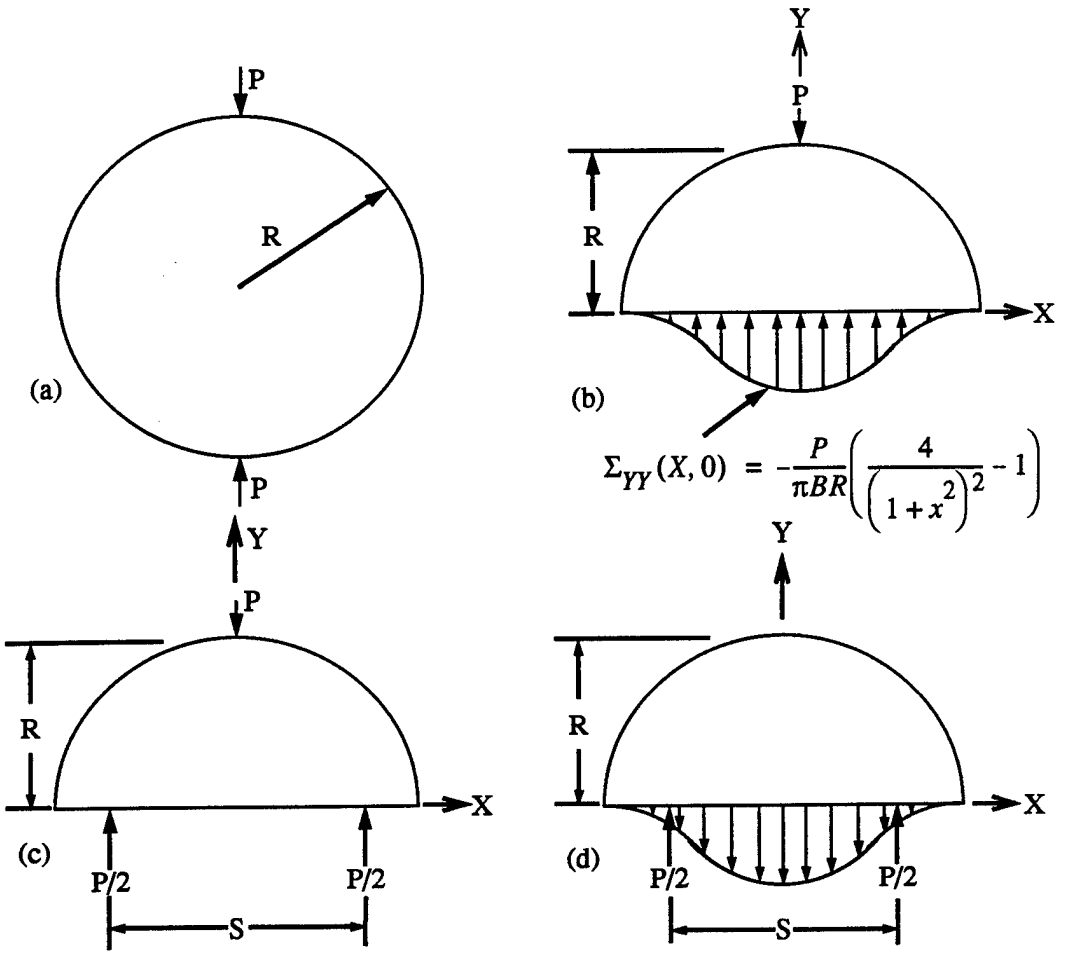

Figure 2.3: Illustration of superposition: (a) diametrically opposing point loads on a disk; (b) stress distribution along Y=0; (c) three point SCB configuraton; (d) equivalent bending configuration

defined in $(2.17)_2$. The loading in Fig. 2.3c is obtained by superposing the loading configurations portrayed in Fig. 2.3b and Fig. 2.3d. A finite element analysis was then conducted for the loading case in Fig. 2.3d for different spans. The resulting stress distributions, $\Sigma_{XX}(0,Y) \equiv \hat{\sigma}(y)$, were curve fit to an N^{th} order polynomial with the form (using $y = Y/R$)

$$\hat{\sigma}(y) = \Sigma_{XX}(0,Y)BR/P = \sum_{i=0}^{N} c_i y^i \tag{2.18}$$

S/R	c_0	c_1	c_2	c_3	c_4
1.0	1.543	-7.720	16.443	-15.776	5.484
1.2	1.792	-7.227	12.026	-9.981	3.122
1.4	2.072	-7.155	9.090	-6.163	1.658
1.6	2.365	-7.086	5.959	-1.957	
1.8	2.702	-7.852	5.679	-1.443	
2.0	3.043	-8.503	5.153	-0.802	

Table 2.1: Coefficients for different spans, S

The coefficients, c_i, are listed in Table 2.1 and the respective stress distributions are plotted in Fig. 2.4a for the different spans. Note that the shorter spans required more coefficients, N=4, to obtain an accurate curve fit. These curve fits provide an accuracy of r^2 better than 0.999. With the solution provided in (2.18), the flexural strength can now be determined by testing an uncracked SCB. For the flexure test, where significantly higher loads will be sustained as compared to a fracture test, the effect of the contact of the upper loading platen on the stress distribution should be considered. Gladwell (1980) developed a relationship between this contact length and the material parameters. Choosing conservative values for the material properties provided a maximum width for the contact surface, about 5% of the radius. Johnson (1985) investigated the case of a disk subjected to such diametrically opposed loads, treating the point load more accurately as a Hertzian contact problem. According to the solution, the finite contact introduces an error of about 0.03% to the point load solution, a negligible effect.

2.5 SCB Fracture

In this chapter, the base-edge-cracked SCB solution for a major span of $S = 1.6R$ (as studied in Chong and Kuruppu, 1984) is studied in depth. By combining (2.18) and (2.4), the normalized SIF solution for the SCB can now be written explicitly as (note

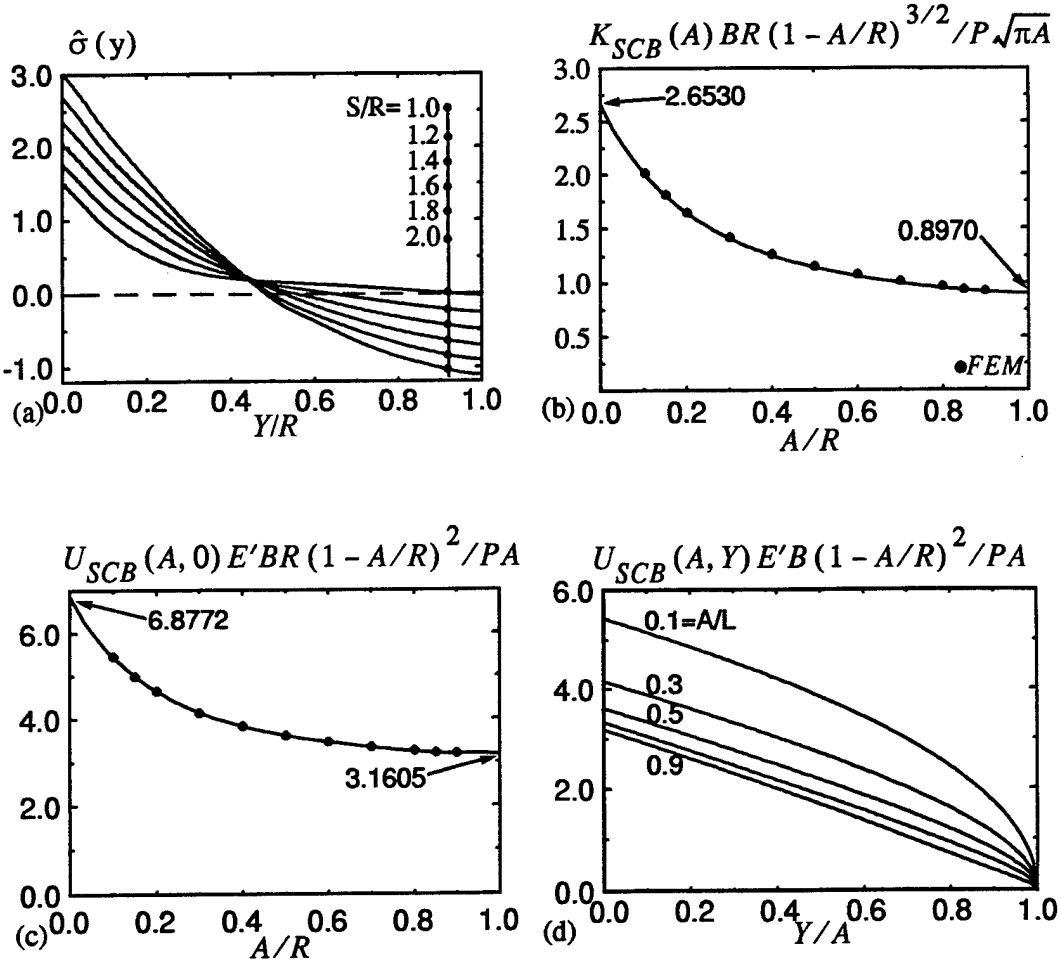

Figure 2.4: (a) SCB stress distributions, $\hat{\sigma}(y)$ for varying spans, S; (b) SIF for the SCB configuration; (c) CMOD for the SCB configuration; (d) COD's for the SCB configuration

the similarity with (2.4)):

$$f_{\rm SCB}(a) = K_{SCB}(A)/\sigma_{\rm SCB}\sqrt{\pi A} = \sum_{i=1}^{5} \mathcal{G}_i(a)\mathcal{R}_i(a) \tag{2.19}$$

where

$$\mathcal{R}_i = \left(\frac{1}{\pi\sqrt{2}}\right)\left[\frac{\sum_{k=0}^{3} c_k a^k}{i-1/2} - \frac{3c_3a^3+2c_2a^2+c_1a}{i+1/2} + \frac{3c_3a^3+c_2a^2}{i+3/2} - \frac{c_3a^3}{i+5/2}\right] \tag{2.20}$$

and

$$f_{\rm SCB}(a) = \frac{F_{\rm SCB}(a)}{(1-a)^{3/2}}, \qquad F_{\rm SCB}(s) = \sum_{i=0}^{7} \alpha_i{}^{\rm SCB} s^i, \tag{2.21}$$

Equation (2.20) applies only to the stress distributions represented by the third order equation (2.18), N=3. The coefficients α_i^{SCB} in (2.21) are

$$\alpha_i^{\text{SCB}} : 2.6530, -8.3354, 24.91, -55.2059, 86.6241, -89.4506, 53.5694, -13.8676 \tag{2.22}$$

The expression for the SIF for the SCB in (2.21) is plotted in Fig. 2.4b as are the FEM predictions from ABAQUS. The SIFs predicted independently by the FEM and the weight function method differ by less than 1% for all A/R.

The normalized CMOD solution for the SCB geometry written following the same definition as in (2.3) is

$$\begin{aligned} V_{\text{SCB}}(A) &= \frac{E'}{\sigma_{\text{SCB}} A} U_{\text{SCB}}(A, 0) \\ V_{\text{SCB}}(a) &= \frac{\bar{V}_{\text{SCB}}(a)}{(1-a)^2}, \qquad \bar{V}_{\text{SCB}}(s) = \sum_{i=0}^{7} \gamma_i{}^{\text{SCB}} s^i, \end{aligned} \tag{2.23}$$

with the coefficients, γ_i^{SCB}:

$$\gamma_i^{\text{SCB}} : 6.8772, -19.784, 70.4978, -199.0382, 393.6767, -479.4072, 314.8848, -84.5462. \tag{2.24}$$

The function $V_{SCB}(s)$ is plotted in Fig. 2.4c with the FEM results showing accuracy of better than 1%. The crack opening profiles for varying crack lengths are shown in Fig. 2.4d. The crack opening area for the SCB is determined applying the same approach used for the concentrated loading solution. It can be expressed explicitly as:

$$\mathcal{COA}_{SCB}(A) BE'/PA = 2V_r(a) \sum_{i=0}^{3} \frac{c_i a^{i+1}}{i+1} \tag{2.25}$$

2.6 Conclusions

The SIF and COD expressions for the SC reference loading case are presented, along with the SIF expression for the special case of concentrated loading at the crack mouth. The analytical expressions for the crack opening area (COA) for both the reference loading and the concentrated crack mouth loading are also obtained. A

detailed analysis of the Semi-Circular-Bend (SCB) geometry is presented, applying both the weight function approach and the finite element method. The full weight function for the SCB is determined, providing SIF and COD results for the entire range of crack lengths. For future applications, the SCB solution may be considered as the reference solution. Now both flexure and fracture information may be extracted from SCB testing. In addition, the solution for the COA for the SCB is determined.

3 ALIGNMENT EFFECTS ON FIRST YEAR SEA ICE*

3.1 Introduction

In 1993 and 1994, a three part field test program at Barrow, Alaska was undertaken as part of the Sea Ice Mechanics Initiative (SIMI). The program was designed to investigate the *in-situ* fracture and constitutive properties of sea ice and see how these properties changed through the growth season. To do so, the trips were made in November (Phase III), March (Phase IV) and May (Phase VI) when the ice was 0.3, 1.38 and 1.77m thick, respectively. Descriptions of the overall objectives, background and site characteristics, ice growth history, ice structure, fabric and micrography, the brine drainage networks, and the equipment and procedures were provided recently by Adamson et al (1995) and Cole et al (1995). The small scale test program was designed to link lab sized tests with the full scale behavior of an ice sheet (Adamson et al, 1995; Mulmule et al, 1995; Dempsey, 1996).

3.2 Background

Over the past two decades researchers have been gathering experimental information on the fracture toughness of sea ice at both laboratory and field scale. Among the authors on this topic are Vaudrey (1977), Urabe et al (1980), Shapiro et al (1981), Urabe et al (1981a,b), Timco and Frederking (1982), Shen and Lin (1986), Parsons et al (1986), Urabe et al (1986), Tuhkuri (1987), DeFranco et al (1991), Bentley (1992), DeFranco and Dempsey (1991,1992, 1994), Parsons et al (1993), Williams et al (1993), and Lazo (1994). A collective history of the experimental information provided by each author has been compiled in Adamson et al (1995). These studies focus primarily on the effects of loading rate, crack orientation, grain size, specimen size, temperature,

*Submitted for publication in the *ASCE Journal of Cold Regions Engineering* (Adamson, Shapiro and Dempsey, 1996)

brine volume and salinity on the apparent fracture toughness. Although these factors have been thoroughly proven to cause significant variations in K_Q, there is another that is often overlooked which can have a measurable influence: crystal orientation or c-axis alignment. The notation K_Q was introduced by Dempsey (1991) to emphasize the lack of a fracture toughness testing standard for ice.

Of the previous articles written on the fracture toughness of sea ice, only a few contain details of the ice fabric beyond the average grain size. In Shapiro et al (1981) there is some discussion regarding the average c-axis direction and its fluctuation with depth. However, there is no quantitative data included from which the degree of alignment can be concluded, nor is there any attempt made to compare c-axis alignment and K_Q. Timco and Frederking (1982) included detailed measurements of fracture toughness versus depth and brine volume, as well as providing thin-section micrographs of the ice through the depth of the sheet. Unfortunately, there was also apparently no attempt made to compare K_Q with the developing c-axis alignment through the depth.

One of the major factors thought to influence the fracture behavior of the Pt. Barrow ice sheet was the c-axis alignment. Examination of the ice fabric at the site (Cole et al, 1995) determined that a very strong horizontal c-axis alignment developed through the sheet. Such strong crystal alignments have been shown (Weeks and Gow, 1979) to be caused by under-ice currents present during the formation of the ice sheet. As part of the SIMI research project at Pt. Barrow, Shapiro and Weeks (1995) examined the effects of c-axis alignment on the flexural strength of small beam samples. Their results indicated that the strong alignment, coupled with brine-drainage networks, played a significant role in the flexural strength of the beams.

As noted above, several previous phases of the SIMI project have included a corresponding small scale testing program. Due to the ease of collection and the minimum amount of handling necessary for testing ice cores, most of the small scale tests have utilized some form of core-based specimen geometry. The geometry selected by the

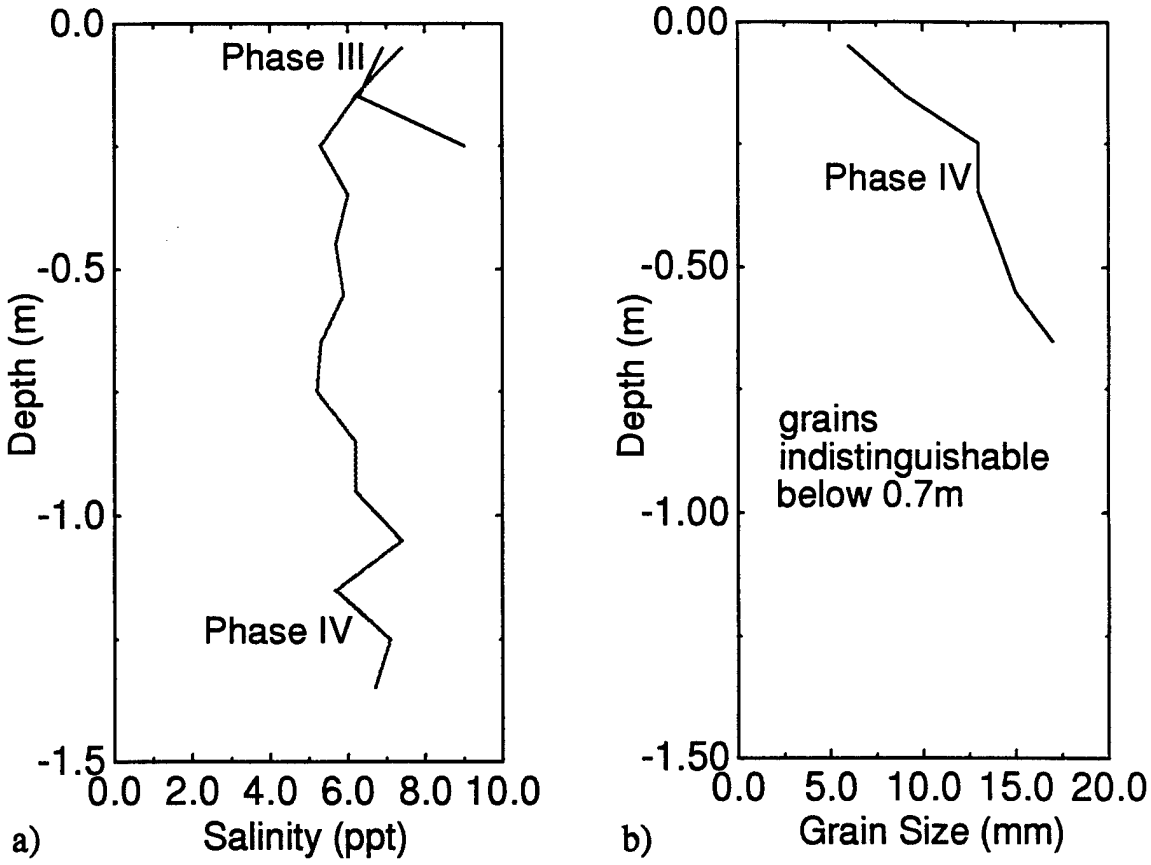

Figure 3.1: a) Salinity and b) grain size profiles for the sea ice in Elson Lagoon

authors for Phases III, IV and VI was the Semi-Circular Bend (SCB), which has the advantage of creating two times the number of specimens from a single core as most other core-based geometries. First developed by Chong et al (1984) for use in rock mechanics research, the SCB has since been rigorously characterized by Adamson et al (1996) using the weight function method. By that solution, the fracture toughness can be determined directly from the load and crack mouth opening displacement (δ_{CMOD}) at failure.

3.3 Characterization

Microstructural analysis of the ice at the Elson Lagoon test site (Cole et al., 1995) showed that the c-axes were strongly aligned as they were elsewhere along the Chukchi

and Beaufort Sea coasts of Alaska (Weeks and Gow, 1979). The alignment influences the fracture behavior by making it strongly anisotropic and creating strong- and weak-fail directions depending on whether a crack propagates parallel or perpendicular to the dominant c-axis orientation (Shapiro and Weeks, 1995). The degree of c-axis orientation tends to increase with depth in the ice sheet. This variation, coupled with the gradients of temperature, salinity and grain size which are also present, produces a vertical variation in strength and fracture behavior through the ice sheet. The small scale tests, along with the tests on the full thickness of the ice sheet, were designed to further investigate these effects (Adamson et al, 1995).

Salinity and temperature profiles through the winter are given in Cole et al (1995) along with data on the grain size, bulk density, platelet spacing and total porosity. Salinity profiles when the sample cores were taken are shown in Fig. 3.1, along with data showing the increase in grain size with depth. In addition, the crystallographic c-axes tend to become more closely aligned as the depth increases making it more difficult to distinguish individual crystals.

3.4 Experimental Program

The results presented in this paper consist of experiments carried out at Barrow, Alaska during the first two Barrow field trips, Phases III and IV, respectively. Both sets of experiments used the semi-circular bend (SCB) geometry. This geometry was chosen as it is very easy to fabricate many experiments from a single core removed from the sea ice sheet. A full fracture analysis of the SCB geometry is provided in Adamson et al (1996). For each field trip, the SCB testing served to provide an analysis of the fracture toughness with depth in the ice sheet. As the SCB tests are isothermal, the test results do not necessarily indicate the performance of the *in situ* sea ice sheet. The test data does, however, indicate the relative effects of brine drainage, drainage channels and voids on the fracture behavior.

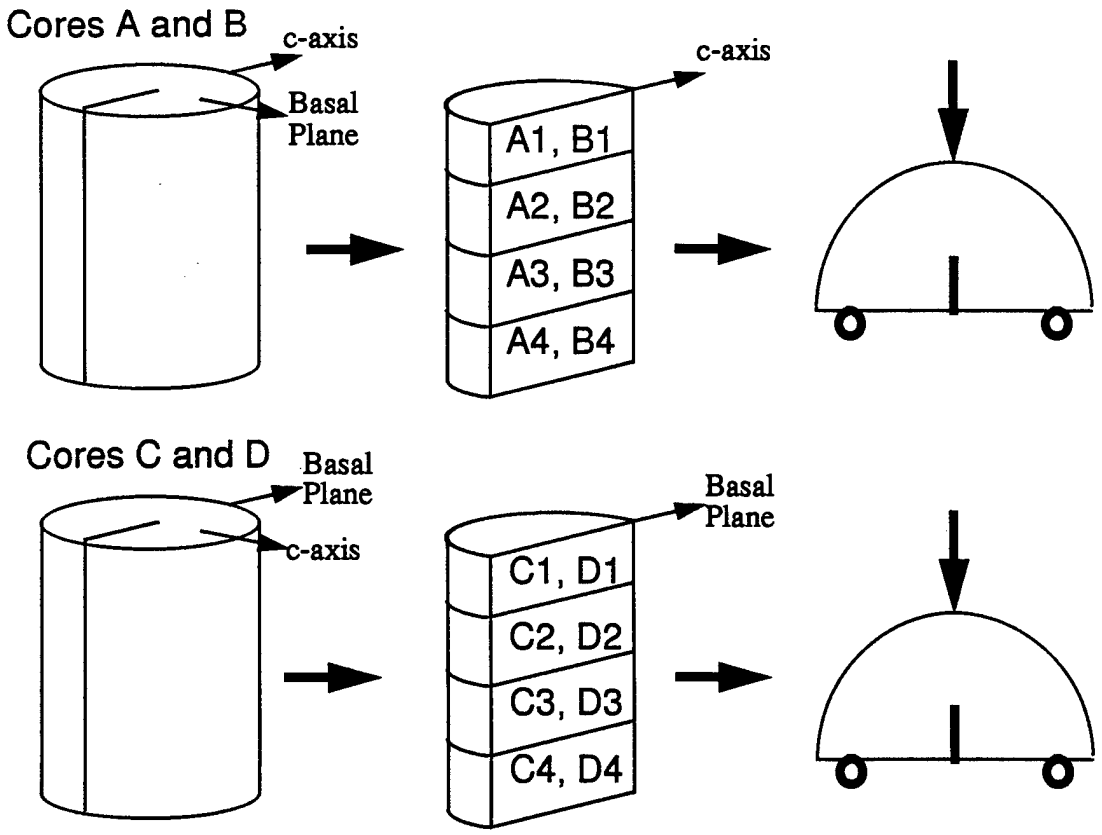

Figure 3.2: Process of machining SCB samples from cores for Phase III

3.4.1 Phase III

During Phase III, the ice sheet was about 0.3m thick and exhibited a strong c-axis alignment caused by currents from tidal activity. Because of this strong alignment, it was imperative that fracture tests with the crack propagating parallel and perpendicular to the c-axis alignment be completed to investigate the alignment effects at small scale. The SCB samples were rough cut from the core halves using a bandsaw and then smoothed using a planing device to a thickness of 7.6cm. The height of the SCB (R) was initially 10cm but the smoothing procedure reduced it to about 8.25cm. Dimensions and results of the experiments are provided in Table 3.1. Four separate cores were taken from the ice sheet and used for full thickness core tests (see Fig. 3.2). In two of the cores (labeled A & B), the precut notch was forced to propagate parallel to the c-axis (hard-fail). The other two cores (labeled C & D)

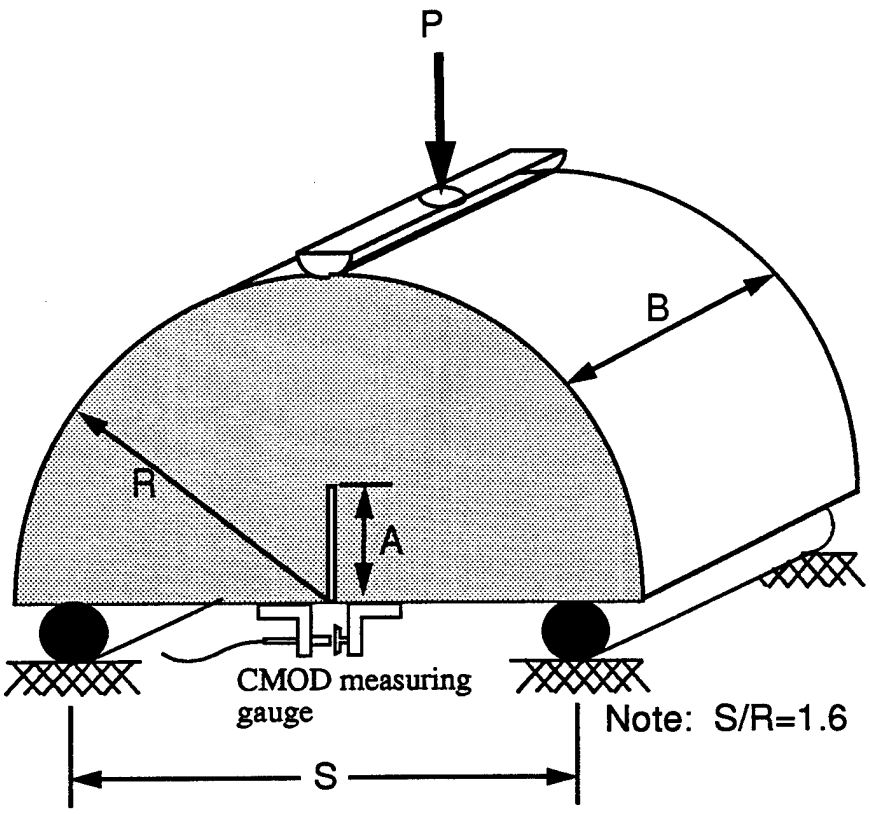

Figure 3.3: Loading configuration for the SCB tests (Note: Phase III experiments did not have CMOD gauges attached to the sample)

featured crack propagation parallel to the basal plane (easy-fail). Following the core experiments, the halved cores were bagged and transported to a cold room near the site. The cold room was maintained at -12° where both SCB preparation and testing were completed. Four SCB samples were machined from each half, creating a total of 32 SCB experiments. 16 of the SCB's were tested unnotched to obtain the flexural strength as a function of depth. The other 16 SCB's were notched and fractured to obtain the fracture toughness through the thickness. This makes it possible to make direct correlations between the tensile strengths determined from both the flexure and fracture experiments. Fig. 3.2 shows the details of preparing the SCB's from the halved cores.

The testing of the SCB's from this field trip were completed in a cold room set at -

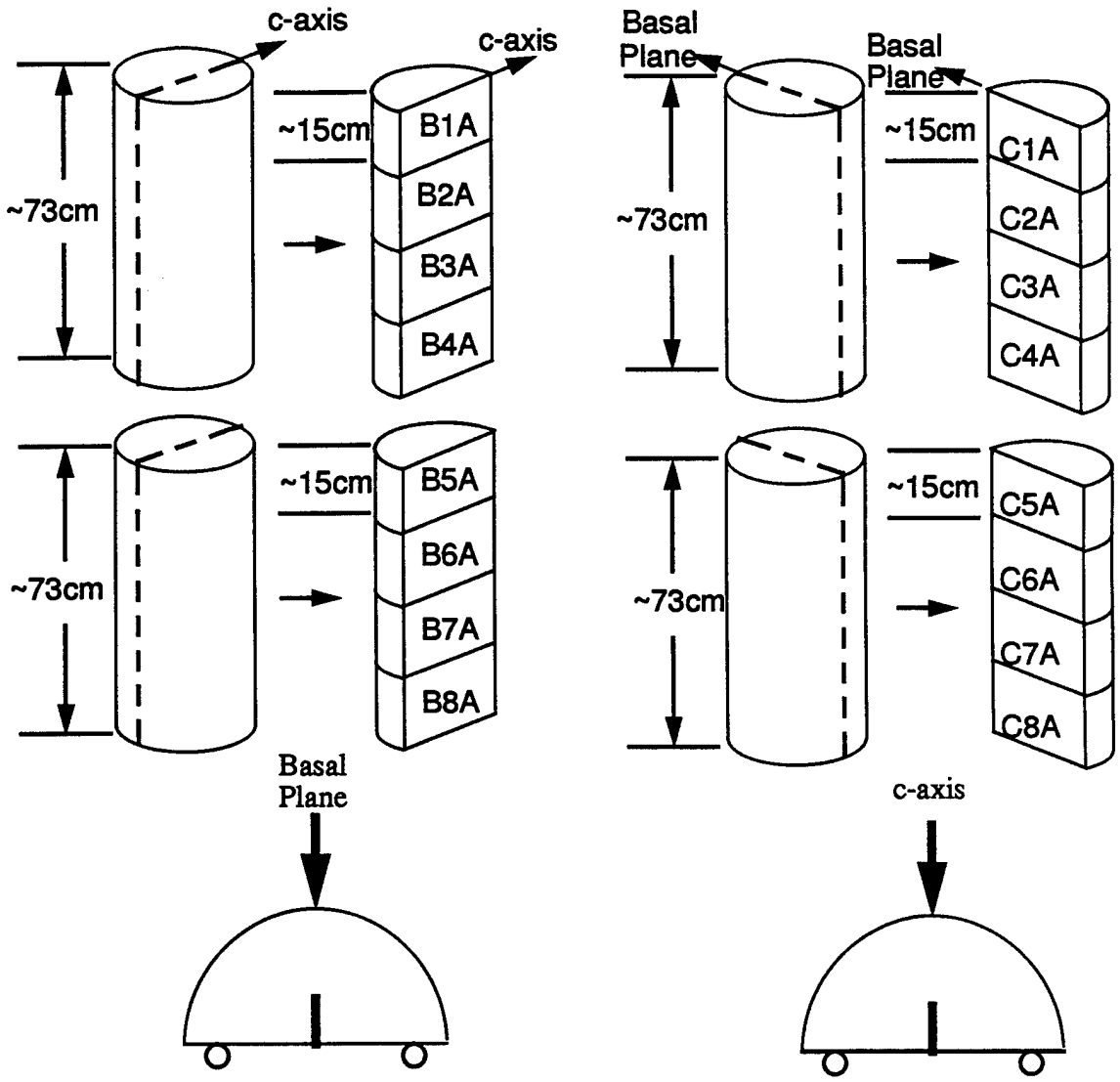

Figure 3.4: Process of machining SCB samples from cores for Phase IV

12°C. A 3.51cm notch was cut in the sample using a bandsaw located in the cold room. The loading surface of the testing device was advanced at a rate of approximately 2.7mm/sec. This resulted in typical failure times between 1 and 4 seconds. Fig. 6.1 shows the SCB fracture geometry with the loading configuration. Due to limited time and equipment constraints, only the load applied to the sample was measured. No displacements were recorded and hence no CMOD and modulus values are available.

3.4.2 Phase IV

By Phase IV, the thickness of the ice sheet had grown to 1.38m, maintaining the very strong c-axis alignment. Again, an analysis of the fracture toughness parallel and perpendicular to the c-axis was conducted. Two full depth cores were extracted from the sheet for the study. Due to time constraints, SCB's were made from only one half of each core (see Fig. 3.4). 8 SCB samples were machined from each core through the thickness of the sheet with an average thickness of about 15cm. To make the SCB samples, each core was sliced into 8 approximately equal thickness core sections. These sections were then cut in half carefully using a fine toothed handsaw. One half was used for the fracture tests, while the other half was saved for flexure testing. Unfortunately, time constraints prevented the testing of the flexure samples. A total of 16 SCB samples were made, 8 easy-fail and 8 hard-fail, from the two cores.

These experiments were completed at the site using a portable 3pt bend testing device. The SCB's were tested at an ice temperature of -35°C. The samples were loaded at about 350N/s resulting in failure times, t_f, of approximately 6 seconds. The crack mouth opening displacement (CMOD) was measured on every sample. Because the samples were about 15cm wide (width being denoted by the letter B in Fig. 6.1) a CMOD gauge was placed on either side detecting any differenceces in the displacement along the width. Interestingly, the easy-fail samples typically had similar CMOD records, whereas the hard-fail samples indicated a large amount of opening on one side and very little on the other (Fig. ??). The CMOD was measured with KAMAN noncontacting displacement gauges with a maximum measuring range of 0.25mm. These results will be discussed in more detail in later sections of this paper. Load and CMOD results from the easy and hard-fail experiments are presented in Fig. 3.6a,b. Because the samples were loaded to failure in about 6 seconds, the load-CMOD curves are show a near linear behavior with catastrophic failure at peak load.

Sample Name	Depth (m)	P_f (kN)	Crack Length (m)	Crack O'n to c-axis	$\dot{K}$ kPa$\sqrt{\text{m}}$s^{-1}	K_q kPa$\sqrt{\text{m}}$	σ_n^t MPa
1A	0.0	0.459	0.0351	$\parallel$	20	68.7	0.45
1B	0.0	0.437	0.0351	$\parallel$	20	65.5	0.43
2A	0.075	0.492	0.0351	$\parallel$	20	73.8	0.48
2B	0.075	0.322	0.0351	$\parallel$	20	48.2	0.31
3A	0.152	0.337	0.0351	$\parallel$	20	50.5	0.33
3B	0.152	—	0.0351	$\parallel$	20	—	—
4A	0.229	0.355	0.0351	$\parallel$	20	53.2	0.35
4B	0.229	0.355	0.0351	$\parallel$	20	53.2	0.35
1C	0.0	0.355	0.0351	$\perp$	20	53.2	0.35
1D	0.0	0.237	0.0351	$\perp$	20	35.5	0.23
2C	0.075	0.389	0.0351	$\perp$	20	58.3	0.38
2D	0.075	0.229	0.0351	$\perp$	20	34.3	0.22
3C	0.152	0.303	0.0351	$\perp$	20	45.4	0.30
3D	0.152	0.159	0.0351	$\perp$	20	23.9	0.16
4C	0.229	0.190	0.0351	$\perp$	20	28.5	0.19
4D	0.229	—	0.0351	$\perp$	20	—	—

Table 3.1: Small-scale SCB results from PHASE III (T=-12°C)

3.5 Results

The results of the SCB experiments are presented in Tables 1 and 2. No CMOD data were taken during the Phase III experiments, so only the apparent fracture toughness K_Q and the nominal tensile strength at failure, σ_n^t, were determined from the data. Nevertheless, comparison of these parameters with those obtained from the Phase IV experiments reveals some interesting differences. Tables 3.1 and 3.2 present the test data as well as computed parameters: K_Q, σ_n^t and E'. As noted earlier, the CMOD results from Phase IV were generally more consistent in the easy fail experiments. The hard-fail tests typically exhibited large openings on one side and very small openings on the other. This difference is possibly caused by the combined effect of the unwillingness of the crack to propagate in the hard fail direction and the existence of macrodefects (relative to the specimen size) near or at the crack front, such as brine drainage channels. Modulus calculations in several of these instances

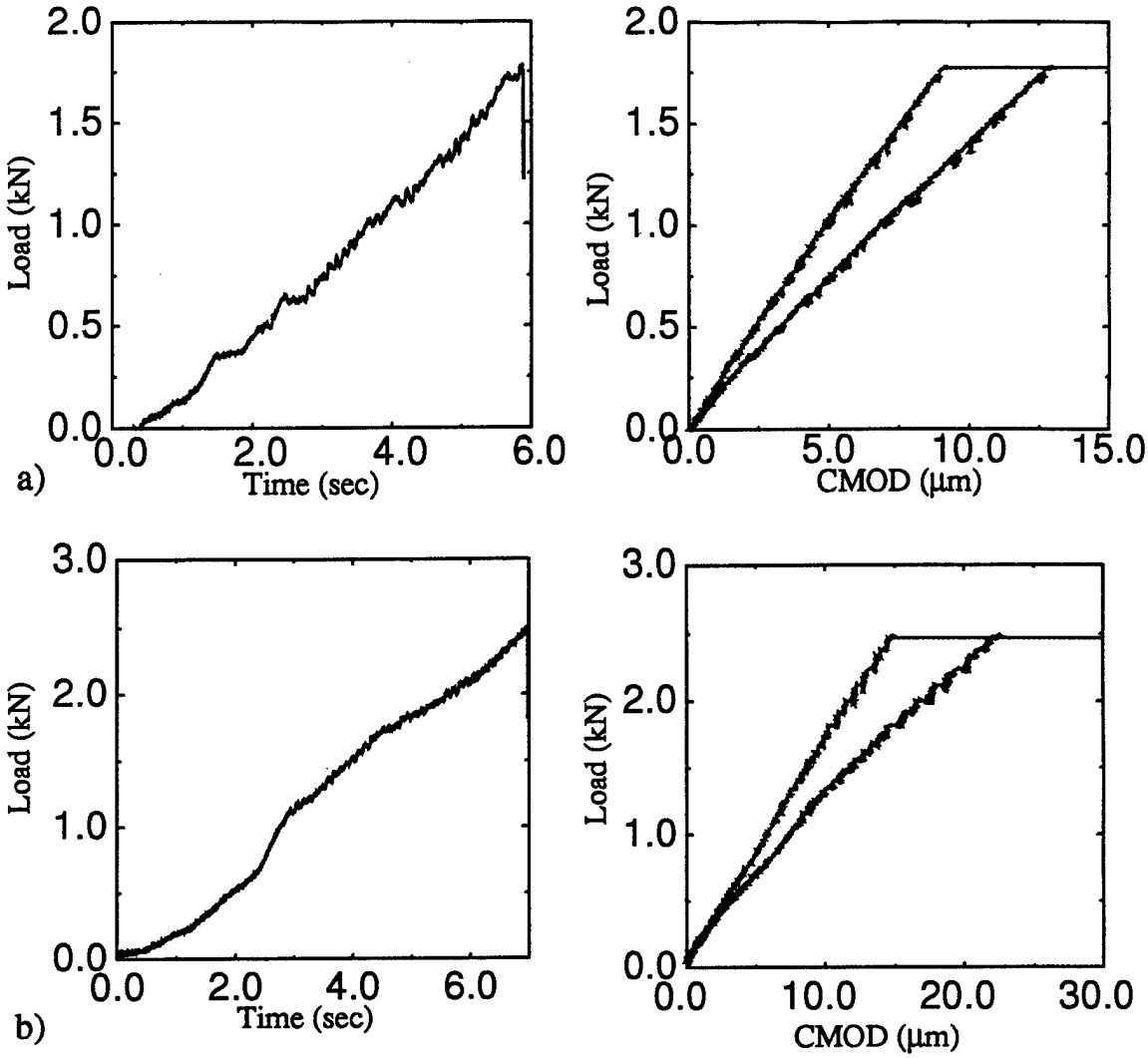

Figure 3.5: Graphs showing typical load and CMOD histories for a) easy fail and b) hard fail experiments

produce unrealistic values, reflecting the non-homogeneous response possible at this scale.

The apparent fracture toughness of each sample was determined by applying the analytical expression derived in Adamson et al (1996) for the SCB fracture geometry:

$$K_Q(A) = \frac{P_f}{BR}\frac{F_{SCB}(a)}{(1-a)^{3/2}}\sqrt{\pi A} \tag{3.1}$$

As is seen, $K_Q(A)$ is a function of the sample radius(R), crack length(A), load at failure (P) and width (B). The nondimensional function, $F_{SCB}(a)$ is a function of

NAME/ O'n	Depth (m)	P_f (kN)	B (m)	A (cm)	$CMOD_f$ (um)	$\dot{K}$ kPa$\sqrt{m}$/s	K_Q kPa$\sqrt{m}$	σ_n^t MPa	E' GPa
B1A ⊥	0.00	2.22	0.15	3.3	11.9	21	126	0.72	3.6
B2A ⊥	0.188	2.17	0.15	3.0	9.8, 3.2	19	113	0.63	4.0, 12.4
B3A ⊥	0.375	1.78	0.14	3.3	9.4, 6.7	18	110	0.62	4.0, 5.7
B4A ⊥	0.563	1.46	0.15	3.3	7.6, 4.8	17	85	0.48	3.8, 6.0
B5A ⊥	0.75	2.20	0.15	3.3	8.5	21	128	0.73	5.2
B6A ⊥	0.938	1.89	0.15	2.8	6.5, 5.8	17	99	0.54	5.3, 5.9
B7A ⊥	1.125	2.13	0.15	3.0	11.7	19	113	0.63	3.3
B8A ⊥	1.313	2.43	0.15	2.9	13.1, 9.0	22	129	0.71	3.4, 5.0
C1A ‖	0.00	2.21	0.14	3.0	30.7, 5.1	21	126	0.70	—,8.5
C2A ‖	0.188	2.44	0.16	2.7	40.5,1.3	20	109	0.60	—,—
C3A ‖	0.375	2.43	0.15	3.1	30.1,10	22	134	0.75	—, 4.6
C4A ‖	0.563	2.1	0.14	3.1	61.1	22	125	0.70	—
C5A ‖	0.75	2.6	0.14	3.0	21.0, 3.7	22	144	0.80	2.4, 13.5
C6A ‖	0.938	2.49	0.16	3.0	15.9, 10.5	21	124	0.69	2.7, 4.1
C7A ‖	1.125	2.28	0.15	2.9	32.3, 8.6	24	120	0.66	—, 4.8
C8A ‖	1.313	2.43	0.14	3.0	9.1	23	136	0.76	5.2

Table 3.2: Small-scale SCB results from PHASE IV (T=-35°C)

the normalized crack length ($a = A/R$) and also the ratio of the span of the lower supports (S) to the sample radius (S/R). It has the form

$$F(a) = \sum_{i=0}^{7} \alpha_i a^i \tag{3.2}$$

The solution derived in Adamson et al (1996) is for $S/R = 1.6$, the ratio chosen for these experiments. The α_i coefficients are also provided in Adamson et al (1996).

The nominal tensile strength at failure provides a way of estimating the tensile strength of fracture samples. For the SCB geometry, the nominal tensile strength was computed by assuming that a linear distribution of the stress field exists along the uncracked ligament (Fig. 2 in LeClair et al, 1996):

$$\sigma_n^t = \frac{P_f}{BR}\left(\frac{[\frac{3}{2}\frac{S}{R} - \frac{2}{\pi}] + \frac{2}{\pi}a}{(1-a)^2}\right) \tag{3.3}$$

The experiments are listed in Tables 3.1 and 3.2, along with the resulting values of K_Q and σ_n^t. The results are also plotted in Fig. 3.6. The difference between the results for the two sets of experiments is clear from the data in Figure 3.6c and d.

The average K_Q values from Phase III are approximately 50 kPa$\sqrt{\text{m}}$ although there is a clear difference in the results for the weak and strong fail directions. The results from the Phase IV tests are about 2.5 times those from Phase III over the same depth range, but do not indicate the effect of the loading direction. As the form of (3.3) and (3.1) are similar, the results for the nominal tensile strength exhibit the same behavior.

The difference in the results between the two sets of experiments probably reflects the difference in the age of the ice sheet and the temperatures of the samples when they were collected and tested. In November, the ice sheet was about 0.3m thick and less than one month old. Over its growth period, the daily average air temperature was never below about -15°C and the samples were stored and tested at -12°C. Under these conditions, the small brine pockets on the interfaces between platelet and grain boundaries, and the channels in the brine drainage networks in the ice were relatively large and open and significant drainage probably occurred when the samples were collected. This distribution of openings enhances the directional properties of the ice as well as providing relatively large voids around which stress concentrations could develop.

In contrast, when the samples were collected and tested in March, the ice sheet had reached a thickness of about 1.4m, and the air temperature was about -35°C and had been colder earlier in the winter. As a result, through most of the ice sheet the brine pockets were smaller than when the samples were collected in November, and drainage channels were narrow and probably isolated so little drainage could take place when the cores were taken. Subsequently, the ice temperature was always low enough that any brine trapped in the ice was frozen solid, so there were undoubtedly many fewer (and smaller) openings in the ice to act as stress concentrators for the tests in March than were present in the November test series.

The results shown in Tables 3.1 and 3.2 and Figures 3.6c and d indicate that for the November tests, the K_Q and σ_n^t values for the hard-fail tests are greater than those in

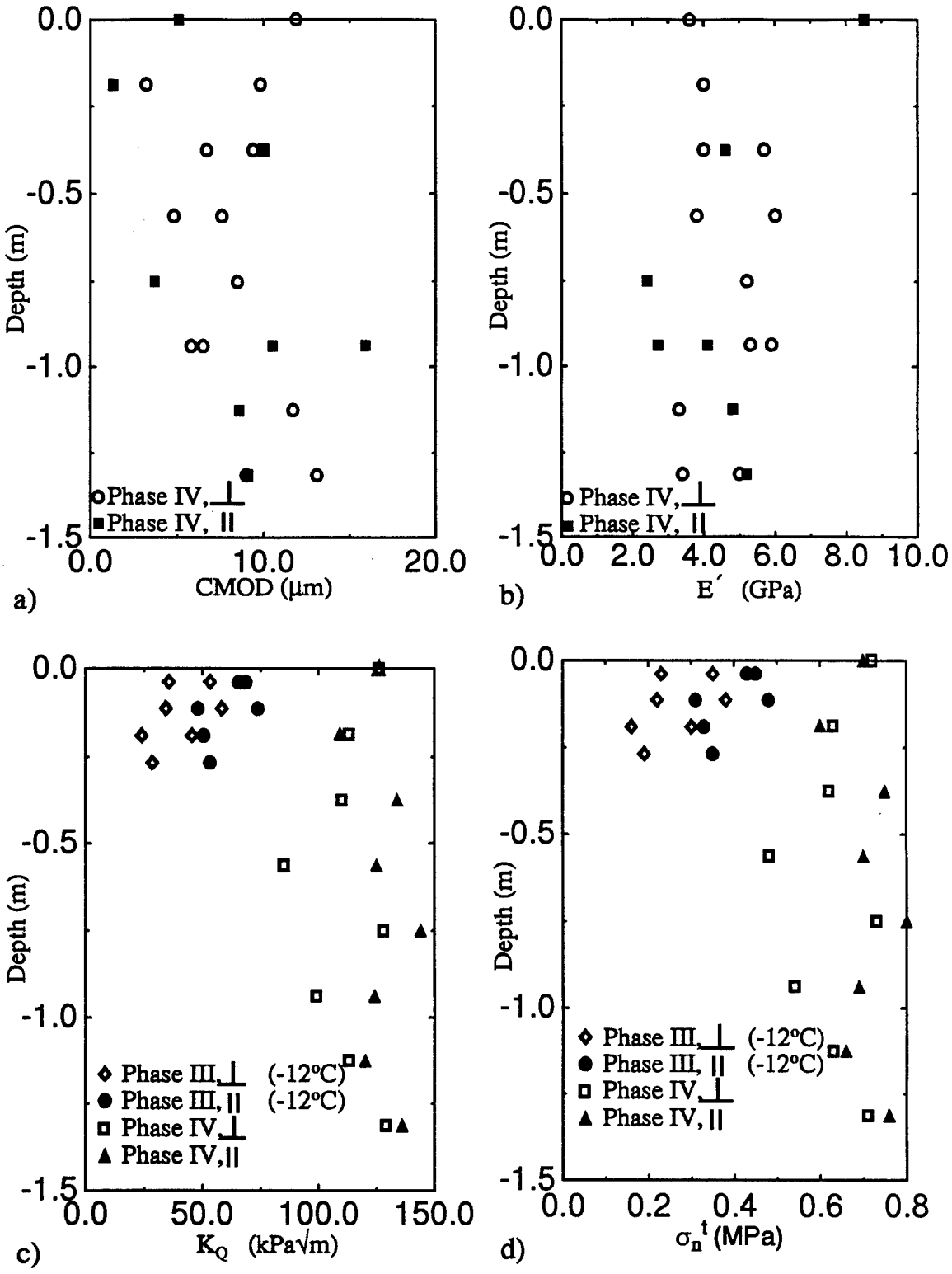

Figure 3.6: Results from the SCB experiments: a) Failure CMOD; b) Modulus of Elasticity; c) Fracture Toughness, K_Q; and d) Nominal failure strength, σ_n. Experiments completed at -35°C unless otherwise specified.

the easy-fail direction at all depths in the ice sheet. This is consistent with the strong mechanical anisotropy imposed by the crystal structure and the distribution of voids in the ice at the time. The results for the March tests show significantly higher values K_Q and σ_n^t but less directionality than those determined in November. Both these factors can be attributed to the decrease in the number and size of voids in the ice (which is primarily controlled by the temperature) between the two test series. This view is supported by data on the flexural strength of laboratory samples collected and tested concurrently with the SCB samples for both November and March, but tested at -12°C. The results of the flexural strength measurements showed a pronounced difference in strength between the strong and weak directions, as has been found previously (Shapiro and Weeks, 1993, 1995).

The tensile strengths obtained from the flexural experiments were very similar to those obtained from the fracture tests, indicating that the prenotching of the sample had little to no affect on the tensile strength. The associated notch insensitivity no doubt indicates the testing of subsized samples (Dempsey, 1991). This aspect of the testing was known prior to the program and was done to make a comparison with fracture toughness and nominal strength values from the larger samples. Results from a similar large scale test program completed in 1993, indicate larger K_Q values and lower σ_n values as the size is increased. Apparently, the sample size must actually be increased significantly to achieve a notch sensitive experiment (Adamson et al, 1995).

3.6 Conclusions

The effects of the inhomogeneity dominate the fracture behavior because the radius R of the cores is of the same order as the brine channel spacing (and possibly other flaw structures); the ratio of the crack length A to grain size varies between 4 or less at the surface to approximately one at depths below 0.7 m. However, it has recently been concluded that to obtain reliable numbers for the fracture toughness of sea ice, the requisite crack length to grain size ratio must be greater than 75

(Dempsey, 1996). This severe specimen size deficiency is judged by the authors to be the principal reason for the mild alignment influence observed. The latter mild influence contradicts observations in the field (one could accurately find the basal plane by simply looking for the few large surface cracks always lying on this plane). The fact that the flexural strengths and the peak nominal fracture tensile strength σ_n^t are of very similar magnitude is another indication of sub-sized tests: the tests were all notch insensitive (Dempsey, 1991). As revealed by Dempsey (1996), there is a dramatic scale effect associated with the fracture toughness parameter K_Q used in this paper. The use of this quantity for the SCB fracture test results presented here is not strictly correct; however, the ultimate purpose is to make comparisons between small-scale and large-scale tests.

4 THE FRACTURE OF S1 FRESHWATER ICE*

4.1 Introduction

The major problem faced by engineers in the design of large structures, be they large rock or concrete containment vessels, earthquake-resistant bridges or buildings, damage resistant icebreakers, or ice-resistant offshore structures in polar regions, is the question of size versus strength. Do the mechanical properties at large scale differ significantly from those at small scale? Can laboratory-scale testing be used to predict properties at large scale? What particular problems are faced with large scale testing? How useful are the size-effect theories developed to date? The answers to these questions are key to cost effective structural design in the fields of ice engineering, concrete design and rock mechanics. The major deterrent to increased arctic oil and gas recovery is the lack of certainty regarding the appropriate ice design loads. In this context, the major task is to ascertain the material behavior of sea ice on the scale of kilometers. This topic itself has far reaching importance: ice forces encountered during offshore structure-ice interactions, loads on submarines while surfacing, the calving rate of icebergs, the design of icebreakers, the ability of the northern countries to keep the Northern Sea Route open, for instance. The scale being attempted here is certainly huge; however, the conclusions will clearly be of interest not only for arctic applications but also for the huge concrete and earthquake-resistant design communities.

A two-phase joint-industry-agency project (JIAP) was initiated in 1990 to calibrate a fracture theory for incorporation into probabilistic global ice load models. Phase I of the JIAP "Large-Scale Ice Fracture Experiments" was completed in January, 1992 near Calgary, Alberta (Kennedy et al, 1993). The primary goal of Phase I was to assess the feasibility of large-scale, full-thickness ice (freshwater and sea)

*Submitted for publication in the *Journal of Engineering Mechanics* (Adamson, Mulmule and Dempsey, 1996)

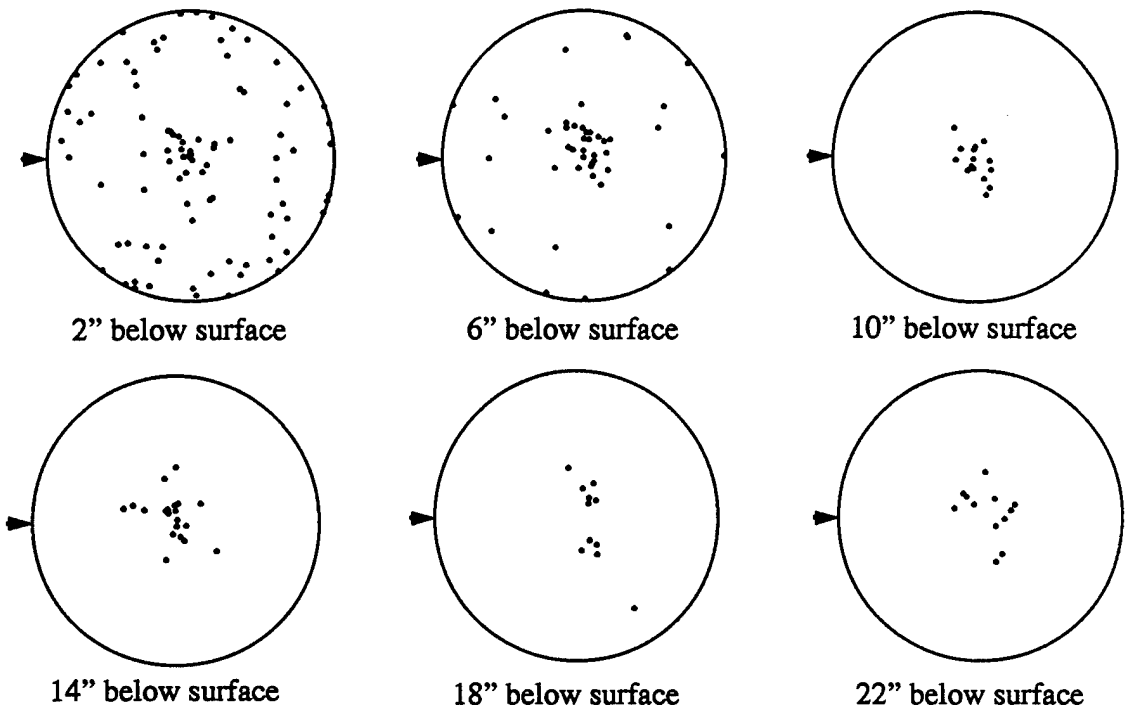

Figure 4.1: Schmidt Net plots for the S1 freshwater ice at Spray Lakes

fracture measurements. Due to the overall success of the project an abundance of data for large scale fracture tests on freshwater ice was recorded. This information serves to link small scale laboratory experiments with large-scale events.

Numerous factors affect the fracture behavior (deformations and failure loads) of prepared freshwater ice specimens such as:

- Temperature.
- Notch tip acuity.
- Rate of loading and process zone size.
- Specimen size and notch sensitivity.
- Material anisotropy.
- Grain size effects and inhomogenities such as grain boundaries.

Of the factors listed above, the specimen size and loading rate have significant

influences on the applicability of Linear Elastic Fracture Mechanics (LEFM). It is advantageous in the study of fracture behavior to be able to apply the principles of LEFM to greatly simplify both experimental as well as analytical aspects of the research. As one varies the specimen size and loading rate, there are three major interactive influences: homogeneity (specimen size to grain size), process zone size (zone of inelasticity ahead of the crack tip) and bulk creep. For severely undersized fracture tests, material homogeneity and small scale creep are both questionable assumptions. Small scale creep conditions hold when the nonlinear zone at the crack tip is sufficiently small (when compared with the crack length, the uncracked ligament, and any other geometric length quantities) such that the K-fields accurately model the stresses and deformations in an annular zone surrounding the crack tip. LEFM for ice is based on the concept of small scale creep (this concept necessarily precludes loading rates that are too slow, the latter causing significant bulk creep). Because of the large grain sizes involved with ice, and especially S1 ice, the applicability of LEFM to ice assumes an adequate specimen size such that material homogeneity holds and the ice can be treated as a continuum. As the specimen size increases, material behavior becomes more homogeneous, and eventually the length of the process zone reaches its maximum extent. With this in mind, it has become apparent that larger tests are required to truly recreate the behavior of a larger sheet of ice and ensure the validity of LEFM.

Dempsey (1991) and Dempsey et al (1992) tentatively proposed for columnar freshwater ice, on the basis of experimental evidence, that the sample size (characteristic length) be greater than $53d_{\mathrm{av}}$ where d_{av} is the average grain size. For the brittle or semi-brittle fracture of columnar S2 freshwater ice, Abdel-Tawab and Rodin (1992, 1993) asserted that only the size and orientation of the actual grain within which the crack tip is confined is important. The latter theoretical analysis neglected mechanisms such as grain boundary sliding and other coupled single crystal-cum-multiple crystal deformation mechanisms.

There is clearly a need for large scale testing to resolve some of the issues alluded to above. Although numerous factors affect the fracture behavior of ice, only a few of them can be investigated if restricted to the testing of laboratory sized specimens. Factors such as notch acuity, ice temperature, salinity and notch sensitivity can be studied independently. However, material anisotropy, specimen size effects, and the true nature of strain localization during fracture can only be addressed by testing large sized specimens. Other interesting aspects of large scale testing result from the possibility of obtaining R-curve information (DeFranco and Dempsey, 1992 & 1994). In-situ testing also incorporates the actual temperature and grain size profiles through the thickness. Furthermore, the testing of ice at ice temperatures above –5°C is really feasible in the field only.

4.2 Site Description

The initial site chosen for the freshwater ice experiments was Bearspaw Reservoir near Calgary, Alberta. The ice at this location was S2 freshwater ice with randomly oriented c-axes in the horizontal plane and grain sizes ranging from 1.5 cm to 5.0 cm. Also, the ice at Bearspaw was highly fractured because of water level changes for hydropower needs. Several experiments were completed at this site, but due to the unseasonably warm temperatures (15°C during the day) sample preparation was extremely difficult and the overall success of the project was in jeopardy. To remedy the situation and save the project, the testing was moved to Spray Lakes Reservoir near Calgary, Alberta. There, S1 freshwater ice grew with very large grain sizes up to 50 cm in diameter at the bottom of the sheet. The ice at Spray Lakes had limited fractures and large areas with no visible cracks. The ice sheet was 0.5m thick with a near vertical c-axis orientation.

4.3 Ice Characterization

Due to the warm temperatures at the test site, no characterization could be done during the field trip. A large block of the ice from Spray Lakes was shipped back to

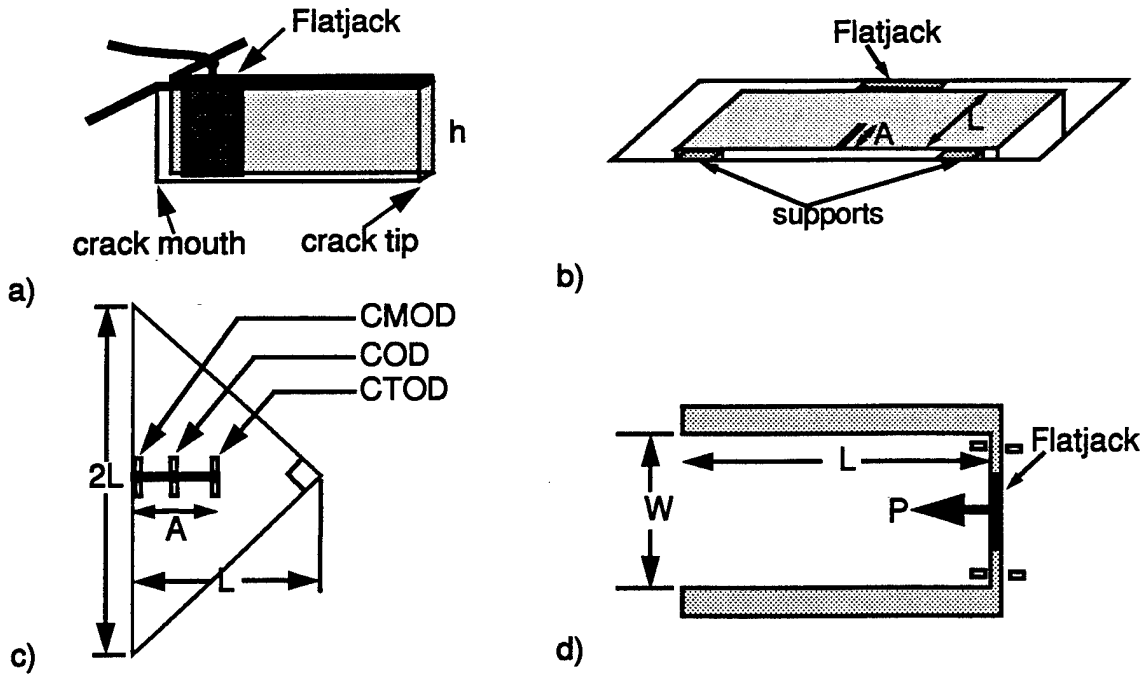

Figure 4.2: Schematic of flatjack in the ice; b) 3 point bend geometry; c) Reversed-taper geometry; d) Cantilever beam geometry

Clarkson University where detailed characterization of the ice was performed (Lazo, 1994). The ice sheet was about 0.5m thick; to obtain a detailed characterization of the ice through the depth, 11 thin sections were made at equal distances apart through the thickness. Grain size distributions and orientations were determined. Near the surface of the sheet the grains were about 0.5cm in diameter with randomly oriented c-axes, mostly horizontal. At the bottom of the ice sheet, the grains had reached diameters of 20cm with near vertical c-axes. For most of the thickness, except for the top few centimeters, the grains exhibited near vertical c-axes, classifying this ice as S1 macrocrystalline freshwater ice. Schmidt net plots (Fig. 4.1) obtained from the thin sections show the increasing trend of vertical c-axes deeper into the ice sheet.

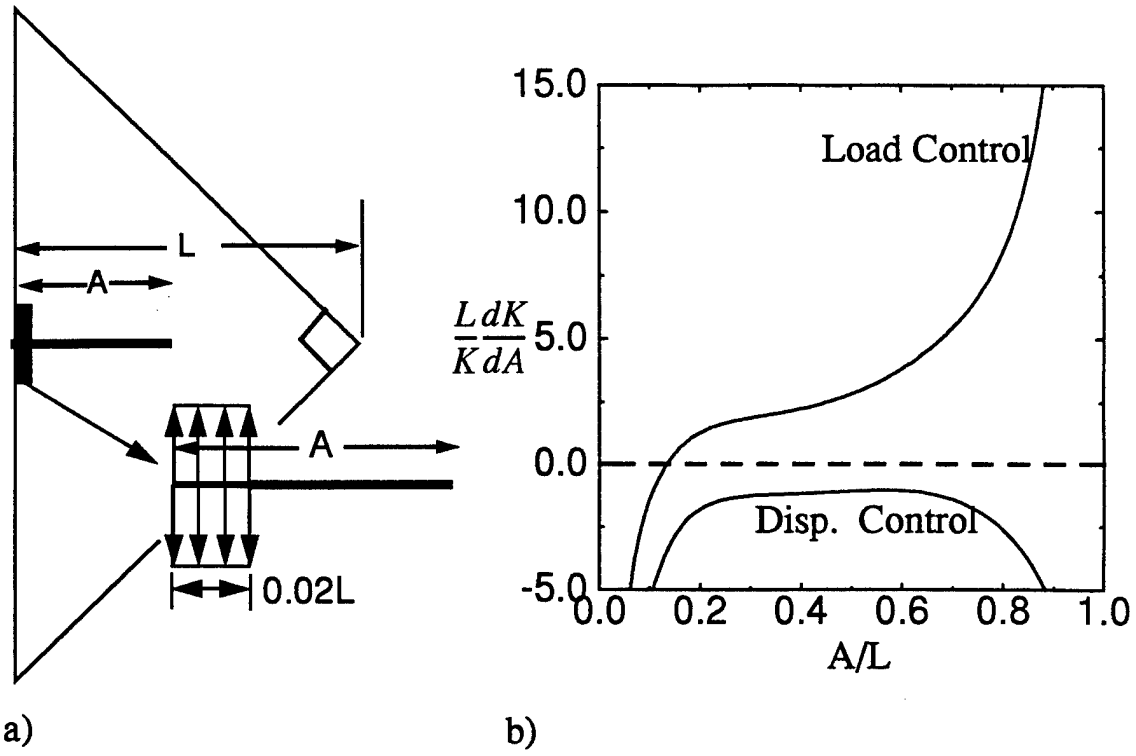

Figure 4.3: Stability of RT geometry subjected to a uniform load under load and displacement control

4.4 Experimental Procedure

All large scale experiments were in-situ tests enabling the testing of large sizes with resident thermal profiles. Experiments were prepared by first cutting the sample free from the parent ice sheet using chainsaws and/or a ditchwitch. The cut was made large enough to avoid refreezing between the specimen and the parent ice sheet. The openings were maintained with shovels and scrapers. While conducting the in-situ ice experiments, it was critical to ensure that the sample did not refreeze to the parent ice sheet.

Load was applied to the test sample using a flatjack loading device (Shapiro and Hoskins, 1978) fabricated by Sandwell, Inc. The flatjack was a thin walled steel blatter pressurized with either nitrogen gas or hydraulic fluid (Fig. 4.2a). Tests performed

with nitrogen gas were controlled by varying the flow of gas from a pressurized tank. These tests resulted in unstable fracture. A servo-hydraulic control system was used on several of the in-situ experiments controlling the load via a feedback signal from a displacement measuring gauge on the crack. These experiments generally involved multiple loadings and stable crack propagation in the form of crack jumps and arrests. Displacement measuring devices, LVDT's and non-contacting sensors, were mounted at several points along the crack as shown in Fig. 4.2b. These locations are labeled CMOD, COD and CTOD for the crack mouth, intermediate crack and crack tip opening displacements, respectively. On smaller experiments, the crack was not long enough to permit the COD gauge. The data from the displacement sensors and the pressure transducer were recorded on two computers equipped with A/D converters and an anologue tape backup system.

4.4.1 Beam Experiments

The geometry initially chosen for the large scale experiments was the three-point bend test with dimensions of 0.17m×0.51m (Fig. 4.2b). Each sample was prenotched with a crack length of 0.3L, or 0.051m. The crack tip was scribed with a fine tipped saw designed to create a very sharp crack. As discovered (Wei et al, 1992), the acuity of the crack tip has a significant influence on the failure load, especially in freshwater ice.

The first two beam experiments were carried out at Bearspaw reservoir. In experiment B2, the loading was controlled using the CTOD gauge for feedback and control resulting in crack propagation and arrest. The next two beams, B3 and B4, were tested at Spray Lakes. As a result of the beam geometry, an excessive amount of cutting was required to free a beam sample with a relatively short characteristic length. In addition, difficulties were encountered when applying the load to the sample. The flatjack was placed at the center of the beam between the sample and the parent ice sheet. On the opposite side two loading supports had to be placed at either end of

the beam. The large space between the parent sheet and the beam coupled with the beam's ability to rotate slightly made it difficult to keep the supports and the flatjack in place.

4.4.2 Reversed-Taper Geometry Experiments

This provoked the adoption of the reversed-taper (RT) geometry (Fig. 4.2c) (Dempsey et al, 1995). This geometry had been previously used for lab work at Clarkson University and proved to be very successful for promoting stable cracking (DeFranco and Dempsey, 1994). Reducing the specimen width with increasing crack length A is conducive to slow crack extension given a rapidly increasing compliance with crack extension. In a following section, the stability characteristics of the RT are investigated. The use of the RT greatly reduced setup time as it required 40% less cutting and the loading device was simplified. Rather than loading the sample by placing the flatjack between the parent ice sheet and the sample, the flatjack was inserted directly into the pre-cut notch (Fig. 4.2a,c), eliminating the need for any supports. Nine RT tests, some with stable crack propagation and multiple loadings, yielded a specimen size range of 1:81 and included the then largest known controlled fracture test specimen ($40.5 \times 40.5 \times 0.57$m).

4.4.3 Cantilever Beams

An additional evaluation of specimen size on the elastic modulus was made using three in–situ cantilever beams as shown in Fig. 4.2d. The sample was cut free from the parent ice sheet on three sides, but remained attached at one end. The flatjack was placed at the opposite end and force was applied in the plane of the sheet. Displacements were measured at the free end between the parent ice sheet and the cantilever beam. Several load/unload trials were performed on each experiment.

Test ID	Length L, (m)	Crack Length (m)	A/d_{av}	K $kPa\sqrt{m}/s$	E_{CMOD} GPa	E_{COD} GPa	$CTOD_f$ μm	Mean Air Temp °C
B1	0.51	0.06		3				-2.4
B2	0.51	0.05		38				+5.3
B3	0.53	0.04	2.2	—				-1.6
B4	0.52	0.05	2.2	2				-2.1
RT1	1.41	0.43	5.13	2.87	4.34	3.54	7	0
RT2	0.41	0.14	1.67	3.77	5.68	-	-	-0.3
RT3	4.42	1.23	14.7	4.79	7.57	5.69	8	-0.6
RT4	0.34	0.95	1.0	5.13	-	-	-	+0.4
RT5	1.04	0.39	4.65	3.71	-	2.79	5	+0
RT6	10.36	3.12	37.3	9.10	3.21	7.66	20	+0
RT7	3.18	0.99	11.8	37.8	2.85	-	8	0
RT8	3.20	0.99	12.2	144	8.0	3.6	11	-3
RT9	28.64	8.98	107	57.8	-	10.0	25	+0
CM1	0.36	N/A		—				0
CM2	1.08	N/A		—				0

B1,B2: Bears Paw; B3,B4, All RT's, CM1,CM2: Spray Lakes, Canmore.

Table 4.1: Large scale experiments completed on Phase I

4.5 The RT Geometry: Stability Aspects

The growth of the crack is as important as the initiation of fracture. The concept of the R-curve has gained wide acceptance in characterizing the resistance of a material to fracture. In the context of ice, efforts to obtain R-curves have been hampered by lack of stable crack growth. DeFranco and Dempsey (1991) were able to obtain the R-curve for lab-scale saline ice tests using the RT geometry.

First, for continued crack advance, given that the current crack length is $A + \Delta A$, the applied stress intensity factor must equate with the resistance to fracture:

$$K = K_R(\Delta A) \tag{4.1}$$

The condition for stable crack growth is

$$\frac{\partial K}{\partial A} < \frac{dK_R}{d\Delta A} \tag{4.2}$$

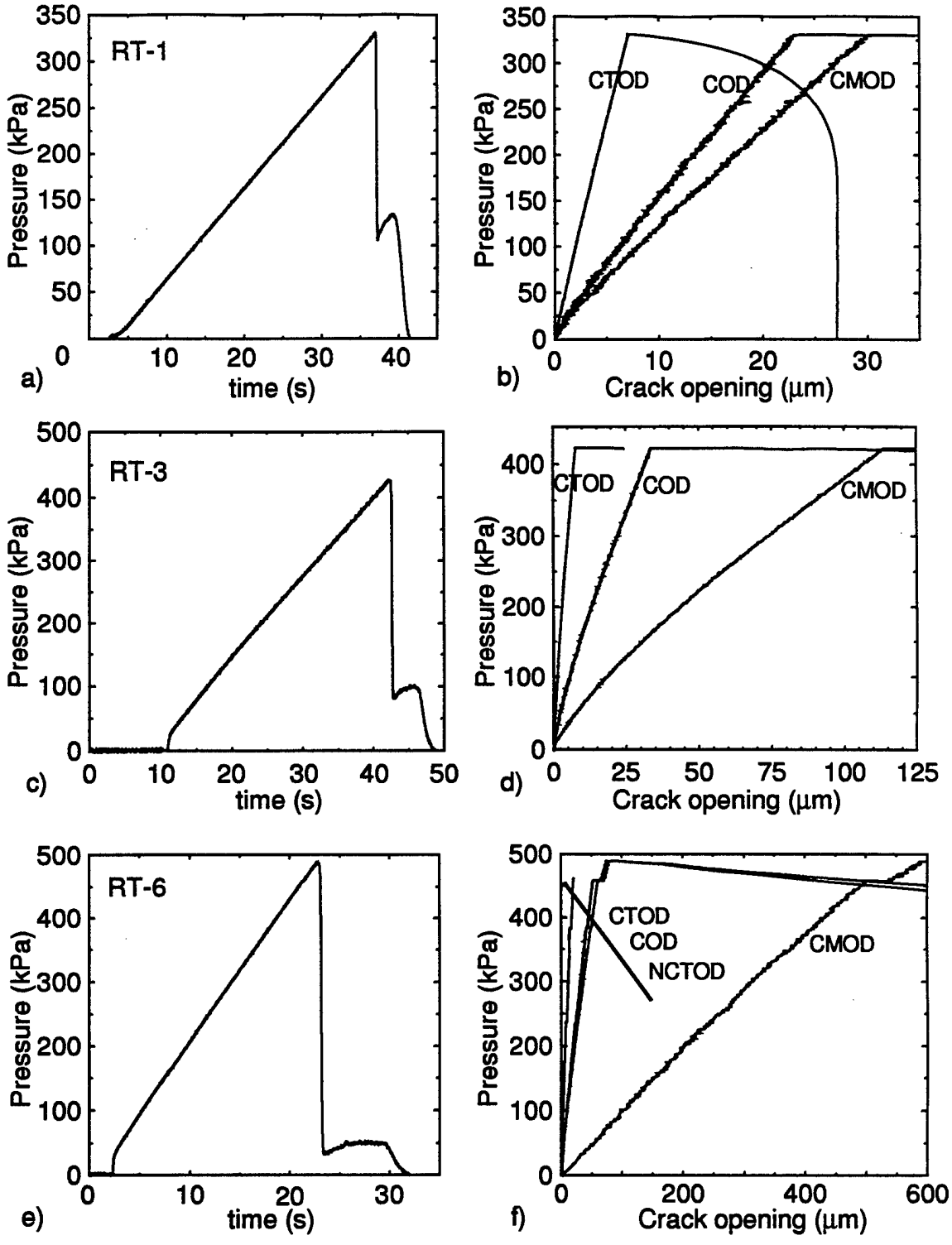

Figure 4.4: Typical Load vs. time and Load vs. COD plots for several experiments

In (4.2), the partial derivative of K with respect to A must be taken with the prescribed loading condition held fixed.

Most common laboratory tested geometries have a positive geometry, that is, a positive $\partial K/\partial A$ curve. In most cases, unless the resistance curve has a higher slope, these tests will result in catastrophic failure upon crack initiation. To promote stable crack growth, the application of the loading can be changed. By using displacement control rather than load control, the test can be made a negative geometry. Suppose the specimen load point displacement is represented by $\Delta = PC$, where $C(A)$ denotes the specimen compliance. In load control, the stability equation is written as:

$$2\frac{L}{K}\left(\frac{\partial K}{\partial A}\right)_P = \frac{C''}{C'} \tag{4.3}$$

In displacement control, the compliance of the testing machine, in addition to that of the specimen, affects the stability of the experiment. For displacement controlled loading, the stability equation is

$$2\frac{L}{K}\left(\frac{\partial K}{\partial A}\right)_{\Delta_T} = \frac{C''}{C'} - 2\frac{C'}{C + C_M} \tag{4.4}$$

where C_M is the compliance of the testing machine. Applying the above equations to the RT geometry used on the freshwater ice experiments, the effects of the loading can be realized. For the simple case of uniform loading along the crack faces of the RT, the stress intensity factor can be written as:

$$K_r(A) = \sigma\sqrt{\pi A} f_r(a), \qquad f_r(a) = \frac{\sum_{i=0}^{7} \alpha_i a^i}{(1-a)^{3/2}} \tag{4.5}$$

where $a = A/L$, and the normalized crack mouth opening displacement (CMOD) as:

$$V_r(A/L) = \frac{E'}{\sigma A} U_r(A, 0) = \frac{\sum_{i=0}^{7} \gamma_i a^i}{(1-a)^2} \tag{4.6}$$

The α_i's and γ_i's can be found in the paper by Dempsey et al (1995). From these solutions, the stress intensity factors and normalized CMOD solutions for any other loading may be obtained using the weight function method. To illustrate the effect of load or displacement control on the stability of an experiment, the loading shown in Fig. 4.3a is chosen. This loading is similar to that applied to the RT geometry field

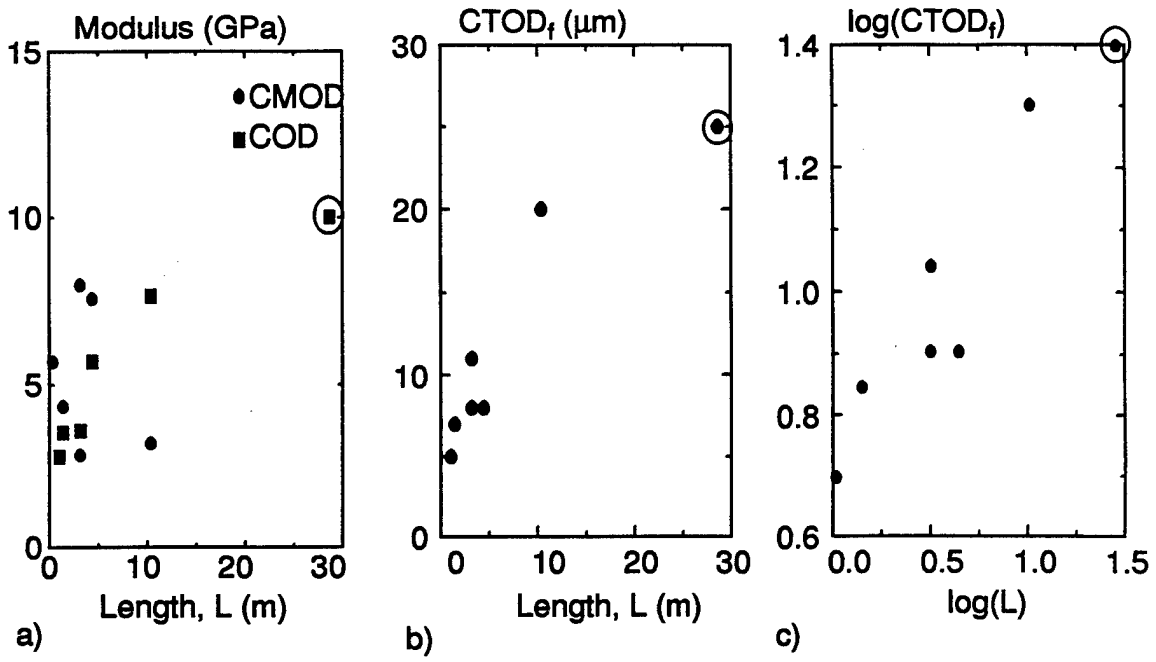

Figure 4.5: Effects of specimen size on a) Elastic Modulus and b) CTOD at failure; c) log-log plot of failure CTOD

experiments. For the case of load control, the stability equation can now be defined as:

$$\frac{L}{K}\left(\frac{\partial K}{\partial A}\right)_P = \frac{1}{2a} + \frac{f'(a)}{f(a)} \tag{4.7}$$

When displacement control is used, and the machine compliance is much less than that of the material ($C_M \rightarrow 0$), the stability is defined as:

$$\frac{1}{K}\left(\frac{\partial K}{\partial a}\right)_\Delta = \frac{1}{2a} + \frac{f'(a)}{f(a)} - \frac{C'(a)}{C(a)} \tag{4.8}$$

As can be seen in Fig. 4.3b, using displacement as a means of controlling the applied load greatly increases the stability of the experiment. In the majority of the RT experiments where load control was used, the sample failed upon initial cracking. When displacement control was used to regulate the loading, stable cracking was witnessed in the form of a series of crack jumps and arrests. The crack would jump up to 1m on some samples before arresting. This can be attributed to the compliance

of the testing system and slow response time relative to the crack jumping speed. In experimental R-curve evaluations, the amount of stable crack growth needed to reach a plateau fracture resistance may be as much as $500d_{av}$ (Peck et al, 1985). If ice behaves similarly, an ice specimen having $d_{av} \approx 20$cm would need at least 100 meters of stable crack growth to reach its plateau resistance.

4.6 Results

A total of 15 in-situ fracture and modulus experiments were completed on beam (BM) (Fig. 4.2a), reversed-taper (RT) (Fig. 4.2b), and cantilever modulus (CM) (Fig. 4.2c) geometries. Most of the experiments were loaded to failure in less than 50 seconds. Table 1 summarizes the experimental details and results. The load vs COD plots in Fig. 4.4 indicate near linear behavior with no noticeable time dependent features. For each of the fracture experiments, the modulus was calculated from the displacement gauges at the CMOD and COD. As can be seen in the load vs. COD plots, the initial behavior of the experiment appears to be nonlinear. This is due to flatjack effects when the flatjack is still forming full contact with the sides of the crack. The modulus was determined from the more linear portion of the curve later in the experiment. Due to the problems encountered with field testing, the displacement records for some of the tests were not recorded. In these cases, the modulus cannot be computed. No discernable trend in the CMOD modulus could be seen and a considerable amount of scatter was present (Fig. 4.5a). The scatter can be attributed to the effects of nonhomogeneity arising from the low flaw size to grain size ratio. It can also be caused by the close proximity of the flatjack loading device. The COD modulus which is farther from the loading shows less scatter with a definite increasing trend with size. A size range of 1:81 was achieved testing RT samples up to 28.6m in length. Even at this size, the crack length to average grain size ratio, A/d_{av}, was only 107 because of the large grain sizes. The displacement measuring gauge at the crack tip, was able to measure deformation prior to crack propagation and indicate the

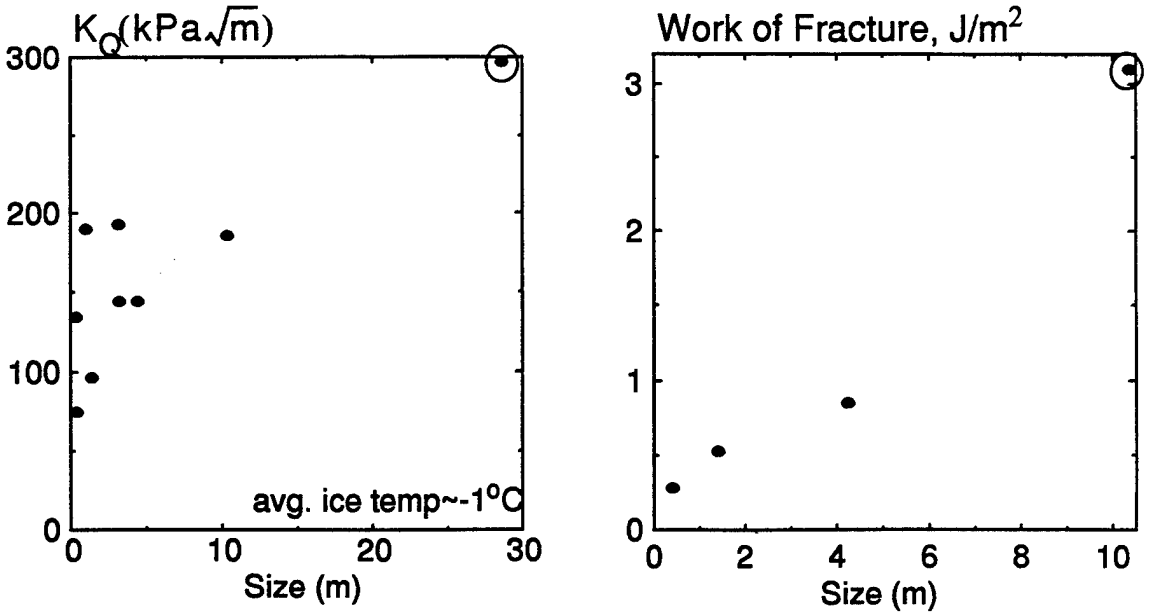

Figure 4.6: a) Apparent fracture toughness vs size for in-situ experiments; b) Fracture energy vs size

exact time of initial macroscopic crack propagation. From this, the crack tip opening at failure was determined for each experiment. An increasing trend in the failure CTOD was noticed (Fig. 4.5b,c), indicating that specimen sizes were not reached at which the failure CTOD was independent of specimen size. Table 1 lists the tests completed with modulus calculations and failure CTOD values. As can be seen, all of the experiments were carried out at very warm temperatures. It is important to note that lab experiments at these temperatures are nearly impossible.

Ratios of crack length and ligament length to average grain size (d_{av}) are also presented in the table. The average grain size was obtained by weighting the size of grain by approximately the length of the crack. For small sizes, this ratio is small. Another feature is seen by considering the effect of grain size on elastic modulus obtained from cantilever beam tests shown in Table 1. The last three tests, namely RT3, RT6 and RT9 have an average elastic modulus of approximately 10 GPa and

are almost constant. This transition occurs when the ligament as well as crack is roughly 15 times the average grain size. It should be noted that the results of RT-9 are somewhat suspect as a significant time period elapsed between sample preparation and final failure during which refreezing of the sides was possible. The results of this experiment are plotted with an open circle around the point for this reason.

4.7 Analysis

The effects of anisotropy and polycrystallinity are very important when considering a material with a very large grain size as encountered in this field study. The inelasticity ahead of the crack tip influences the behavior of the ice especially in the smaller samples. Other factors that affect the fracture of freshwater ice are thermal profile, notch tip acuity, loading rate and notch sensitivity. A large enough specimen must be tested to assume a homogeneous isotropic response. In this ice, the basal plane or weak plane is predominantly parallel to ice surface. Because the ice is being fractured along stronger planes, the weakness introduced by the grain boundaries and therefore the grain size play an important role in the strength of the sheet.

4.7.1 Fracture Toughness

The fracture toughness is a measure of a material's ability to resist fracture and is represented by the critical stress intensity factor, K_{Ic}. Because no fracture toughness testing standard exists for ice and several assumptions are made to justify the applicability of LEFM to freshwater ice, the following notational change has been recommended [*Dempsey,* 1991] and since adopted:

$$K_Q = K_{apparent}^{initiation} \tag{4.9}$$

to replace the parameter K_{Ic}. Apparent fracture toughness values were computed from the load at the onset of cracking as determined from the CTOD gauge. The fracture toughness as a function of size is plotted in Fig. 4.6a and shows a rise in the toughness with size without achieving a plateau K_Q value. This is indicative of

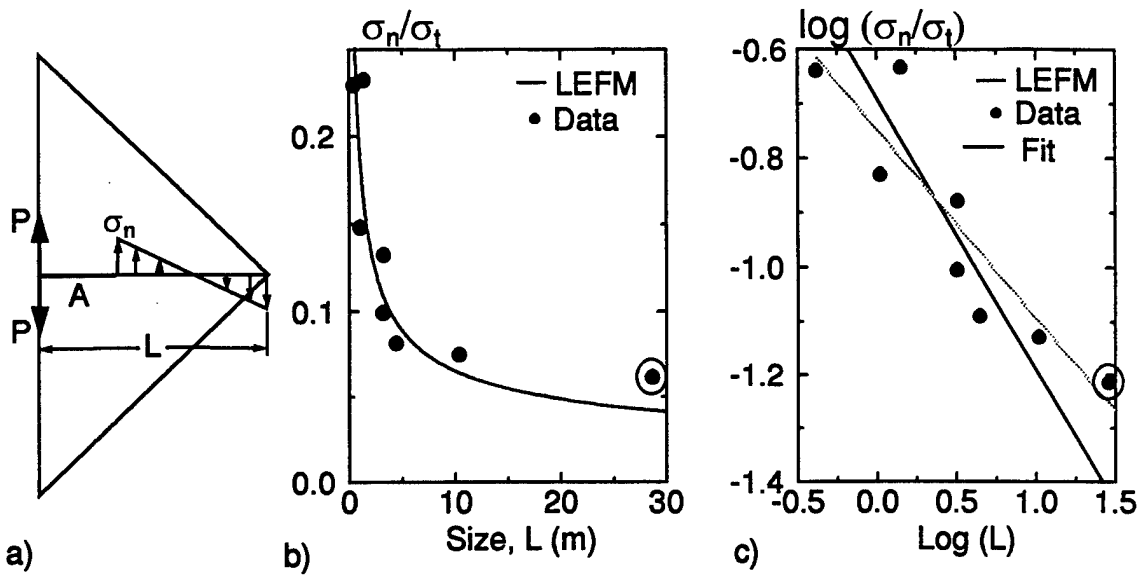

Figure 4.7: a)Nominal stress, σ_n, at the crack tip; b) Normalized nominal stress at failure for in-situ fracture experiments; c) Log-log plot of nominal failure stress versus size

softening mechanisms (grain boundary sliding, dislocations, microcracking) around the crack tip dominating the failure of the smaller samples with a transition to brittle failure at the larger sizes. A plateau in the fracture toughness was not reached, possibly because still larger sizes are required for this large grained S1 ice.

4.7.2 Nominal Strength and Size Effects

The nominal strength provides a way of estimating the tensile stresses of similar test samples and predicting size effects. It is defined as the maximum nominal stress sustained at the crack tip before failure. For the RT geometry, the nominal stress was computed by replacing the load from the flatjack with an equivalent load and moment at the center of the uncracked ligament. From this, the maximum nominal stress at the crack tip was computed. The tensile strength can be found from the

flatjack load with the following equation:

$$\sigma_n = \frac{2P_f(A+2L)}{h(L-A)^2} \tag{4.10}$$

Fig. 4.7b shows the plot of the maximum nominal stress vs. the sample size. The solid curve represents the size effect as predicted by LEFM. This prediction assumes a constant fracture toughness and similar geometries; that is the same geometry with the same nondimensional crack length, A/L. Note that the curve can be shifted vertically by assuming a different fracture toughness. The curve is found by solving (4.5) for σ. It can be seen σ will decrease as a function of $\sqrt{L}$. It is plotted over the field results to simply show how well the data follows the LEFM size effect. Fig. 4.7c is a log-log plot of the stress vs. size with the LEFM prediction as well as a linear regression of the data. Because of the large scatter in the data, the linear regression line should not be considered to be the size effect, but only used as a comparison with the LEFM size effect. A thorough investigation of the flexural strength of S1 freshwater ice was completed by Gow et al (1978, 1988). Large-scale (0.3m $\times$ 0.3m $\times$ 2.0m) flexural experiments on a freshwater lake (Gow et al, 1978) exhibited lower strengths than comparable smaller experiments (Gow et al, 1988) on model S1 freshwater ice. These results are consistent with those obtained from the Phase I fracture experiments.

If an LEFM size effect exists, a linear scaling in the strength will be evident with a slope of -1/2 on a log - log plot of the nominal stress vs. size (Fig. 4.7c). If other size effects are present, the scaling will be different. Attempts were made to analyze the large scale fracture data using the fictitious crack model (FCM) and existing size effect laws. The FCM makes use of the CTOD data for determining the size of the process zone, and subsequently determining the size effect. In the large scale experiments, the mounts used for the CTOD gauges on the large scale tests were approximately 2cm wide parallel to the crack. For this CTOD data to be representative, the size of the predicted process zone should be much larger than the width of the CTOD mounts. In these experiments, the process zone size was determined to be much less than the

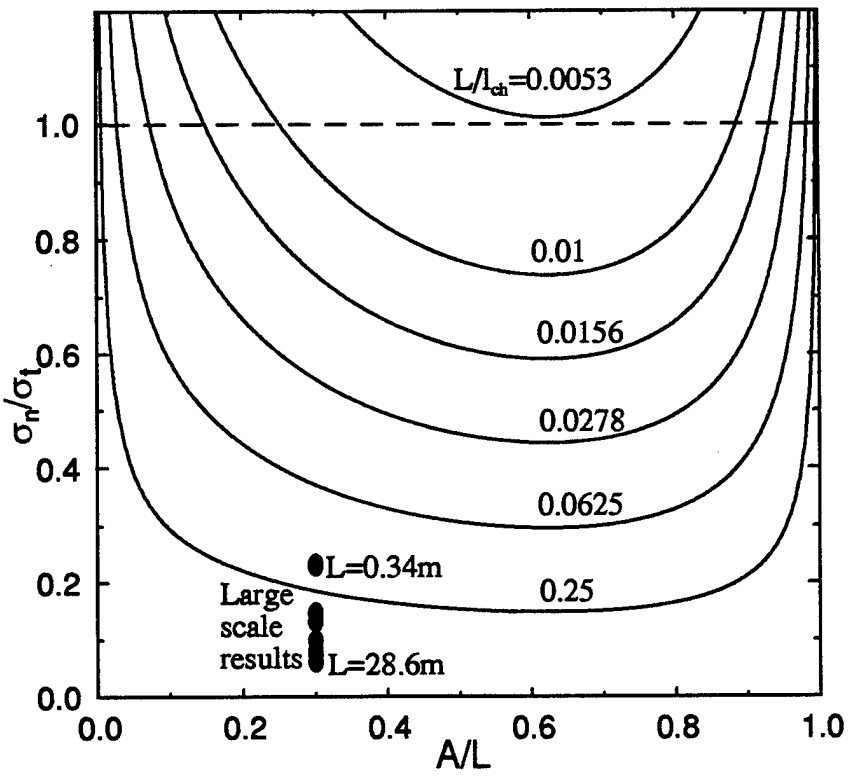

Figure 4.8: Brittleness plots for the RT geometry subjected to flatjack loading (w/L=0.02).

size of the mounts, rendering modelling based on the FCM unreliable. In addition, since the process zone size was found to be so small, the fictitious crack model is not necessary. The very small amount of nonlinearity found in the experiments can be attributed to bulk behavior.

Attempts to fit any of the existing size effect laws also proved to be unsuccessful. The linear fit obtained for the experimental data, although not accurate because of the large scatter in the data, indicates that other size effects are present. These are possibly due to effects of grain size and inhomogeneity.

4.7.3 Notch Sensitivity

Surprisingly, very little attention has been paid to the study of the fracture behavior of S1 freshwater ice (Kolle, 1981; Danilenko, 1985; Dempsey et al, 1988; Dempsey and Wei, 1989; Stehn et al, 1994, 1995a, 1995b). The most recent studies (Dempsey et al, 1988; Dempsey and Wei, 1989; Stehn et al, 1994, 1995a, 1995b) appear to be the most comprehesive with investigations of the effects of crack vs c-axis orientation, grain size and specimen size on the fracture. When conducting fracture experiments, it is imperative to make the specimen notch sensitive, that is, the crack and uncracked ligament must both be long enough for the crack tip to be surrounded by a volume in which the elastostatic stress and displacement field is accurately portrayed by LEFM theory. For cracks that are too short or even too long, the notch sensitivity decreases and flexural or tensile failure may preclude a true fracture failure. The procedure for determining the notch sensitivity as outlined by Walsh (1972) and Carpinteri (1982) and applied to freshwater ice by Dempsey (1991) is used. Dempsey (1991) completed a thorough investigation of the brittleness and notch sensitivity of S2 columnar freshwater ice.

The stress intensity factor expression for the RT geometry with partial crack face loading as applied by the flatjack is given as:

$$K_Q = \frac{P_f}{wh} f(a) \tag{4.11}$$

where w is the width of the flatjack. The peak nominal stress (σ_n) acting on the uncracked ligament at failure is given in [4.10]. Now, the nondimensional σ_n/σ_t can be written as:

$$\sigma_n/\sigma_t = \frac{C_N}{\sqrt{L/l_{ch}}}, \tag{4.12}$$

where l_{ch} denotes the size-independent characteristic length

$$l_{ch} = \left(\frac{K_{1c}}{\sigma_t}\right)^2 \tag{4.13}$$

and

$$C_N = \frac{2(a+2)}{(1-a)^2}\frac{(w/L)}{\sqrt{\pi a}f(a)}\frac{K_Q}{K_{1c}} \tag{4.14}$$

Fig. 4.8 plots the normalized σ_n as a function of the crack length. It is evident that fracture tests completely lose meaning for L/l_{ch} below values of about 0.005. The plot in Fig. 4.8 is more acceptable if a restricted range in size were to be tested. The curves drawn were generated by first assuming that $K_Q = K_{1c}$ in (4.14). This is of course not true for sub-sized tests. To compound the latter deficiency, the apparent fracture toughness, K_Q, is size dependent (see Fig. 4.6), but then so is the tensile strength, σ_t (see Fig. 4.7). The large scale results shown were calculated, on the other hand, using

$$\frac{\sigma_n}{\sigma_o} = \frac{2(2+a)}{(1-a)^2}\frac{P_f/hL}{\sigma_o} \tag{4.15}$$

with the reference tensile strength, σ_o, given by $\sigma_o = 1$MPa. Despite the abovementioned interpretive difficulties, Fig. 4.8 qualitatively underscores the influence of scale and crack length. Moreover, given that $\sigma_o = 1$MPa is a realistic estimate, it is clear that all the fracture tests were decidedly notch sensitive.

4.7.4 Work of Fracture

The fracture energy per unit crack area for a cracked body can be expressed as:

$$G_f = \frac{1}{h(L-A)}\int_0^\infty P d\delta_{LL} \tag{4.16}$$

where P is the applied load normal to the crack and δ_{LL} is the load line displacement. Equation 4.16 represents the area under the load versus load-line displacement curve and is an estimate of the work of fracture. It assumes that all of the work of the load is dissipated in creating the crack. For an ideally britttle material, the equation reduces to $G_f = P_f\delta_{LL}/2h(L-A)$. For the large scale experiments, very little nonlinearity was observed in the P versus LLD curves, so the behavior was assumed to be linear. As for the unloading portion of the curve, numerous reasons account for excluding any area under the unloading portion of the curve. Once the ice sample fractures,

the two halves are further pushed apart by the flatjack. Their motion is resisted by hydrodynamic forces as well as interaction with the parent ice sheet. This force is recorded and cannot be uncoupled from the unloading response of the ice sample. In addition, where load control was used for the fracture test, brittle cleavage fracture was observed. Fig. 4.6b shows the work of fracture vs size as an increasing function. This tends to indicate that larger sizes are needed to reach a plateau fracture energy. These results are consistent with tendencies of the other material properties calculated (i.e. $CTOD_f$, K_Q).

4.7.5 Non-Universal Scaling

If the crack growth were a self-similar process described by a law invariant with size, one could speculate on the existence of a universal fracture mechanism governed by either a constant fracture toughness or a constant material strength. As noted in the preceeding discussions, it is not the case with this S1 freshwater ice. S1 freshwater ice has two major length scales affecting its fracture behavior: ice thickness and grain size. The grain size relative to the other length scales appears to be the most influential scale. The average grain size for the ice was about 15 cm with crack lengths ranging from 0.14 to 8.98 m. To investigate the presence of non-universal scaling, the dependence of the CTOD at crack growth ($CTOD_f$) versus the pre-notched crack length (A) is plotted in Figures 4.5b,c. Fig. 4.5c reveals no significant change in scaling. This is also consistent with the K_Q results in Fig. 4.6a which indicate that a scale invariant fracture toughness was not obtained. Unfortunately, the effect of scaling on the nominal failure stress (Fig. 4.7b,c) is clouded by the wide scatter in the data and therefore no reliable predictions can be made with those results. Nevertheless, the results undeniably indicate larger sized experiments are required to successfully reveal a change in fracture mechanism and ultimately obtain scale invariant fracture and strength parameters.

4.8 Conclusions

A field investigation of macrocrystalline S1 freshwater ice was completed to determine the effects of specimen size on fracture and strength parameters. The experiments were in-situ fracture tests using beam and reversed-taper geometries. The size study used the RT geometry and produced very interesting results. The grain sizes were very large relative to the largest sample size tested; as a consequence, issues of specimen homogeneity and the applicability of LEFM proved very important. While a distinct size effect does exist, it appears to be less pronounced than the size effect predicted by LEFM. Larger test sizes are necessary to achieve a more homogeneous sample and obtain the scale invariant fracture and strength parameters for macrocrystalline S1 freshwater ice.

5 THE FRACTURE OF S2 SEA ICE*

5.1 Introduction

Ice is very unique in the broad range of sizes over which it must be understood. An abundance of lab scale investigations have been completed on sea ice as well as investigations above the 1 km scale. Very little data exists for the scales between 0.1 and 1000m. The objective is to evaluate the scale effect on the fracture behavior of sea ice over the range 10^{-1}m (laboratory) to 100m (full thickness field experiments) employing a combination of on-site and laboratory experiments linked to theoretical fracture and constitutive models as well as theoretical ice property models. Nonlinear fracture models can then be used to predict the scale effect over the range $10^{-1} \approx$ 1000m. The long term modeling objectives include: (a) Quantitatively validate the near-tip processes and relaxation processes. In this context, the effectiveness of the currently available size effect laws in terms of their predictions for fracture energy and process zone size must be established; (b) Quantitatively verify a process zone model for fracture in saline ice at any scale by linking the experimentally determined information with an analytical treatment of the process zone.

A two-phase joint-industry-agency project (JIAP) was initiated in 1990 to calibrate a fracture theory for incorporation into probabalistic global ice load models. Phase I of the JIAP "Large-Scale Ice Fracture Experiments" was completed in January, 1992 near Calgary, Alberta (Kennedy et al, 1993; Adamson et al, 1996). The primary goal of Phase I was to assess the feasibility of large-scale, full-thickness ice fracture measurements. Due to the overall success of the project, Phase II was initiated to study arctic sea ice at large scales.

Most of the experiments carried out to obtain the fracture toughness of ice have been performed on lab sized specimens. Because of the material anisotropy, nonhomo-

*Submitted for publication in the *Journal of Engineering Mechanics* (Adamson, Mulmule and Dempsey, 1996)

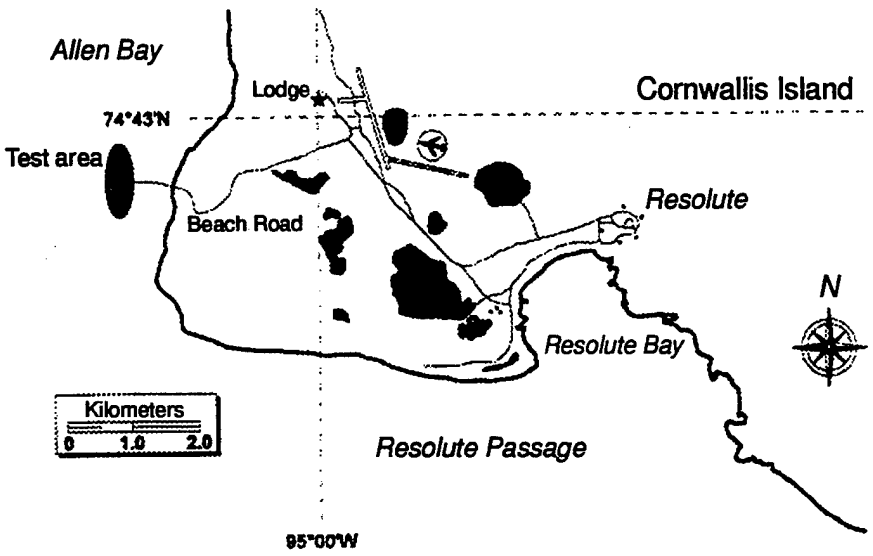

Figure 5.1: Map of Resolute Bay indicating the test site

geneity of the ice due to large grain sizes, brine drainage channels and the very high homologous temperature at which fracture tests are usually carried out, the fracture toughness obtained at lab sizes can not be considered as a true material property. Dempsey (1991) defined an apparent fracture toughness K_Q as obtained from lab tests and advocated the use of larger sized specimens. With this in mind, large scale experiments coupled with small scale field and laboratory tests were completed on sea ice in Phase II. The experiments have yielded an abundance of information related to the fracture and constitutive behavior of sea ice.

The various influences on the fracture of ice are reiterated below

- Salinity and temperature.
- Notch tip acuity.
- Rate of loading.
- Material anisotropy.
- Grain size effects and inhomogenities such as grain boundary sliding, brine drainage channels.
- Specimen size and notch sensitivity.
- Inelasticity ahead of crack tip.

Each of the above factors are examined below as related to the current investigations. A full thickness ice sheet has both a temperature and salinity profile through the depth: the isolated effect of either parameter is not obtainable. The issue of crack tip acuity for saline ice was explored by DeFranco et al (1991) who found a decrease in K_Q with increase in crack tip acuity. Notch tip acuity was maintained in these experiments by sharpening and scribing the cracks with a special apparatus. The quantification of rate effects demands a large number of tests to be carried out over a range of rates. Large scale testing with its time consuming test setups and limited time precluded any such possibility. Notch sensitivity for first year sea ice was experimentally investigated by Parsons et al (1993). The length of the pre-cut crack was always such that the specimens were notch sensitive and failure occurred by fracture.

The specimen size and loading rate have significant influences on the applicability of Linear Elastic Fracture Mechanics (LEFM). It is advantageous in the study of fracture behavior to be able to apply the principles of LEFM to greatly simplify both experimental as well analytical aspects of the research. As one varies the specimen size and loading rate, there are three major interactive influences: homogeneity (specimen size to grain size), process zone size (zone of inelasticity ahead of the crack tip) and bulk creep. For severely undersized fracture tests, material homogeneity and small scale creep are both questionable assumptions. Small scale creep conditions hold when the nonlinear zone at the crack tip is sufficiently small (when compared with the crack length, the uncracked ligament, and any other geometric length quantities) such that the K-fields accurately model the stresses and deformations in an annular zone surrounding the crack tip. LEFM for ice is based on the concept of small scale creep (this concept necessarily precludes loading rates that are too slow, the latter causing significant bulk creep). Because of the large grain sizes involved with ice, and especially S1 ice, the applicability of LEFM to ice is also based on an adequate specimen size such that material homogeneity holds and the ice can be treated as a continuum.

As the specimen size increases, material behavior becomes more homogeneous, and eventually the length of the process zone reaches its maximum extent.

Due to the large grain size of ice and anisotropy of grains, the crack size to grain size and the ligament size to grain size ratio of the fracture specimen dictate the size of specimen if micromechanical simulations are to be avoided. For polycrystalline S2 freshwater ice, it was decided that if the uncracked cylindrical test specimen diameter spanned approximately 15 grain diameters, then a homogeneous response would be obtained (Earle et al, 1984). For the same ice, but with cracked test pieces, it was proposed that the fabricated crack and ligament each be greater than approximately 15 grain diameters (Dempsey, 1991; Dempsey et al, 1991; Abdel-Tawab and Rodin, 1992). Significantly, for very much larger test sizes of this S2 freshwater ice (Bentley et al, 1989), the fracture toughness was found to have increased by approximately 50%.

For sea ice, theoretical estimates of the minimum notched specimen size necessary to observe homogeneity were revised from 1700 grain diameters (Abdel-Tawab and Rodin, 1992) down to 400 (Abdel-Tawab and Rodin, 1993). In this context, note that the ratio of specimen size to the average grain size in the experiments reported have ranged from 40 to 6000.

Inelasticity ahead of the crack tip may be caused by many reasons. Inelasticity is the cause of the size effect being milder than LEFM size effect. The fracture theory adopted must address the dominant cause producing this inelasticity. A detailed discussion follows in Section 6 regarding the ice fracture modelling.

Although many issues affect the fracture toughness of ice, only a few of them can be investigated if restricted to the testing of laboratory sized specimens. Factors such as notch acuity, ice temperature, salinity and notch sensitivity can be studied independently. However, material anisotropy, specimen size effects, and the true nature of strain localization during fracture can only be addressed by testing large sized specimens. In-situ testing also incorporates the actual temperature, grain size

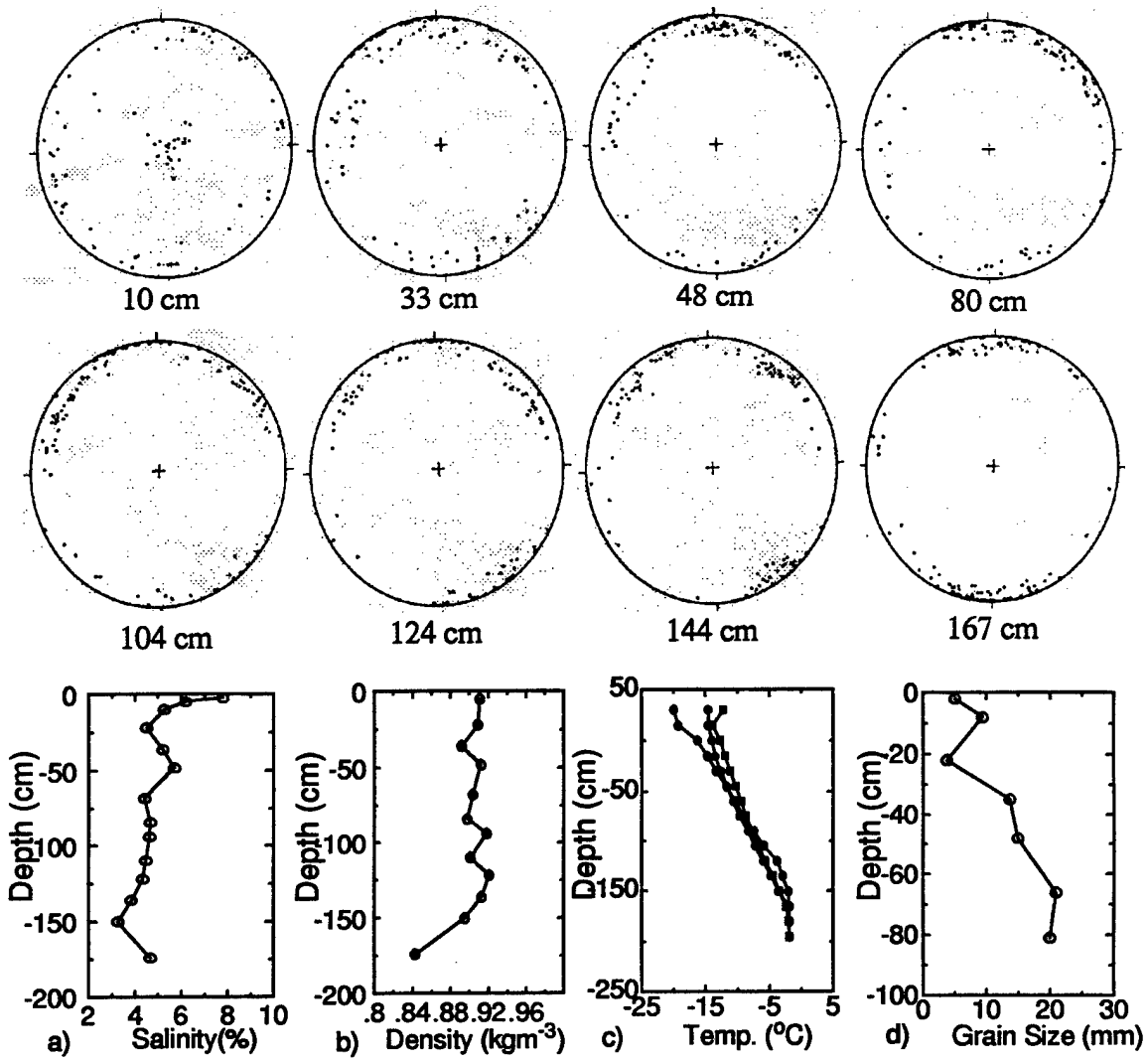

Figure 5.2: Schmidt Net plots for the ice at Resolute Bay

and salinity profiles through the thickness. Furthermore, the testing of ice at ice temperatures above –5°C is ideal in the field, but fraught with difficulties in the lab.

5.2 Site Description

The site chosen for the large scale sea ice experiments was Resolute, Northwest Territories in Canada. It was chosen primarily for the availability of logistical support and the growth of uniform, thick sea ice. The history of the temperatures, snow cover and average ice thickness in Resolute Bay served to indicate the most favorable

time period and location for testing. April 17 - May 8, 1993 was the chosen time frame for the experimental program and the testing area was established in Allen Bay, approximately 6 km from the lodge (Fig. 5.1). The ice was first year sea ice with a thickness of approximately 1.8 meters. The snow cover on the surface of the ice sheet ranged from 5cm to 40cm deep. Temperatures during the program typically remained between -15°C and -20°C. More details of the site and conditions can be found in Kennedy et al (1993).

5.3 Ice Characterization

Proper characterization of the ice being tested is a key element when testing any kind of ice. It is essential to realize its microstructural aspects to better explain its behavior under applied load. Because of time restrictions it was not feasible to do any microstructural work prior to the large scale testing. A tent was set up at the site where the tests were being done to eliminate transporting ice blocks to a cold room. Ice characterization and micrography were conducted at intervals through the thickness of the sheet. Approximately 14 horizontal thin sections were done specifically for grain size and orientation studies. Fig 5.2 shows eight of the Schmidt net plots at successive depths in the ice sheet. A slight c-axis alignment develops after the first 10cm. The average grain size is about 1.2cm for the first meter of ice. Lower in the ice sheet it was difficult to distinguish individual grains (Fig 5.2e). More details of the characterization and microstructure are given in the paper by Wei et al (1995).

5.4 Large-scale In-situ Fracture And Flexure Experiments

All large scale experiments were in-situ tests enabling the testing of large sizes with resident thermal profiles. Experiments were prepared by first cutting the sample free from the parent ice sheet using a R-100 DitchWitch equipped with special cutting teeth. It achieved cutting speeds of approximately 90 meters per hour, creating a slot about 15cm wide. Most of the slush created from the cutting remained in the slot

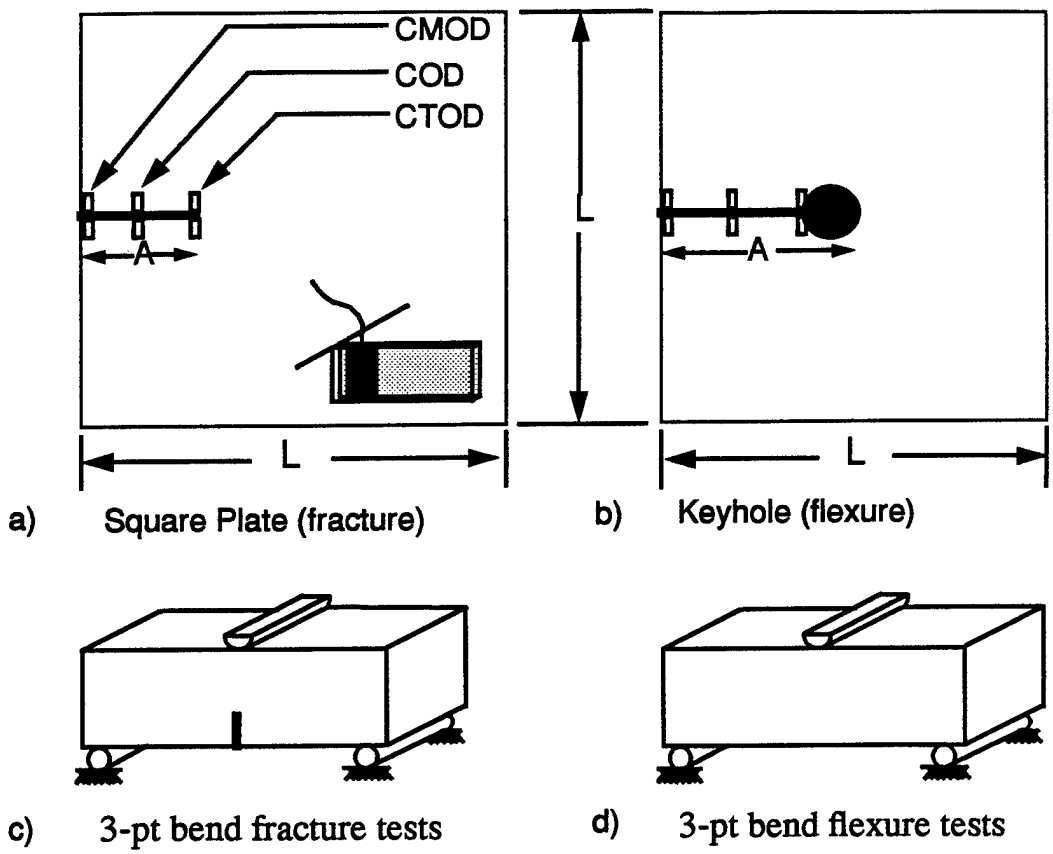

Figure 5.3: Geometries used for the in-situ sea ice experiments

and was removed to prevent refreezing. While conducting the in-situ ice experiments, it was critical to ensure the sample does not refreeze to the parent ice sheet, changing the boundary conditions of the experiment. A second smaller Ditchwitch was used to cut the crack in the specimens. This machine cut a notch 1.6 cm wide, enough to insert the loading device, the flatjack. Because it was a narrow cut, it had to be constantly cleaned to prevent refreezing.

Load was applied to the test sample using the flatjack loading device (Shapiro and Hoskins, 1978) inserted in the pre-cut crack. A flatjack is a thin walled steel bladder pressurized with either nitrogen gas or hydraulic fluid (Fig. 5.3c). Tests performed with nitrogen gas were controlled by varying the flow of gas from a pressurized tank

and generally resulted in unstable fracture. A servo-hydraulic control system was used on several of the in-situ experiments controlling the load via a feedback signal from a displacement measuring gauge on the crack. These experiments generally involved multiple loadings and stable crack propagation in the form of crack jumps and arrests. Displacement measuring devices, LVDT's and non-contacting sensors, were mounted at several points along the crack as shown in Fig. 5.3a. These locations are labeled CMOD, COD and CTOD for the crack mouth, intermediate crack and crack tip opening displacements, respectively. At each point, two displacement gauges were used, an LVDT and a KAMAN non-contacting displacement gauge. The KAMAN gauge had a finer resolution, but went out of range much earlier. As the crack opened, the KAMAN gauge would go out of range while the LVDT would continue measuring, providing a continuous record of the crack opening deformation. On smaller experiments, the crack was not long enough to permit mounting the COD gauge. On larger samples, it was possible to place a fourth set of displacement transducers between the COD and the CTOD, labelled as the NCTOD. The data from the displacement sensors and the pressure transducer were recorded digitally on two computers equipped with A/D converters. One computer was set up to provide real time viewing of the pressure and displacements as well as to record the data. The other computer was dedicated to data acquisition and sample rates up to 5 kHz were possible for 8 channels. Recording the data directly to the computer made it possible to do preliminary analysis and determine if any changes to the test plan were required.

5.4.1 Fracture experiments

The square plate geometry (Fig. 5.3a) was used for the fracture experiments. In Phase I, the RT geometry was used for its stability characteristics, but the square plate (SQ) actually required less cutting and was easier to lay out. In the field it is essential to reduce sample preparation in order to maximize test time. The sample

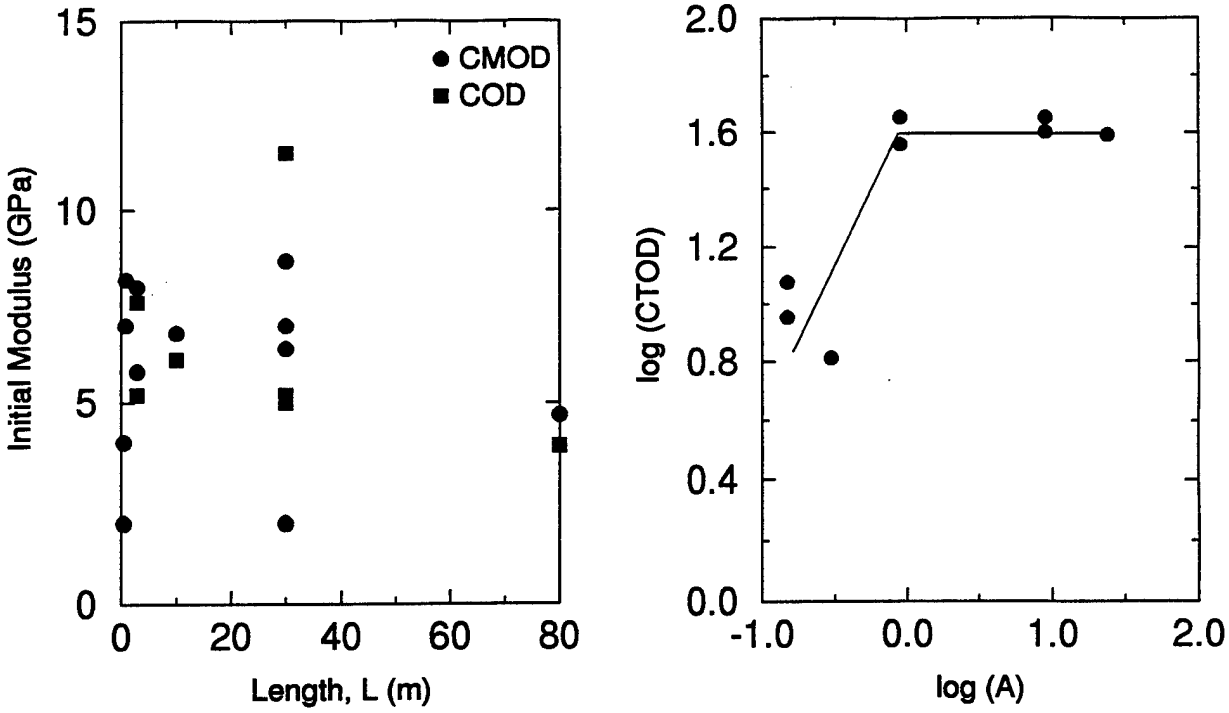

Figure 5.4: Effects of specimen size on a) Initial modulus and b) failure CTOD

Test ID	Length (m)	Crack Length (m)	K kPa$\sqrt{m}$/s	Control	E_{CMOD} GPa	E_{COD} GPa	$CTOD_f$ μm	Mean Ice Temp. °C
SQ1	1.0	0.3	0.48	Load	8.2	—	6.5	-9
SQ2	0.9	0.28	0.42	Load	7.0	—	—	-13
SQ3	10.0	3.0	0.45	Load	—	—	—	-13
SQ4	10.0	5.02	0.32	Load	6.8	6.1	—	-13
SQ5	30.0	9.0	0.21	Load	7.0	5.0	40	-13
SQ6	30.0	9.0	0.22	Load	6.4	5.2	35	-14
SQ7	30.0	9.0	0.46	Load	8.7	11.5	35	-15
SQ8	3.0	0.9	0.4	Load	8.0	7.6	36	-15
SQ9	3.0	0.9	5.14	CMOD	5.8	5.2	45	-3
SQ10	0.5	0.26	220	Load	2.0	—	9	-3
SQ11	30.0	9.0	1944	NCTOD	2.0	—	14	-14
SQ12	0.5	0.25	0.26	CMOD	4.0	—	12	-14
SQ13	80.0	24.0	0.17	Load	4.7	3.9	39	-12
SQ14	30.0	9.0	8.33	NCTOD	—	—	—	-12
SQ15	3.0	0.9	15.0	CMOD	—	—	—	-17
KH1	3.0	1.5		Load			N/A	-6
KH2	3.0	1.5		Load			N/A	-6

Table 5.1: Large Scale Sea Ice Experiments @ Resolute Bay

size was varied from 0.5m on a side to 80m, accomplishing the largest controlled

Depth in sheet (m)	Length m	Width m	Thickness (m)	Crack Length A (m)	Failure Load, P (N)	E_{CMOD} GPa	K_Q kPa$\sqrt{m}$	Ice Temp. °C
0.05	0.80	0.10	0.10	0.05	117.9	8.06	75	-14.8
0.05	0.80	0.10	0.10	0.05	91.7	5.25	77	-17.4
0.05	0.80	0.10	0.10	0.05	117.2	3.87	86	-18.0
0.15	0.80	0.10	0.10	0.05	121.4	4.21	77	-20.5
0.15	0.80	0.10	0.10	0.05	142.9	4.93	91	-20.4
0.20	0.80	0.10	0.10	0.05	96.6	5.51	83	-15.7
0.55	0.80	0.10	0.10	0.05	90.7	5.85	74	-18.2
0.71	0.80	0.10	0.10	0.05	82.6	4.36	64	-16.1
0.71	0.80	0.10	0.10	0.05	65.7	5.19	53	-16.8
1.05	0.80	0.10	0.10	0.05	80.0	6.45	66	-17.1
1.05	0.80	0.10	0.10	0.05	73.2	4.43	59	-16.8
1.22	0.80	0.10	0.10	0.05	77.9	5.12	69	-16.5
1.22	0.80	0.10	0.10	0.05	55.2	7.54	67	-17.7
1.40	0.80	0.10	0.10	0.05	83.7	4.58	72	-15.1
1.40	0.80	0.10	0.10	0.05	93.8	4.17	77	-16.7
1.40	0.80	0.10	0.10	0.05	110.6	4.90	90	-16.5
1.59	0.80	0.10	0.10	0.05	108.3	5.04	88	-15.9
1.59	0.80	0.10	0.10	0.05	79.5	4.32	64	-16.7
1.75	0.80	0.10	0.10	0.05	72.3	4.30	58	-14.7

Table 5.2: Small Scale Isothermal Sea Ice Experiments @ Resolute Bay

fracture test to date on any material (Table 5.1).

5.4.2 Flexure experiments

The testing of in-situ flexure beams (FL) proved to be a difficult task in Phase I. One flexure beam was tested in Phase II. The test was unsuccessful and required an excessive amount of preparation. It was found that test specimens using self-equilibrated loading (the RT on Phase I and the square plate on Phase II) were inherently easier to setup, minimizing the preparation time. This encouraged the use of the square plate keyhole geometry (KH) shown in Fig. 5.3b. This was a flexure test similar to the square plate fracture tests with a 20cm hole bored at the crack tip. The displacement gauges were placed at points on the crack, similar to the fracture tests. A finite element analysis of this geometry was done in order to obtain the tensile strength from these tests.

5.5 Small-scale Isothermal Fracture And Flexure Experiments

A complementary small-scale program was carried out during the large-scale testing (Williams et al, 1993). The three-point bend geometry (Fig. 5.3c and 5.3d) was used for both fracture and flexure experiments. Sixty fracture experiments as well as 42 flexure experiments were completed varying size, depth in the sheet and orientation. In this paper, only the fracture tests with the same orientation as the large scale experiments are investigated for comparative purposes. Most of the beams were machined to dimensions of 1.2m × 0.1m × 0.1m. The fracture tests were loaded at a rate of 200 kPa$\sqrt{\text{m}}$/s. The load and CMOD were recorded providing fracture toughness and modulus values for each of the fracture tests (Table 5.2).

5.6 Experimental Results

The experimental results are summarized in Table 5.1. Since the data covered such a large size range, the effect of size on the results provides tremendous insight to the size effects present in first year sea ice. Tangent moduli values were computed from the CMOD and COD records and are plotted vs. size in Fig. 5.4. A fair amount of scatter is evident in the results, an expected outcome from sea ice testing. No discernable trend in the modulus values is seen. The failure CTOD values, on the other hand, show a drastic change in behavior above crack lengths of 0.9m (or specimen sizes above 3m).

5.6.1 Fracture Toughness

The fracture toughness is a measure of a material's ability to resist fracture and is represented by the critical stress intensity factor, K_{IC}. The stress intensity factor for any cracked body can be written as:

$$K_I = f(a)\sigma\sqrt{\pi A} \tag{5.1}$$

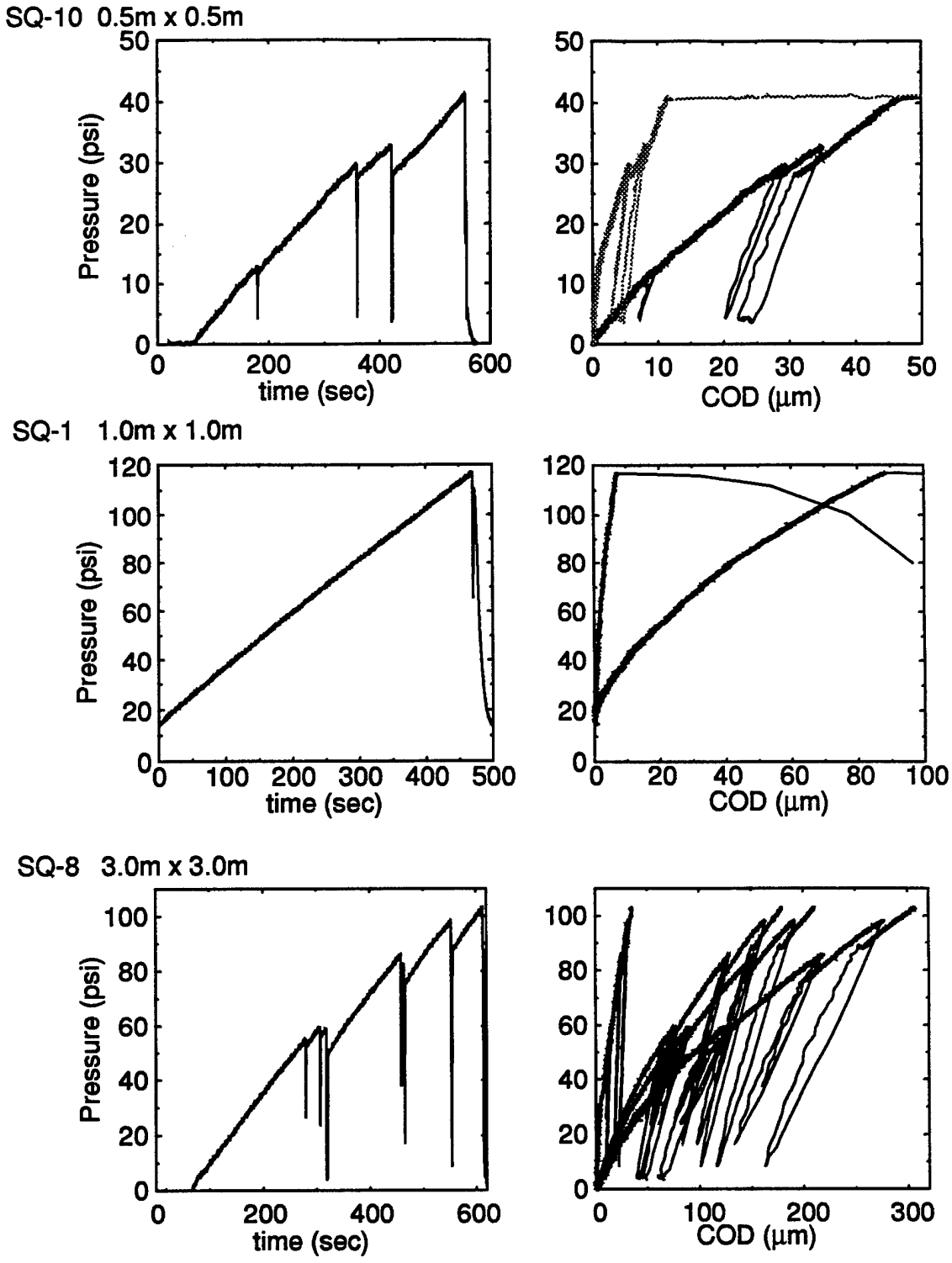

Figure 5.5: Load vs. time and load vs. COD plots for selected square plate experiments

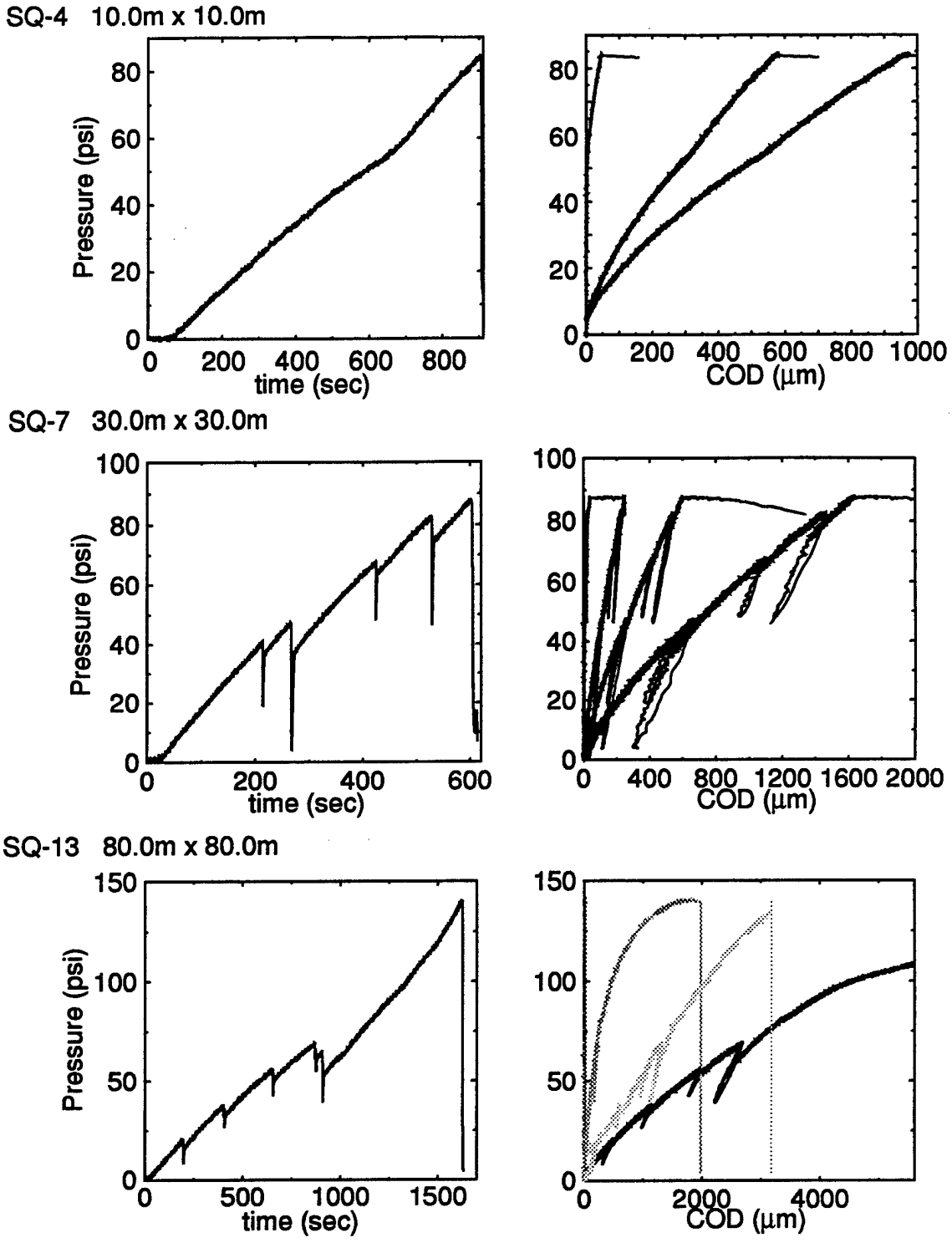

Figure 5.6: Load vs. time and load vs. COD plots for selected square plate experiments

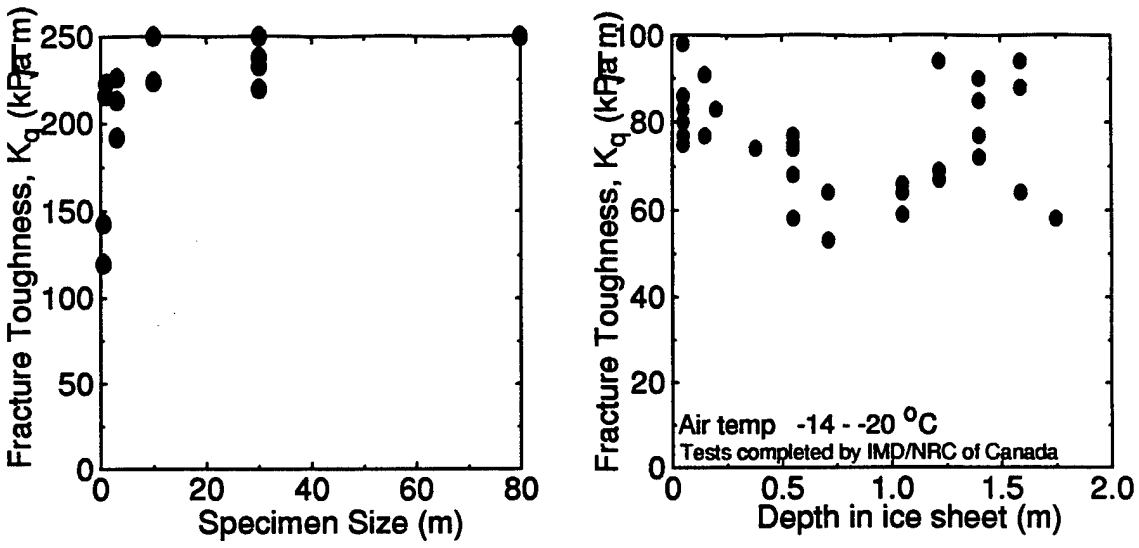

Figure 5.7: a) Apparent fracture toughness vs. size for in-situ experiments; b) Apparent fracture toughness vs. depth in sheet for isothermal small scale experiments

where f(a) is a non-dimensional function unique for each geometry and loading. The f(a) function for the square plate geometry subjected to uniform loading was obtained from Wu and Carlsson (1991). Further finite element work has been done at Clarkson University to obtain the linear elastic CMOD solution, V(a) for the square plate. Using the weight function technique as described by Wu and Carlsson, the stress intensity factor for the square plate subjected to the partial crack face loading applied by the flatjack was determined. Because of the uncertainties in applying LEFM to fracture testing of sea ice as alluded to earlier, $K_Q = K_{apparent}^{initiation}$ will be used throughout this paper to represent the apparent fracture toughness. Apparent fracture toughness values were computed from the load at the onset of cracking as determined from the CTOD gauge. The fracture toughness as a function of size is plotted in Fig. 5.7a and shows a rise in toughness with size and seems to approach a plateau K_Q value above a size of about 3m. This is indicative of softening mechanisms (grain boundary sliding, dislocations, microcracking) around the crack tip dominating the failure of the smaller samples with a transition to brittle failure at the larger sizes.

5.6.2 Non-Universal Scaling

If the crack growth were a similar process described by a law invariant with size, one could speculate on the existence of a universal fracture mechanism governed by either a constant fracture toughness or a constant material strength. As noted in the preceeding discussions, it is not the case with this S2 sea ice. S2 sea ice has two major length scales affecting its fracture behavior: ice thickness and grain size. The grain size relative to the other length scales appears to be the most influential scale. The average grain size for the ice was about 15 cm with crack lengths ranging from 0.14 to 8.98 m. To investigate the presence of non-universal scaling, the dependence of the CTOD at crack growth ($CTOD_f$) versus the pre-notched crack length (A) is plotted in Figure 5.4b. Fig. 5.4b reveals no change in scaling below 0.9m (L=3m). It appears that the scaling changes above A=0.9m and becomes invariant with size. These results are consistent with findings by Hatton et al (1994) in a study of fracture in the lava flows of the Krafla fissure swarm. This is also consistent with the K_Q results in Fig. 5.7a which seem to indicate a scale invariant fracture toughness above L=3m.

5.7 Analysis of Size Effect Laws

The nominal failure stress (derived from failure loads via a strength of materials approach by treating the crack as a notch) from fracture tests on self similar specimens of increasing size can be fitted to an equation that is a function of size. Bazant (1984) proposed such an equation, size effect law (SEL). The underlying analysis is similar to the fictitious crack model and provides for an increasing apparent fracture toughness which reaches a plateau at a certain specimen size. The form of the size effect law is such that it provides for a gradual transition from strength failures at small sizes to linear elastic fracture mechanics at large sizes. To get away from the self-similarity of the specimen as well as the failure processes, Carpinteri (1993) proposed a multifractal scaling law (MFSL). The multifractal scaling law has a mathematical form which predicts very high strength for small sizes while at large sizes the strength

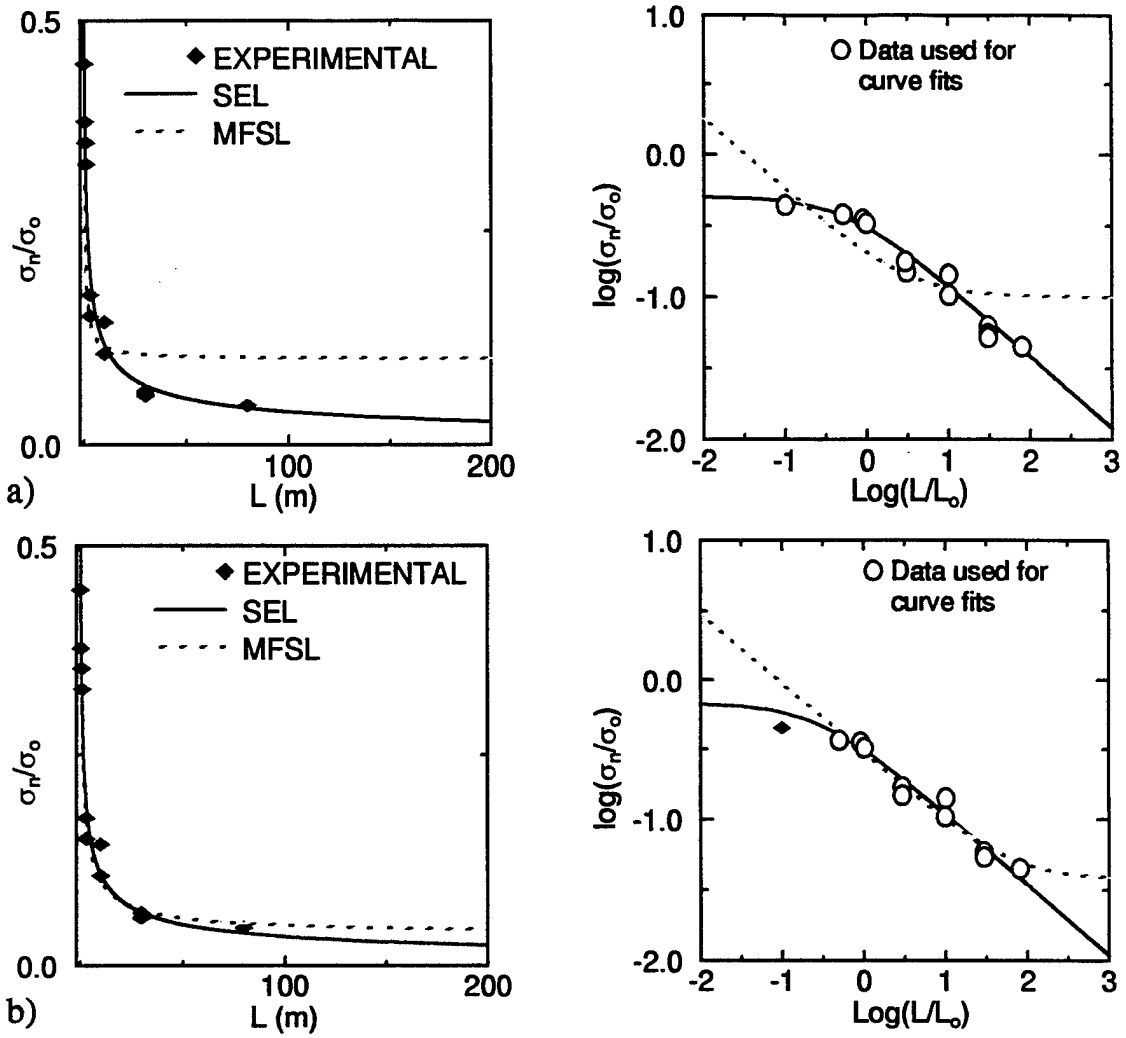

Figure 5.8: Normalized nominal stress at failure for in-situ fracture experiments: a) Curve fits using all data and b) Curve fits using only the large-scale data

reaches a size independent constant value. The advantage of using the size effect laws is that reasonable estimates of fracture properties like fracture energy can be obtained without complicated analysis. The largest known size range of fracture specimens tested makes it possible to assess the dependence and variability of the fitted parameters on the size range used for calibration of size effct laws. Of interest is the accuracy of the size effect laws outside their range of calibration.

The forms of the size effect laws are given below.

$$\sigma_n = \frac{A}{(1 + L/B)^{1/2}} \qquad \text{BZ} \tag{5.2}$$

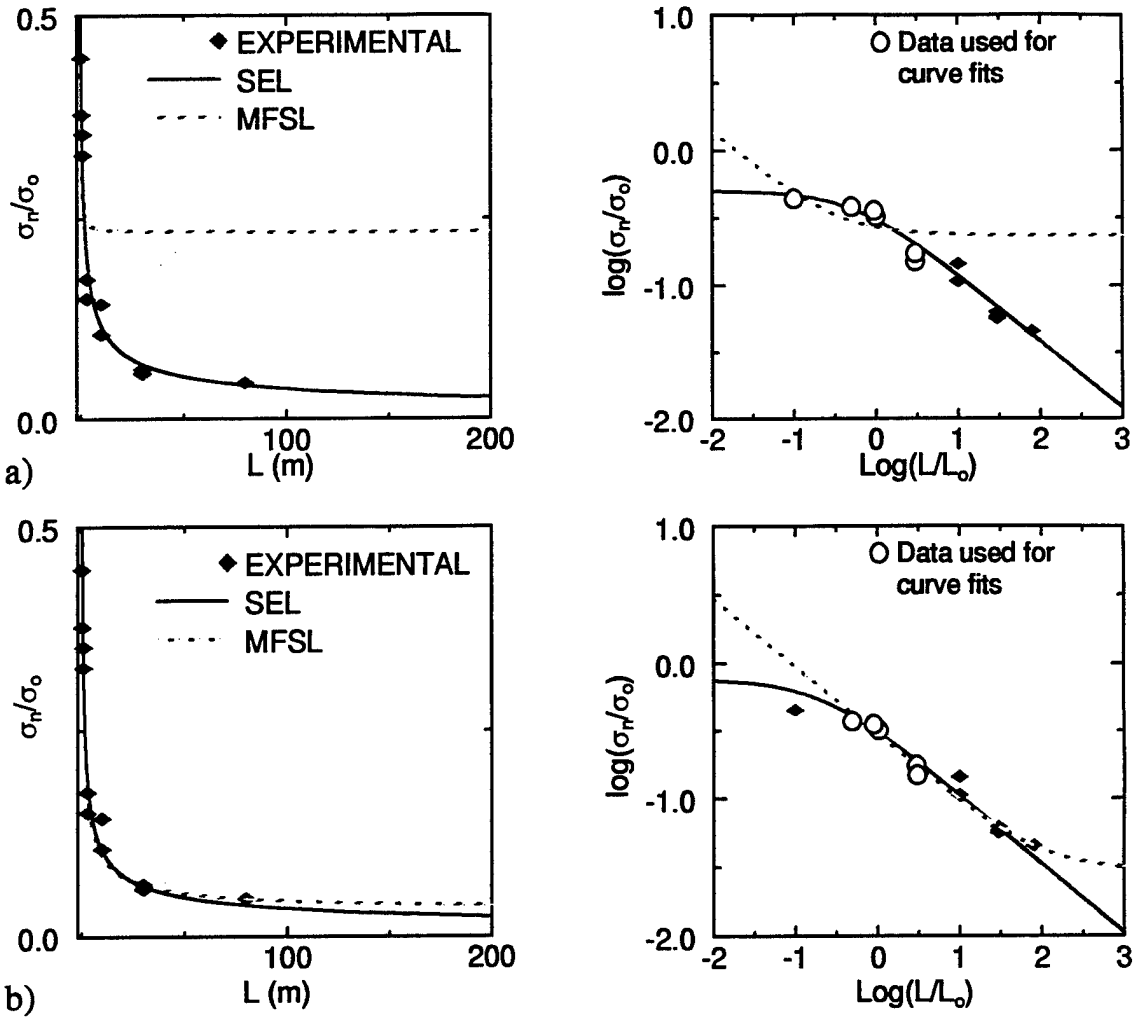

Figure 5.9: Normalized nominal stress at failure for in-situ fracture experiments: a) Curve fits using 0.1 - 3m data and b) Curve fits using 0.5 - 3m data.

$$\sigma_n = C(1+10^B/L)^{1/2} \qquad \text{MFSL} \tag{5.3}$$

(5.4)

Size effect laws were fitted to the entire size range on which tests were performed as well as various subranges of the data. The average nominal failure stress obtained from the small scale fracture tests shown in Table 5.2 was also included extending the size range studied to 0.1m - 80m. The undetermined constants were determined by using Tablecurve (an automated nonlinear curve fitting program that uses 64-bit Levenburg-Marquardt algorithm). The size range and the constants are tabulated in

Table 5.3: Size Effect Laws

FIT	RANGE (m)	LAW	A MPa	B (m)	C MPa
FIT1	0.1–80	BZ MFSL	0.50 -	0.56 0.50	- 0.10
FIT2	0.5–80	BZ MFSL	0.68 -	0.26 1.80	- 0.04
FIT3	0.1–3	BZ MFSL	0.50 -	0.56 -0.47	- 0.23
FIT4	0.5–3	BZ MFSL	0.76 -	0.19 1.97	- 0.03

Table 5.3.

The curve fits are plotted along with the data in Fig. 5.8a,b and Fig. 5.9a,b. FIT1 (Fig. 5.8a) covers the complete size range of the data. While the SEL covers the data with acceptable accuracy, the MFSL does not. The MFSL is strongly influenced by the small scale data at 0.1 m. Removing this data point makes MFSL achieve same accuracy as that of SEL in FIT2 (Fig. 5.8b). It is difficult in practice to perform tests over such a wide range, however sizes up to 3 m can be tested in basins. Hence FIT3 was restricted to 0.1 m to 3 m size range (Fig. 5.9a). It can be seen that changing the range of calibration changes the values of the undetermined constants. Especially from FIT1 and FIT2 of SEL, it can be seen that increasing the minimum size in the size range tested increases the value of constant A, which represents the tensile strength in the limit of small scale. Though the parameters are seen to change considerably, the accuracy of the predicted response outside the

range of calibration is within the scatter of experimental results. The MFSL law again suffers because its mathematical structure predicts infinite strength in the limit of zero size. Removing the smallest size of 0.1 m as in FIT4 (Fig. 5.9b), removes this problem. From the data, it can be seen that the transition from predominantly strength to predominantly fracture dominated failures occurs in the size range up to 3m. However this can only be seen from the experimental data. If the tests are conducted on smaller physical sizes and size effect law is calibrated on this range, the conclusions may not be accurate.

5.8 Conclusion

Preliminary analyses for the large-scale fracture tests from Phase II is presented. For Phase II (columnar S2 sea ice), the inclusion of bulk viscoelastic deformation has been found to be essential for proper numerical analysis. Various available size effect laws have been compared. The behavior of these laws over portions of the available size range was examined to study the effect of change in size range as well as change of the absolute sizes. The predictive capability of the size effects laws was shown to be rather fickle. By examining the various size effect laws in Fig. 5.8 outside of the data range for which they were calibrated, a large difference is seen. This difference is imposed by the mathematical structure of the laws which have been constructed on the basis of specific beliefs. If a larger size range than what has been tested were to become available then all the size effect laws would again span this larger size range in the same fashion as Fig. 5.8a with the same order of disagreement in the extrapolated region. Future research on this topic does not lie within the proposition of various curve fit or size effect laws such as those just examined. There is a clear need for a quantitative basis to the predicted size effects. The latter basis will reside with approaches reflective of the true material behavior.

6 A PNEUMATIC LOADING SYSTEM FOR FIELD TESTING*

6.1 Introduction

This chapter presents the design and implementation of a closed loop servo controlled field loading system. The system was used in the arctic to test large in-situ plates of sea ice in order to determine the mechanical behavior of sea ice sheets subjected to various loading sequences (Adamson et al, 1995).

In order to track the seasonal evolution of the mechanical and physical properties of first year sea ice, three field trips were conducted at Barrow, Alaska: November 9–19, 1993, March 9–20 and May 8–19 of 1994. This was a joint field trip with members of the group from Clarkson University, CRREL, and the University of Alaska at Fairbanks (UAF). A total of thirty large scale tests were completed covering a wide range of sizes, temperature profiles, and loading paths. Each set involved a large scale in-situ (full ice thickness) matrix of experiments and a complementary small scale (partial thickness) matrix of experiments. An additional large scale program was completed in April of 1994 where experiments on lead ice and a multi-year floe were carried out. When going to such lengths to prepare a large ice sample, it is of utmost importance to extract as much quantitative information from the sample before final failure.

Ice exhibits two unique features that make such a project feasible: it grows to very large sizes in nature and it floats. Large sheets of freshwater ice are readily available in any area where the climate in conducive to ice growth on lakes and rivers and an abundance of sea ice is available in the polar regions. Because the testing must be completed in-situ, the accessibility of the test sites is restricted to a degree. This necessitates the design and fabrication of portable testing systems that can

*To be submitted to the *ASCE Journal of Cold Regions Engineering* (Adamson and Dempsey, 1996)

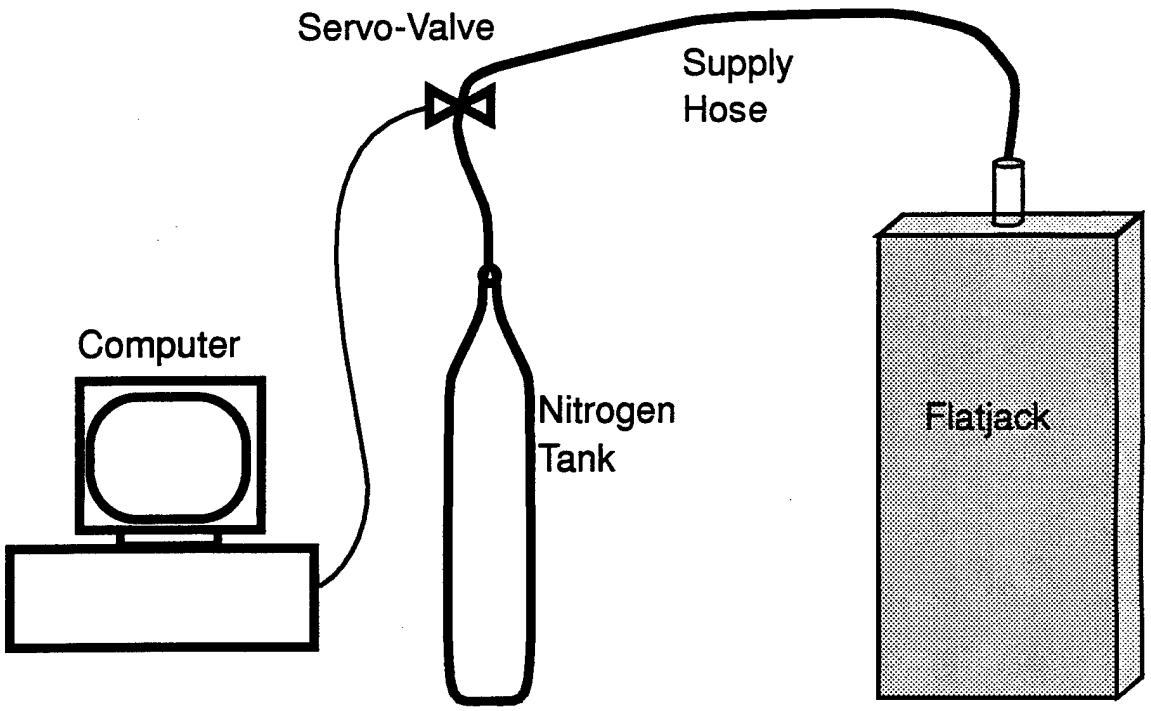

Figure 6.1: Schematic showing the components of the loading apparatus

be flown or transported by vehicle to the site. The design must be simple enough to reduce the chance of malfunction yet sophisticated enough as not to restrict the goals of the project. These factors were taken into account when making the servo-pneumatic computer controlled loading device used to obtain constitutive and fracture information for arctic sea ice.

6.2 Servo-pneumatic Loading System

The system was designed to minimize the required equipment and maximize the systems performance. The basic components of the system included: a 486 computer equipped with analog input and output capabilities, a servo-valve, a nitrogen pressure supply and a flatjack loading device. Fig. 6.1 shows a schematic of the assembly of the field testing system. High pressure air lines (1/4in inside diameter) were used to connect the supply tank, servo-valve and flatjack.

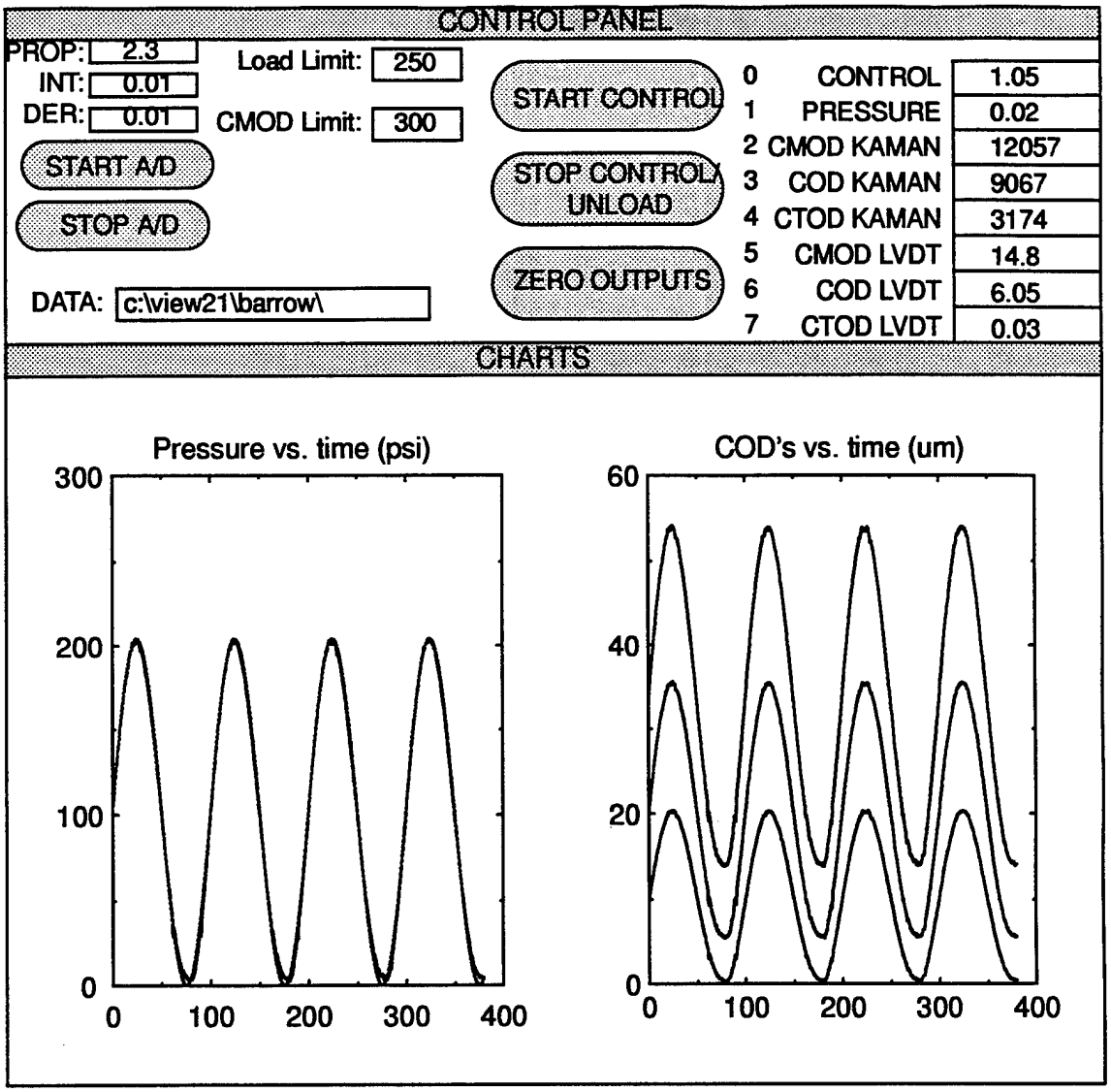

Figure 6.2: View of control panel and monitoring charts as seen on the monitor

6.2.1 Closed Loop Computer Control

The computer system was a standard 486 PC equipped with an 8 channel differential ended analog to digital (A to D) board. The board also had two analog outputs. The typical field data consisted of one pressure measurement and six displacement measurements. These transducers were connected to channels 1 through 7 on the A to D board. The transducer that was to be used for controlling the experiment, called the feedback signal, be it load or displacement, was connected to both channel 0 and the channel to which it was typically connected. For the sake of simplicity, channel 0 was

always used for control avoiding changes in the software setup. Data acquisition and control were done through the VIEWDAC software, a Keithley Metrabyte product. All channels of data were brought into the computer at 50 Hz and were recorded to a file in ASCII format at 10Hz. The data acquisition system on this computer only served as a backup to two other higher speed systems. Its main function was to control the test and provide real time viewing of the load and displacement transducers via scrolling strip charts on the monitor. Fig. 6.2 shows the interactive Viewdac control panel as seen on the monitor. Through this panel, data logging to the harddrive was controlled, servo control was started and stopped, and the pressure and displacements were viewed in real time. This provided an immediate indication of the status of the experiment.

To control the test, a desired waveform (monotonic ramp, cyclic) for the load or displacement feedback signal to follow was created. The PID (Proportional Integral Derivative) algorithm was used to monitor the feedback signal, compare it with the desired waveform (setpoint) and output the controlling signal to the servo valve. The PID control function has the following form:

$$O(t) = Pe(t) + \int_0^t I(t')e(t')dt' + D\frac{de(t)}{dt} \tag{6.1}$$

where

$e(t) = s - y(t)$ is the error term

s is the setpoint (desired waveform)

$y(t)$ is the actual transducer response (feeback signal)

P is the proportional gain coefficient

$I(t')$ is the integral coefficient at time t'

D is the derivative coefficient

For the purposes of our testing it was sufficient to keep the $I(t')$ and D coefficients low and vary the P coefficient to optimize the system response. The servo valve operated over a -5 to 5 volt range. At -5 volts, the system would be fully open to

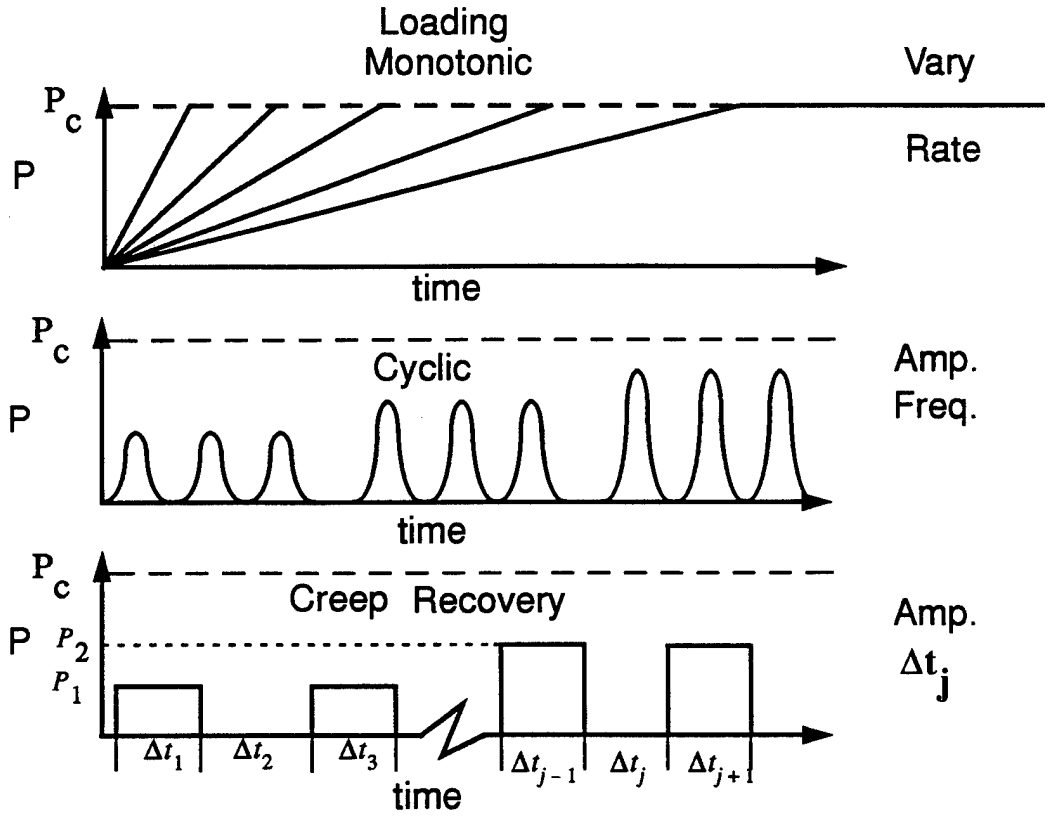

Figure 6.3: Schematic showing monotonic, cyclic and creep recovery loadings applied with the loading device

discharge air pressure; at 0 volts status quo was maintained; and at +5 volts, pressure in the system would be increased at a maximum rate. If the response of the system indicated that the pressure needed to be increased to follow the specified waveform, a positive voltage was applied to the servo controller. The controller was sent updated information at a rate of 50 Hz. Now, although this is decades slower than a servo-hydraulic laboratory test frame, it was sufficient for the loading sequences performed. The desired waveform was plotted in real time with the controlling transducer on the strip chart to monitor the controlling capabilities of the system.

6.2.2 Pneumatic Servo Valve

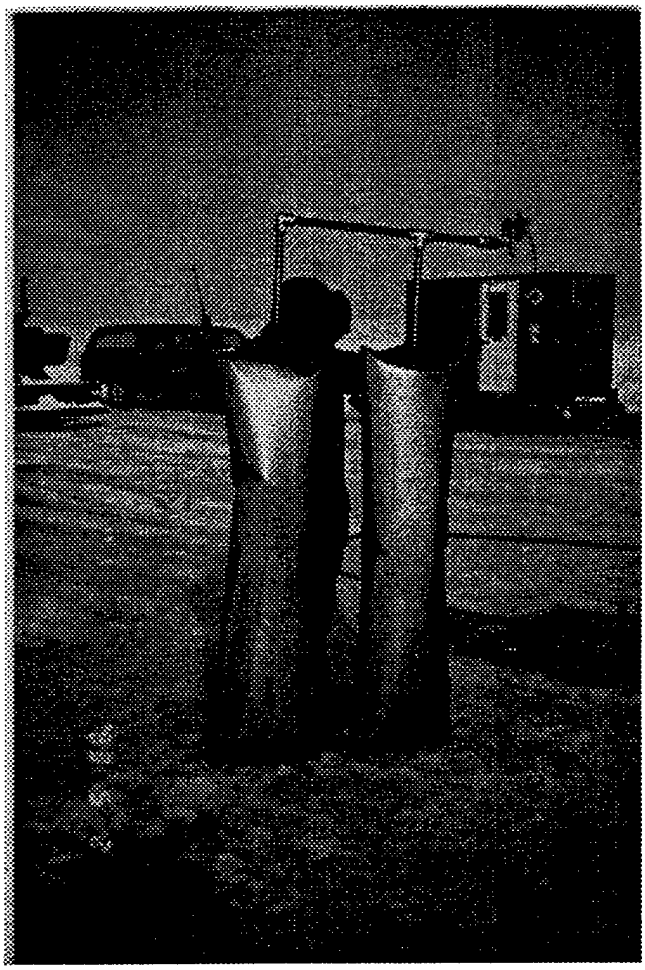

Figure 6.4: Two 0.45m x 1.5m long flatjacks used to load 1.8m thick first year sea ice

The system was controlled via a 1000 psi max working pressure, 4 port, pneumatic servo valve. Since this system had only one supply line to the flatjack, only 3 ports of the valve were used; input from pressure supply, output to flatjack and a vent to the atmosphere. The position of the servo valve was controlled by a control amplifier. As mentioned above, it would interpret an analog signal sent from the computer to position the valve. Fig. 6.3 shows the various loading sequences applied to the ice in an effort to elucidate some constitutive information needed for modeling purposes. To control unloading as was necessary for the cyclic and creep recovery sequences, the rate at which the pressure was released from the flatjack was controlled through the servo valve. Since the unloading was limited by the flow rate of air through the fully open servo valve, cyclic loadings faster than 0.2 Hz were unable to be completed.

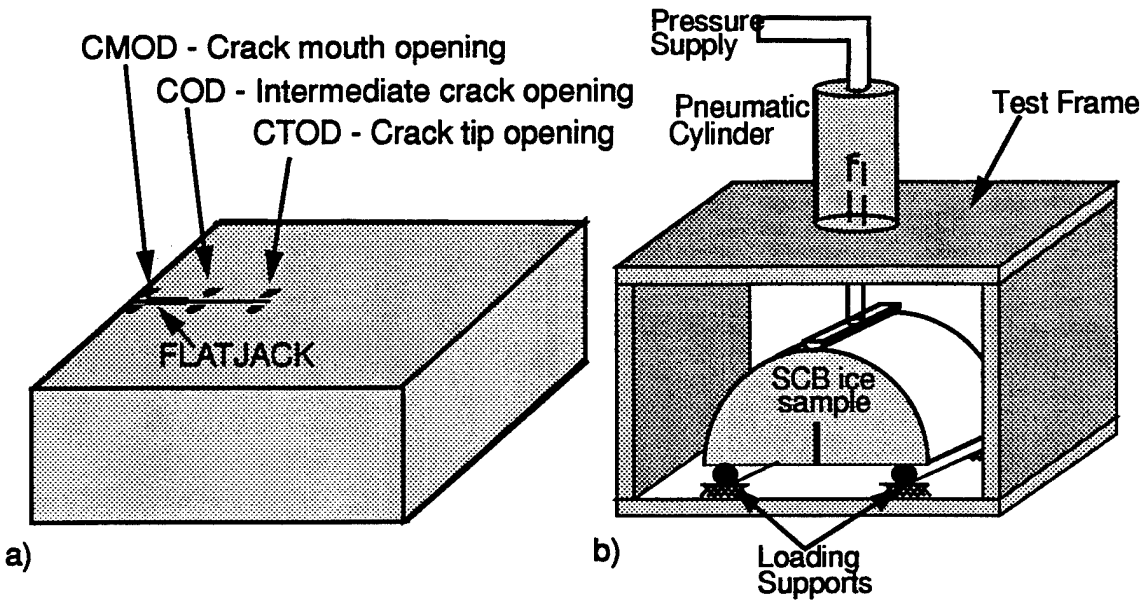

Figure 6.5: Experimental setups: a) Large scale square plate fracture tests; b) small scale SCB experiments

This could be increased if a vacuum pump was attached to the vent port of the servo valve. To attain frequencies above 1 Hz, more sophisticated equipment is necessary; for the purposes of the sea ice experiments, this system was sufficient.

6.2.3 Pressure Supply

Bottles of compressed nitrogen gas were used to supply the pneumatic pressure. A pressure regulator maintained a constant pressure delivery to the servo valve. Considering the nitrogen tank was pressurized to about 3000 psi and typical system pressures never exceeded 150 psi, the bottle was capable of servicing several experiments, even when cyclic loading sequences were applied. Bottled nitrogen gas was chosen over an air compressor for two reasons. First, because of the fine ports and mechanisms of the servo valve, it was necessary to provide a very clean air. It was also a guaranteed supply of air that could not malfunction. Even in the remote locations where we tested, the bottles were available.

6.2.4 Flatjack Loading Device

Pressure was applied to the ice through a thin-walled steel bladder called a flatjack (Hoskins and Shapiro, 1975) (fabricated by Sandwell, Inc.). The flatjack is made of two very thin steel sheets welded together at the edges with an inlet fitting at the top to which the pressure supply was attached. It is air tight and can expand to about 8cm. Different sized flatjacks were used depending upon the dimensions of the experiment. Each flatjack of differing size had to be calibrated individually to determine its efficiency. All of the flatjacks had linear calibration curves for low displacements (<0.7cm) and therefore only a single efficiency value (γ) was required for each flatjack. The following equation is used to convert the flatjack pressure to the actual applied pressure:

$$\sigma_{ice} = \gamma \sigma_{fj} \tag{6.2}$$

Fig. 6.4 shows a typical flatjack used for the in-situ sea ice experiments. The length of the flatjack was usually about 3/4 of the ice thickness. It was designed this way because the sea ice near the bottom of the sheet is very soft and offers very little resistance to load. If the flatjack were to extend the full depth of the sheet, it would balloon out at the bottom and tend to pull the flatjack down through the ice.

6.2.5 Small-Scale Testing Device

To provide a link from the small-scale results to the large-scale, it was imperative that a set of small-scale isothermal field tests be completed. These tests used the same computer controlled system with a 3-point bending device replacing the flatjack. The air line was attached to a pneumatic cylinder (Fig. 6.5) which would apply pressure to the top of a semi-circular bend (SCB) (Adamson et al, 1995) fracture sample of sea ice. The sample was easily fabricated from a core taken from the ice sheet. With this setup, similar loading scenarios as applied to the larger tests could be repeated for the isothermal small scale (0.1m) tests.

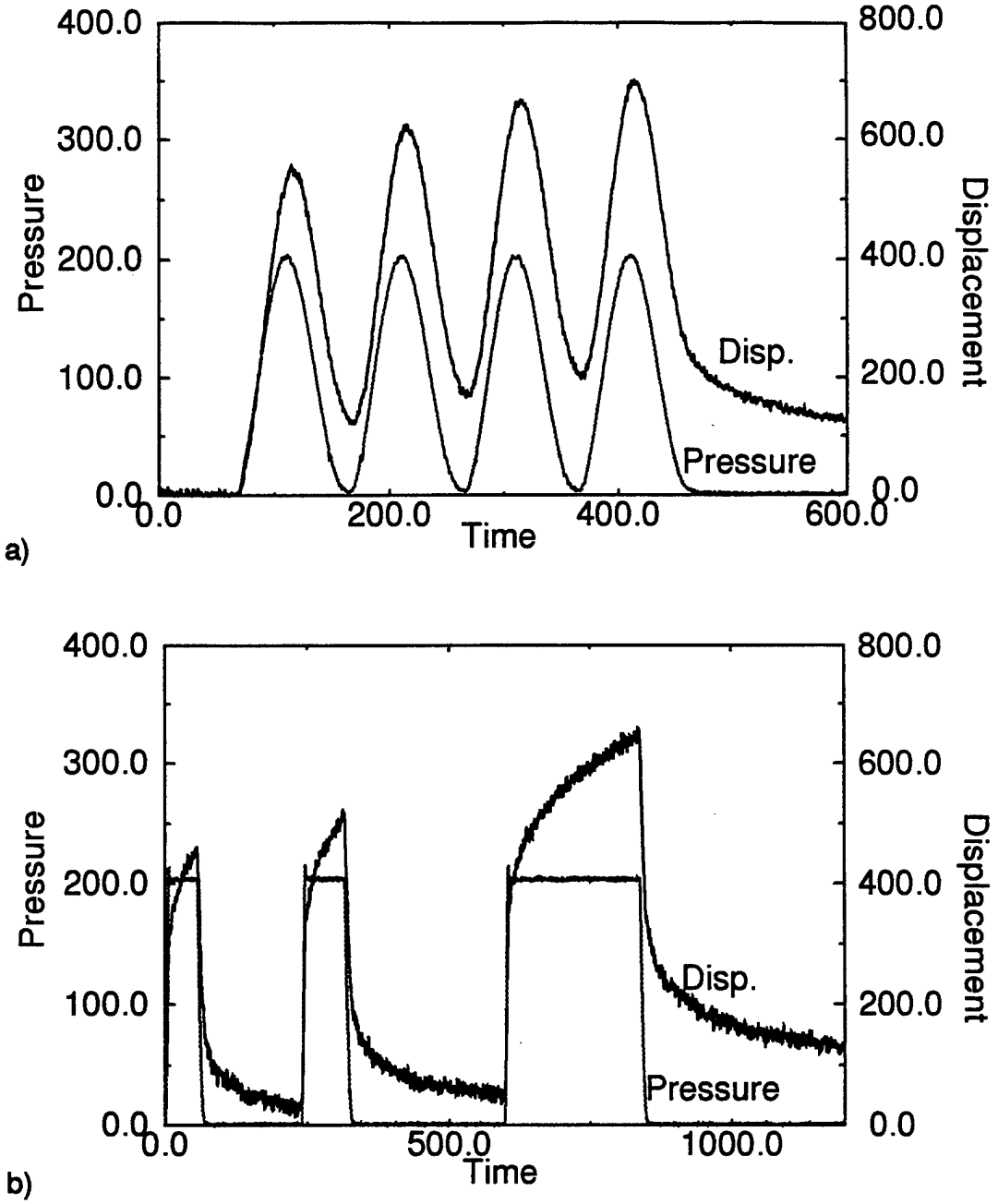

Figure 6.6: Results from the field tests on first year sea ice a) cyclic loading; b) creep recovery sequences.

6.3 Results

About 40 large scale in-situ tests were successfully completed using this system. Cyclic, creep recovery, and monotonic sequences were applied to many of the experiments, several using the CMOD gauge for control. Figures 6.6 show load and

displacement results from applied cyclic and creep recovery loadings. Very smooth load cycles can be seen, showing the system's ability to follow a prescribed load path. Details of the experiments completed are provided in Adamson et al (1995).

6.4 Conclusions

The design and application of a closed loop computer controlled field testing system is presented. Its ability to control both load and displacement and follow virtually any prescribed loading path enables one to extract an abundance of information from a single field experiment. This system provided the ability to apply loading sequences previously limited to lab experiments using hydraulic test frames. The sea ice behavior at the large scale can now be compared in detail to its behavior under laboratory conditions.

7 THE CREEP BEHAVIOR OF FIRST YEAR SEA ICE*

7.1 Introduction

In 1993 and 1994, a three part test program was undertaken as part of the Sea Ice Mechanics Initiative (SIMI). The program was designed to investigate the fracture and constitutive properties of sea ice and to see how these properties changed through the growth season. Consequently, the field trips were made in November, March and May where the ice was 0.3, 1.38 and 1.77m thick, respectively. Changes in temperature and salinity profiles were recorded and are provided in Cole et al (1995).

In May, the ice sheet was at a rather unique stage for testing purposes having reached its maximum thickness and exhibiting almost a vertical temperature profile. In most laboratory settings it is almost impossible to test ice this close to its melting point ($\geq -5°C$). This prompted the desire to extract as much constitutive information from the fracture experiments as possible. To this end, loading sequences (creep recovery, cyclic, monotonic ramps) below the failure loads were applied prior to complete fracture of the sample. The creep recovery sequences analyzed in this paper were applied following the recommendation from Schapery. From these loadings, the viscoelastic nature of the ice can be explored, determining the stress and time dependence as well as the extent to which the different strain components (ie, elastic, delayed elastic, viscous) contribute to the overall deformation.

The creep of saline and sea ice has been investigated experimentally by Sinha (1992) and Cole (1993). The purpose of our investigations of the creep behavior of sea ice is to elucidate the effects that creep has on the failure loads and deformations in order to develop a failure criterion for fracture modeling. The immediate objective of the creep studies has been to determine the effects of temperature, strain rate and

*To be submitted for publication in the *International Journal of Fracture* (Adamson and Dempsey, 1996)

stress levels on the creep components (primary and steady state) present in the ice. Subsequently, the purpose is to link these results with fracture information to build a comprehensive data set capable of verifying creep based fracture models. The recent PhD thesis by Abdel-Tawab (1995) provides a comprehensive and recent servey of the constitutive modeling literature for sea ice. A review of Abdel-Tawab's model is provided by Schapery (1996) in which clear evidence was provided as to the advantages of a nonlinear viscoelastic characterization. LeClair et al (1996a) augmented this evidence with further analysis using nonlinear viscoelastic characterization of S2 lab-grown saline ice subjected to a uniform stress field. The formulation suggested therein is here applied to the Phase VI experiments.

This chapter presents the experimental results and subsequent analysis of creep recovery and cyclic loading measurements recorded on Phase VI of the Sea Ice Mechanics Initiative (SIMI) project at Barrow, Alaska. This was part 3 of a 3 trip program to track the seasonal evolution of the mechanical and physical properties of first year S2 sea ice. This was a joint field trip with members of the group from Clarkson University, CRREL, and the University of Alaska at Fairbanks (UAF). Seven large-scale in-situ experiments were completed covering a size range of 1:30 with the largest test having dimensions of 30m$\times$30m. Through recommendations from David Cole (CRREL) and Richard Schapery (U of Texas at Austin) sequences of cyclic and creep recovery loadings were applied to each sample before final fracture. The strain response from the creep and recovery loadings is examined in this paper to determine the coefficients and time and stress dependence in a non-linear viscoelastic model developed by Schapery (1969, 1996). This model is then applied to the cyclic response to quantify its ability to predict behavior for a variety of loading paths.

7.2 Experimental Program

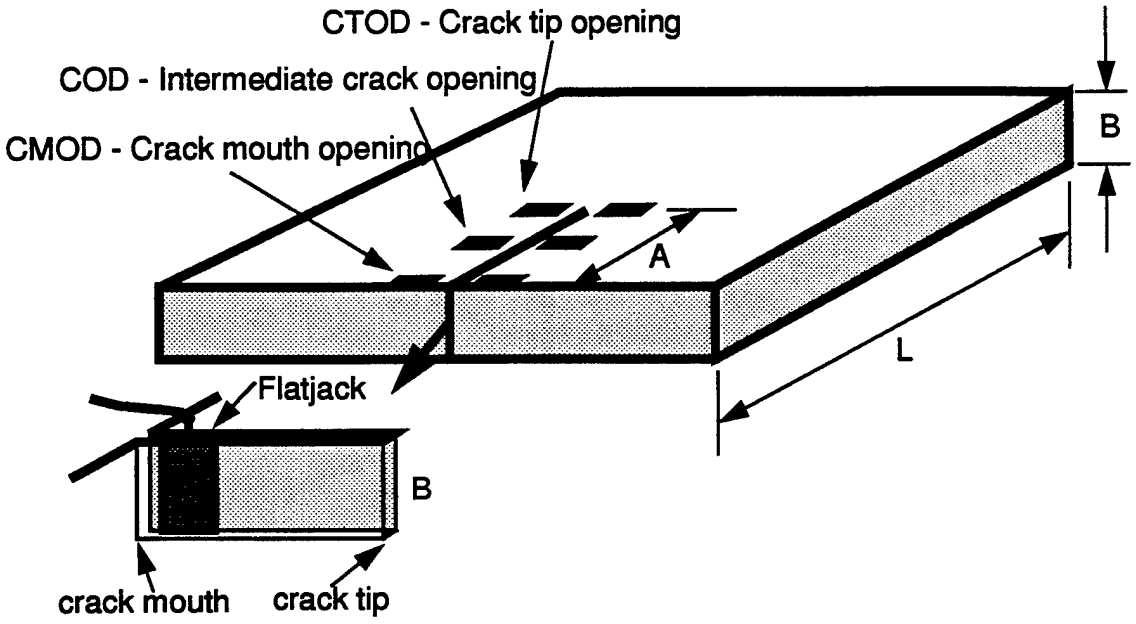

Figure 7.1: Square plate geometry showing loading configuration and crack opening measuring locations

7.2.1 Sample Preparation and Testing Procedure

The experimental portion of this program was completed in Elson Lagoon near Barrow, Alaska (Adamson et al, 1995; Cole et al, 1995). Elson Lagoon is separated from the Chukchi Sea by a narrow strip of land yet the tidal activity of the sea still affected the lagoon, causing under ice currents. These currents caused an alignment of the grains (Weeks and Gow, 1979) which, in turn, had a significant effect on the behavior of the ice (parallel versus perpendicular to the alignment). The effects of the alignment are discussed in papers by Adamson et al (1996), LeClaire et al (1996b) and Cole et al (1996).

The large scale experiments completed in the lagoon were in-situ, thus enabling the testing of large sizes with resident thermal profiles. The experiments were prepared by first cutting the sample free from the parent ice sheet using a specially designed cutting device for the smaller tests and a ditchwitch for the large experiments. Most of the slush created by cutting the sample free remained in the slot and was removed to prevent refreezing. When conducting these in-situ ice experiments, it was critical to

prevent the sample from refreezing to the parent ice sheet as it changes the boundary conditions of the experiment for analysis considerations and could jeopardize the success of the test. The special cutting device was also used to prenotch the fracture samples. The typical geometry used for the in-situ experiments was the square plate (Fig. 7.1). On the first trip the square plate geometry was found to be insufficient when trying the propagate the crack parallel to the c-axis (typically the direction of the current flow). A strength failure would occur with the crack propagating along the basal plane, the plane perpendicular to the c-axis, also called the easy-fail direction, rather than along the c-axis of the grains. For tests with the crack parallel to the c-axis, the geometry was modified to a rectangular plate.

Load was applied to the test sample using a flatjack loading device (Shapiro and Hoskins, 1978) inserted in the pre-cut crack. The flatjack is a thin walled steel bladder pressurized with nitrogen gas (Fig. 7.1). A closed-loop computer controlled system was used to control the pressure in the flatjack. The computer was used to monitor the feedback signal from the controlling transducer and send a command signal to the servo-valve (Adamson and Dempsey, 1996). The servo-valve regulated the nitrogen gas pressure in the loading system. This system could operate using load or displacement control and apply virtually any desired load sequence.

Displacement measuring devices, LVDT's and non-contacting sensors, were mounted at several points along the crack as shown in Fig. 7.1. These locations are labeled CMOD, COD and CTOD for the crack mouth, intermediate crack and crack tip opening displacements, respectively. At each point, two displacement gauges were used, an LVDT and a KAMAN non-contacting displacement gauge. The KAMAN gauge had a finer resolution, but went out of range much earlier. As the crack opened, the KAMAN gauge would go out of range while the LVDT would continue measuring, providing a continuous record of the crack opening deformation. On smaller experiments, the crack was not long enough to permit mounting the COD gauge. On larger samples, it was possible to place a fourth set of displacement transducers between the

COD and the CTOD, labelled as the NCTOD.

The data from the displacement sensors and the pressure transducer were recorded digitally on two computers equipped with A/D converters. One computer was set up to provide real time viewing of the pressure and displacements as well as record the data. The other computer was dedicated to data acquisition and sample rates up to 5 kHz were possible for 8 channels. Recording the data directly to the computer made it possible to do preliminary analysis and determine if any changes to the test plan were required. A digital DAT recorder was used to record all data directly to tape at 6 kHz. This method ensured no loss of experimental data.

7.2.2 Sea Ice Characterization

As mentioned earlier, an in depth microstructural analysis of the S2 sea ice from the three field trips was carried out by Cole and Weeks and is presented in the paper by Cole et al (1995). Salinity and temperature profiles are given in the paper for the ice sheet as it developed through the season. Additional investigations of the grain size, platelet spacing, bulk density and total porosity given in Cole et al (1995) are provided for the May trip (Phase VI). Horizontal micrographs of the ice show the strong c-axis alignment of the grains. As was determined by the large scale experiments, the alignment of the grains has an extremely strong influence on the direction of crack propagation.

7.3 Experimental Results

A detailed look at the creep recovery sequences is provided in this paper. The cyclic sequences were completed as part of a study of the anelastic behavior of first year sea ice. The cyclic responses are examined here to show the ability of the non-linear viscoelastic model to predict the strain behavior for different loadings.

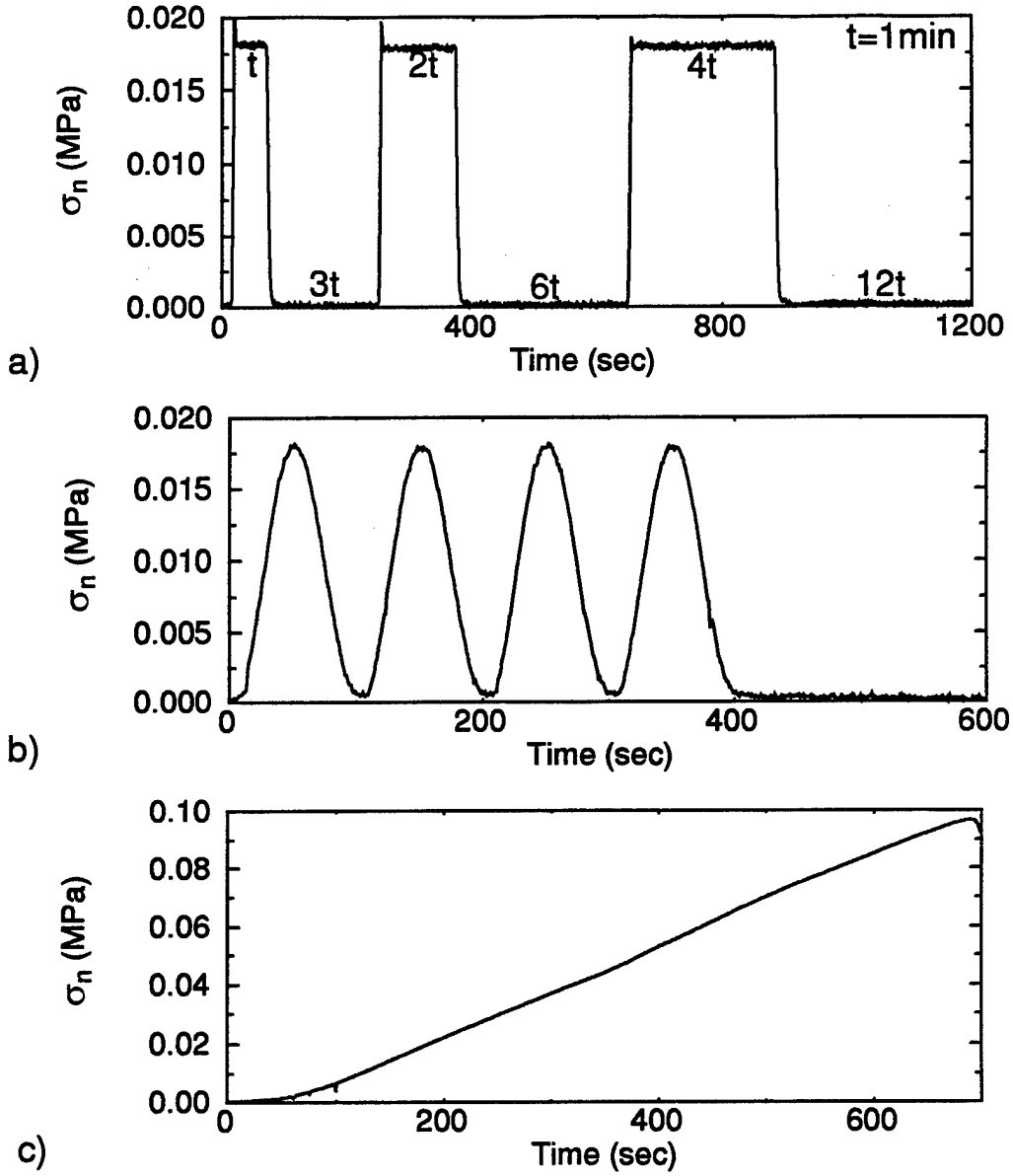

Figure 7.2: Loading sequences applied to each sample before final fracture: a) creep recovery; b) cyclic and c) monotonic.

7.3.1 Creep Recovery Experiments

Typically, the experiment was started by first applying a low level, low frequency (0.01 Hz) cyclic loading to ensure all gauges were operating properly. Since one computer was set up with real time viewing of the pressure and displacements, the gauge response was determined immediately. When all was working properly and measureable displacement responses were seen, creep recovery sequences were applied.

This consisted of three load and holds at the same load level, each separated by a recovery period three times the prior loading time. Each load application was twice as long as the previous loading (Fig. 7.2). For instance, with the first creep loading being 1 minute long, the unload period was 3 minutes. This was thought to provide sufficient time for full recovery, but was later determined to be too short to achieve full recovery. Figure 7.6 shows the applied creep recovery loadings along with the displacement response for the 30m×30m experiment.

7.3.2 Cyclic Loading Experiments

Following the creep recovery sequence, a cyclic loading with a frequency in the range of 0.001 to 0.1 Hz was applied. Figure 7.7 schematically shows the applied cyclic loadings, depicting how the the cycles oscillated from 0 to 2 times the amplitude. This provided a mean value equal to the amplitude of the given cycle. The peak cycle value was chosen to be the same as that of the prior load and hold cycles. Due to time restrictions and limitations of the loading system, the above mentioned range of frequencies was chosen. This data is currently being analyzed to investigate the anelastic nature of the ice and compare results with those of small scale isothermal laboratory experiments. Cole (1995) has developed a physically based model for predicting the cyclic response and anelastic behavior of sea ice. It has been successfully applied to S2 saline and sea ice and its application to these experiments will be investigated.

7.3.3 Fracture Loading

At the completion of the low level loading sequences, the sample was loaded to failure on a monotonic load or CMOD controlled ramp. Failure times were on the order of 1 minute. From final failure, the critical CTOD, nominal tensile strength and the apparent fracture toughness could be obtained. Future publications will investigate these results.

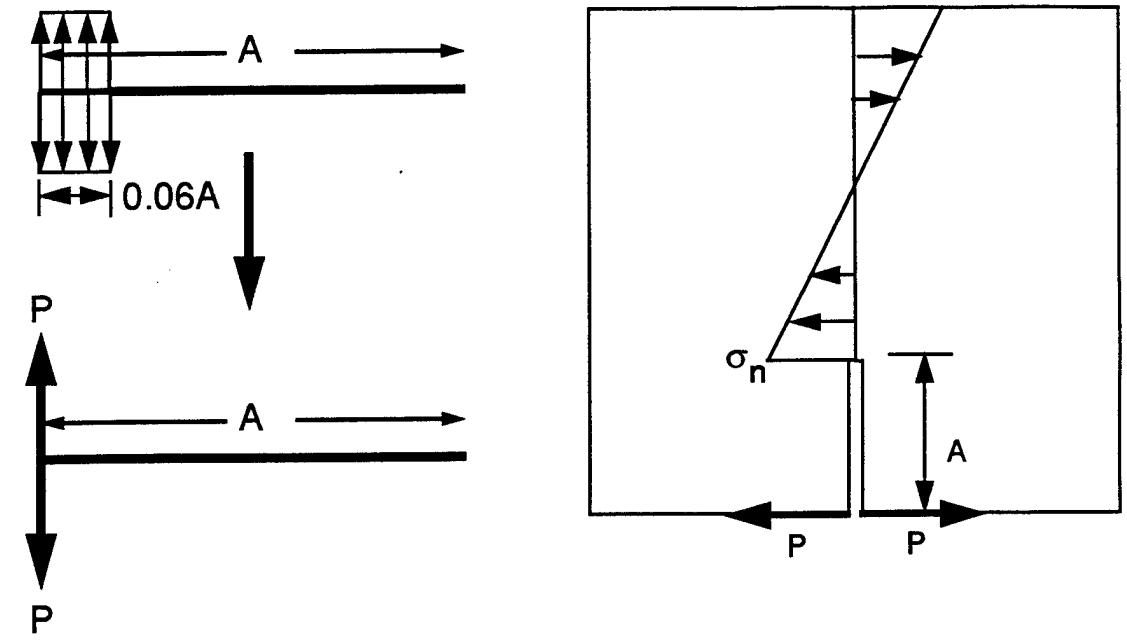

Figure 7.3: a)Simplification of flatjack distributed loading to a point load at the crack mouth; b) Square plate geometry showing stress distribution along the uncracked ligament

7.4 Non-linear Viscoelastic Modeling

The model presented here is the same model used by LeClair et al (1996) to model creep recovery behavior of S2 sea ice subjected to uniaxial, isothermal, tension loading. Following a brief description of the model, its application to the large scale field experiments is presented.

7.4.1 Non-linear Viscoelastic Constitutive Equation

The general form of the non-linear equations are fully described by Schapery (1969, 1996) as derived from multiaxial linear theory. This theory presents the total strain (ε) as a composition of three strains: elastic (ε_e), delayed elastic(ε_d), and viscous(ε_v):

$$\varepsilon = \epsilon_e + \epsilon_v + \epsilon_d \tag{7.1}$$

where

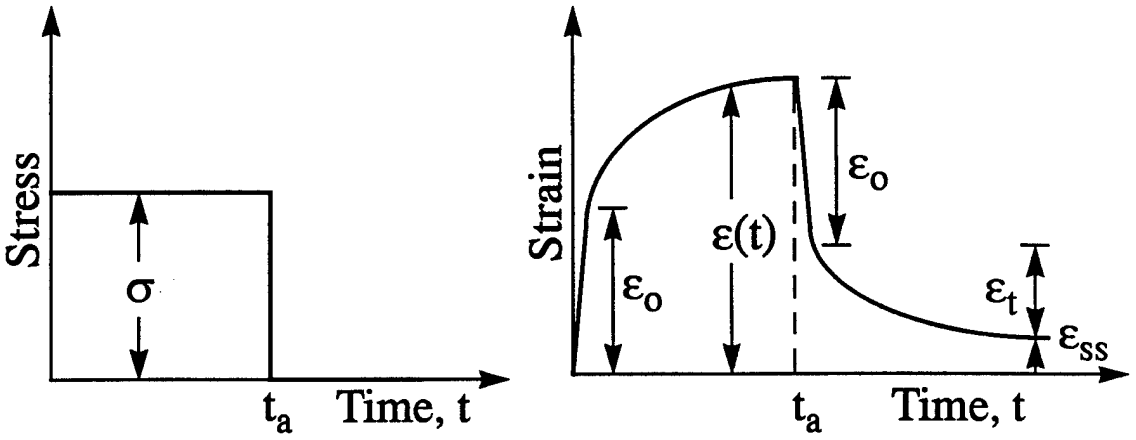

Figure 7.4: Schematic of creep recovery sequences indicating the various strain components

$$\varepsilon_e = g_o S_e \sigma \tag{7.2}$$

$$\varepsilon_v = S_v \int_{-\infty}^{t} g_v \sigma dt' \tag{7.3}$$

$$\varepsilon_d = g_1 \int_{-\infty}^{t} S_d(\psi - \psi') \frac{dg_2\sigma}{dt'} dt' \tag{7.4}$$

and

$$\psi - \psi' = \int_{t'}^{t} dt''/a_\sigma \left[\sigma(t'')\right] \tag{7.5}$$

In the above equations, g_o, g_v, g_1, g_2 and a_σ are typically functions of stress. As will be shown later, these parameters assume values of one in the linear range of behavior, greatly reducing the complexity of the equations. The coefficients, S_ϵ, S_v and S_d, are the elastic, viscous and delayed elastic compliances, respectively, and σ is the applied stress. Although a slight temperature profile does exist through the thickness of the sheet, the sheet is assumed to be isothermal ($\Delta T = 0$), so no temperature effect is included in these simplified equations.

As described by Schapery (1969), it is possible to determine the unknown quantities in the above equations via the strain response to one type of stress history. In

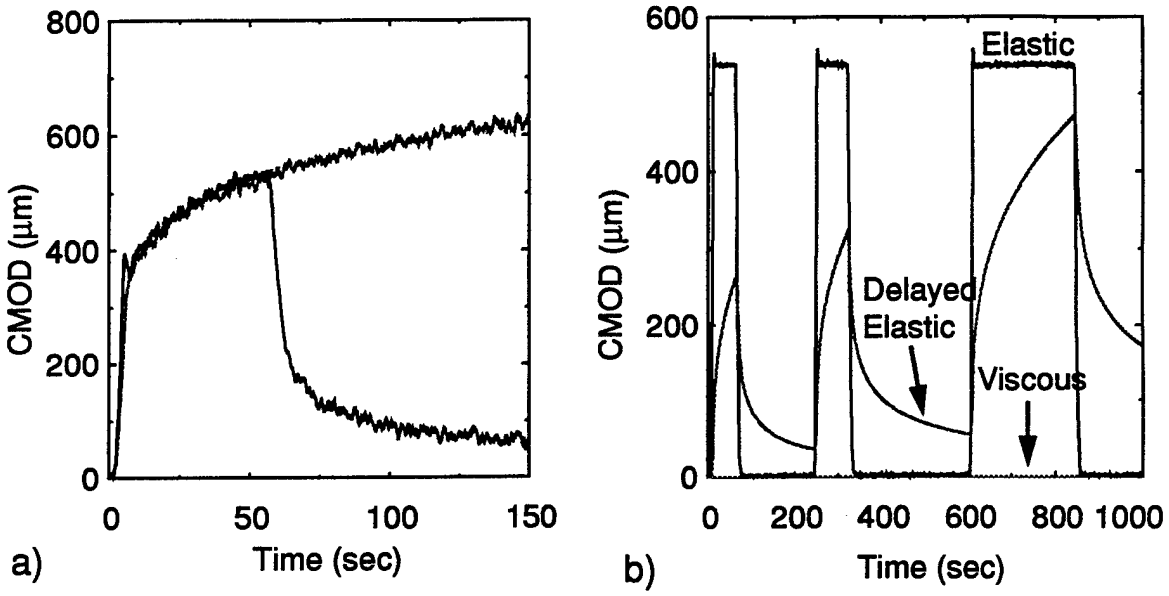

Figure 7.5: a) Superposition of the first and third creep cycles; b) Contribution of each strain component to the total strain

the case of creep recovery sequences, the first loading and recovery cycle will suffice for obtaining the necessary parameters. The following cycles are used to fine tune the parameters to obtain the optimal solution. The methods for obtaining the unknown functions are fully described by Schapery (1969) and summarized in LeClaire et al(1996). At this point, it is redundant to again repeat the derivation.

Schapery (1996) and LeClair et al (1996) have applied this nonlinear viscoelastic creep compliance function to the same set of experiments (LeClair et al, 1996) analyzed by Abdel-Tawab (1995). The robustness of this approach still needs to be evaluated but preliminary analysis looks promising. The strain is a nonlinear function of stress which further complicates modeling efforts. The same form of the creep compliance function has been applied to the large scale sea ice experiments with encouraging results. At present, this creep based modeling is not physically based as the coefficients of the compliance terms have not been soundly linked to properties of the ice (salinity, density, temperature, grain size).

7.5 Analysis

The constitutive model was applied to a 30m × 30m square plate of first year sea ice. The sheet was 1.8m thick with a near vertical temperature profile. The loading was applied to the plate via a flatjack inserted in the precut notch at the crack mouth. Because of the size of the sample (30m) relative to the flatjack dimensions (0.6m), the pressure in the flatjack could be converted to a point load applied at the crack mouth with very little loss of accuracy and thus simplifying the computations (Fig 7.3a). Prior applications of this uniaxial model assumed a uniform tensile stress was applied to the sample. The field experiments were fracture tests with the loading distributed along a small portion of the crack length. This provides a varying stress field through the plate with high stresses at the crack tip. The flatjack loading distribution must be normalized to a stress which can be consistently defined at any sample size. Because failure occurs due to the stress concentration at the crack tip, the nominal stress at the crack tip as defined in Dempsey (1996) for the square plate is used. This formula presents the flatjack loading as an equivalent stress applied at the crack tip. Figure 7.3b shows the assumed stress distribution and the stress, σ_n, at the crack tip defined as:

$$\sigma_n = \frac{2P(A+2L)}{B(L-A)^2} \tag{7.6}$$

As discussed above, the coefficients g_o, g_1 and a_σ are assumed to have values of one for the analysis presented in this paper. Assuming the elastic behavior is linear with stress and independent of time, g_o=1 is immediately evident. If the experimental data exhibits the ability to predict the recovery strain from the superposition of the creep strains, the coefficients g_1=a_σ=1. By plotting the creep loading of the first cycle with that of the third cycle, the superposition can be seen. Figure 7.4 shows the idealized creep and recovery response of a linear viscoelastic material. When

$$\varepsilon_r = \varepsilon(t) - \varepsilon(t - t_1) \tag{7.7}$$

in a nonlinear viscoelastic material, g_1=a_σ=1 must be true. As can be seen from

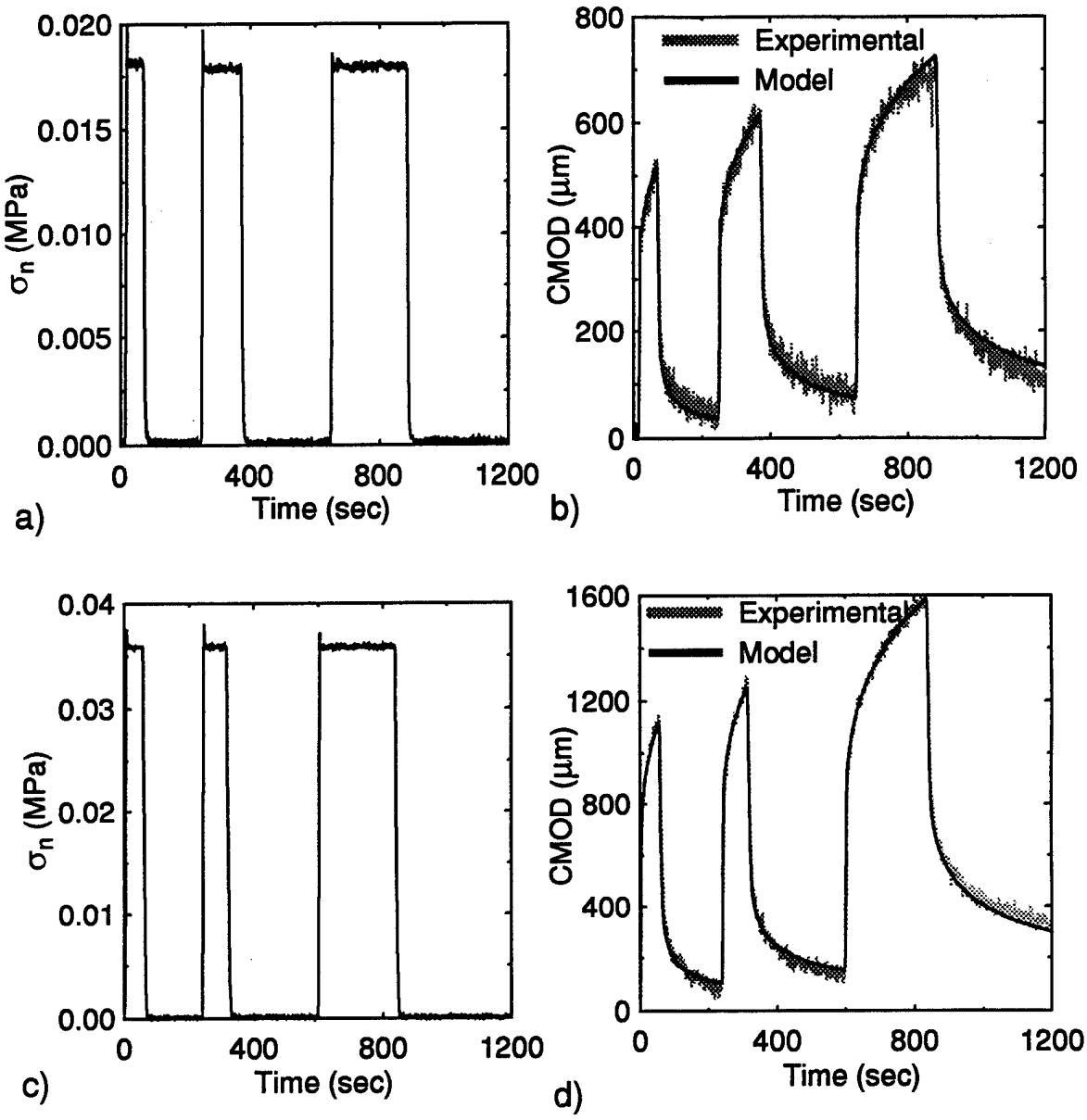

Figure 7.6: a) Creep recovery sequences and b) crack opening displacement responses at 0.018 MPa nominal stress; c) Creep recovery sequences and d) crack opening displacement responses at 0.036 MPa nominal stress

the overplot of the first and third cycles in Figure 7.5a, the special case of $g_1=a_\sigma=1$ exists.

The coefficents, g_v and g_2, are functions of stress causing the nonlinearity of the equation. Combining these terms with the associated viscous and delayed elastic compliances, respectively and incorporating the assumptions made above, (7.1) can

be rewritten as:

$$\varepsilon(t) = S_e\sigma + S_1\int_0^t \sigma^p dt + S_2\int_0^t (t-t')^n \frac{d\sigma^q}{dt'}dt' \qquad (t \geq 0) \tag{7.8}$$

The experimental results are the measurement of crack opening and not strain, therefore the strain equation defined in (7.8) actually has the units of displacement. The time, stress and stress history dependence in the delayed elastic component of the displacement make it a difficult equation to solve so ε_d was computed by solving it as a convolution:

$$\varepsilon_d = S_2\int_0^t (t-t')^n \frac{d\sigma^q}{dt'}dt' = S_2(t^n \otimes \frac{d\sigma^q}{dt}) \tag{7.9}$$

Each component of the total displacement was computed using the DADiSP data analysis software package. The exponents on the stress and time functions, n, p and q were chosen based on the prior investigations by Schapery (1996) and LeClaire et al (1996). The stress exponent for the viscous term, p=3, is a commonly used stress power used in dislocation theory models. A stress exponent of 3/2 was chosen for the delayed elastic with a time exponent, n, of 1/3. An iterative procedure was used to then obtain the compliances, S_e, S_v and S_d. First, a value for the elastic compliance, S_e, was chosen by determining the elastic modulus from the initial slope of the loading to be 5.2 GPa. Knowing the strain required to produce this modulus, the compliance was chosen to also achieve the known displacement. Because the unloading period was not long enough for full recovery of the delayed elastic deformation, the remaining deformation at the end of the unloading was a combination of both delayed elastic and viscous displacement. Knowing the viscous deformation was only a part of the remaining deformation, a value for S_v was assumed. S_v and S_d were then modified to produce the best fit of the data. After obtaining the compliance coefficients, the model was applied to the next creep recovery sequence at 0.036 MPa. The model consistently overpredicted the CMOD. It was determined that the stress exponent for the delayed elastic was too large. When an exponent of 1 was used the CMOD

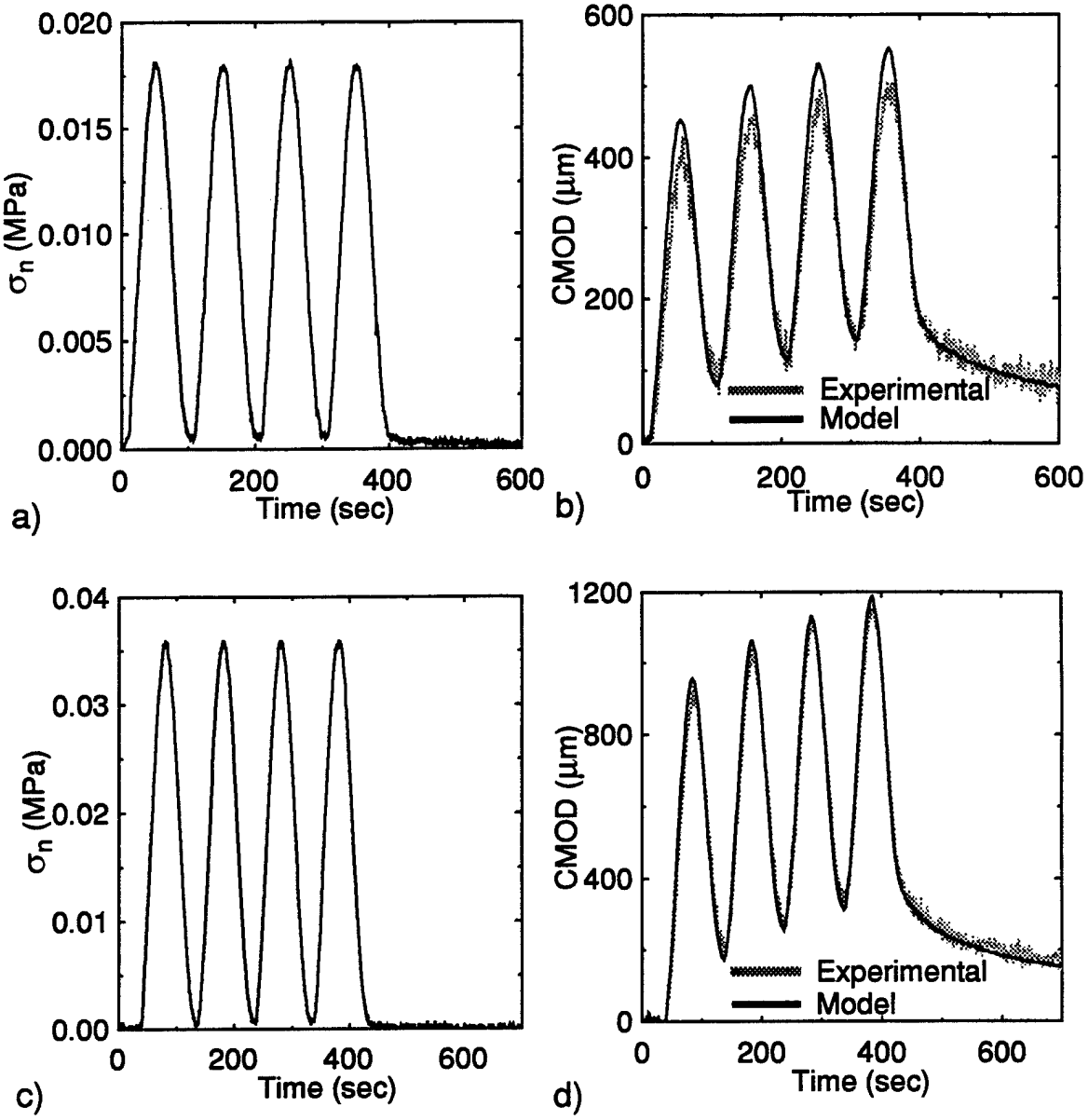

Figure 7.7: a) Cyclic loading sequences and b) crack opening displacement responses at 0.018 MPa peak cyclic stresses; c) Cyclic loading sequences and d) crack opening displacement responses at 0.036 MPa peak cyclic stresses

was underpredicted, indicating the most suitable value to lie between 1 and 1.5. A value of 1.2 for the exponent best fit the experimental data at both load levels (Fig. 7.6). Agreement within about 5% was achieved. The final compliance values used for the model were: S_e=0.015, S_d=0.0082 and S_v=0.0001. The contribution of each strain component to the total deformation is shown in Fig. 7.5b. The elastic and

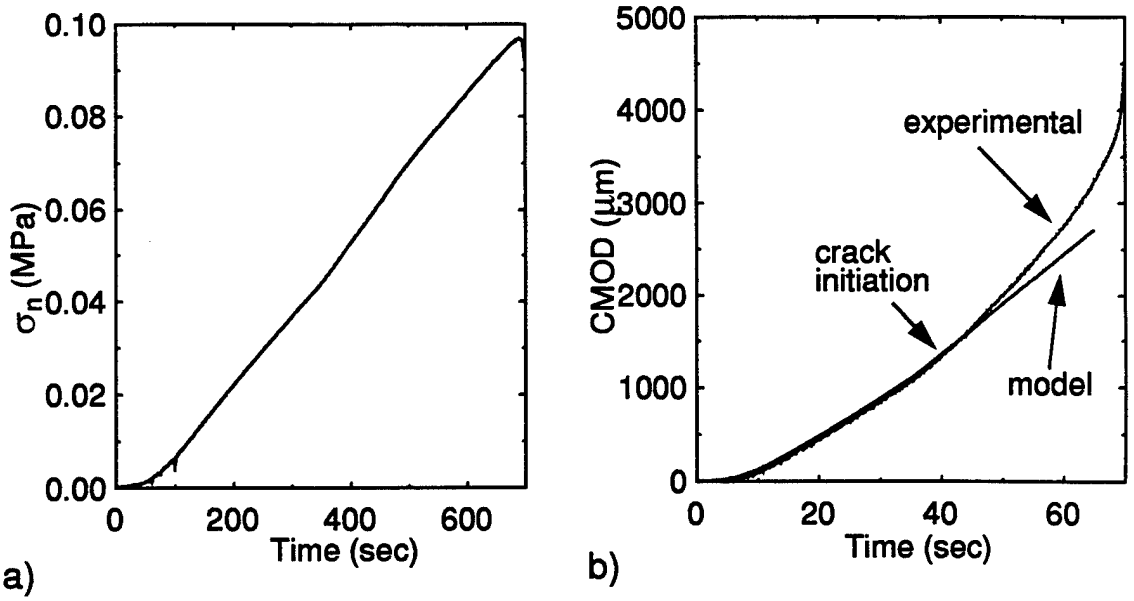

Figure 7.8: a) Monotonic load ramp to fracture and b) crack opening displacement response

delayed elastic components account for most of the deformation with the viscous strain being a very small but not negligible component.

7.5.1 Comparison with cyclic responses

For the same experiment, two sets of 0.01 Hz cyclic sequences were completed with load cycles to 0.018 MPa and 0.036 MPa to compare with the applied creep sequences. Now, although each cycle is completed in 100 seconds, 4 to 6 cycles are run consecutively with no relaxation after each cycle. Because these cycles do not oscillate about a zero mean stress, they are equivalent to the superposition of a creep loading and the same cycles shifted vertically to oscillate about zero loading. The longest creep recovery cycle used for calibrating the model was 240 seconds whereas the cyclic sequences are about 500 seconds long. The ability of the model to accurately predict the cyclic response indicates how well it can be extrapolated to longer loading durations. As shown in Fig. 7.7 the model predicts the cyclic responses for both load levels quite nicely as well as the final recovery.

7.5.2 Comparison with monotonic fracture loading

Following the cyclic and creep recovery interrogation of the ice sample, the ice plate was ramped in load control until it fractured. Although the time to complete failure was approximately 1 minute, the crack began to propagate after about 40 seconds of loading. The onset of the small cracking events was picked up by the fine resolution displacement gauge placed at the crack tip. Because of the relatively large displacements at the crack mouth, the CMOD gauge does not show a sharp rise in opening, but rather a steadily increasing specimen compliance. The crack tip displacements are very small so when any microcracking occurs, the crack tip gauge (CTOD) sees it.

Using the same methods as applied to the creep and cyclic loadings, the monotonic displacement response was modeled. It predicted the CMOD very well until the crack began to propagate (Fig. 7.8). As the crack slowly propagated over the next 20 seconds until complete failure, the sample became more compliant as is seen in the CMOD record. Since the model doesn't account for crack propagation, it under predicts the CMOD after initial crack propagation.

7.6 Conclusions

The application of a non-linear viscoelastic model to an *in-situ* sea ice experiment is presented. As a preliminary effort, the model fits the data quite well. Its ability to predict strain responses resulting from various loading scenarios is promising. As this was a simplified model, assuming the ice to be isothermal, the effects of the thermal gradient through the depth are not handled. Further applications of this model to the in-situ plates should incorporate a temperature dependent component.

8 CONCLUSIONS

A fracture mechanics analysis of the semi-circular (SC) and semi-circular-bend (SCB) fracture geometries is presented. The weight function method is implemented to obtain wide ranging stress intensity factor (SIF) and crack opening displacement (COD) expressions. This study has as its basis a finite element analysis of the semi-circular disk (SC) subjected to a reference loading case. The latter is required to determine both the associated reference stress intensity factor and the weight function for the base-edge-cracked semi-circular geometry. With this information, SIF and COD expressions for the full range of crack lengths are obtained. The special cases of the SC subject to a concentrated crack mouth loading and the SCB are analyzed in detail. The weight function for the SCB is fully developed, with an accurate expression for the SIF and and a numerical result for the crack mouth opening displacement (CMOD). The latter wide ranging expressions can, in turn, be applied as a reference solution. From this weight function approach, SIF's and COD's for the SC and SCB subject to any other loading can be obtained.

The results of two small scale first year sea ice testing programs using the SCB geometry are presented. The effects of the strong c-axis alignment as well as the age of the ice are investigated. Ice cores pulled from very young, thin sea ice are much weaker than cores removed from the same depth of the same sheet later in the growth season. Also, the effects of the c-axis alignment are quantified showing a higher fracture toughness and tensile strength was exhibited by samples fracturing along the c-axis. Due to a wide band of scatter in the data, it was difficult to distinguish any differences in the CMOD and modulus results. This work completes the complementary small-scale test program part of the SIMI large scale fracture testing program.

A set of large scale fracture and flexure tests were conducted on S1 freshwater

lake ice at Spray Lakes, Alberta (Phase I). Details of the experimental aspects of the large scale freshwater ice fracture test program are presented. Analysis of the results reveals the dramatic effect polycrystallinity and anisotropy have on the fracture of ice. S1 freshwater ice is typically composed of large grains (up to a meter at the bottom of the sheet) with predominantly vertical c-axes. Unless large enough sizes are tested, the macrocrystalline, not polycrystalline behavior is seen. The goal of this program was to test progressively larger sizes in an effort to transcend the macrocrystalline behavior and obtain the fracture behavior of the ice sheet. Unfortunately, due to the large grained ice encountered in this program and the limitations of the equipment, sizes at which the material properties and behavior were independent of size were not accomplished. Nevertheless, important information linking the small scale to the large scale was obtained.

Preliminary analyses for the large-scale fracture tests from Phase II is presented. For Phase II (columnar S2 sea ice), the inclusion of bulk viscoelastic deformation has been found to be essential for proper numerical analysis. Various available size effect laws have been compared. The behavior of these laws over portions of the available size range was examined to study the effect of change in size range as well as change of the absolute sizes. The predictive capability of the size effects laws was shown to be rather fickle. Future research on this topic does not lie within the proposition of various curve fit or size effect laws such as those just examined. There is a clear need for a quantitative basis to the predicted size effects. The latter basis will reside with approaches reflective of the true material behavior.

The design and application of a closed loop computer controlled field testing system is presented. Its ability to control both load and displacement and follow virtually any prescribed loading path enables one to extract an abundance of information from a single field experiment. This system provided the ability to apply loading sequences previously limited to lab experiments using hydraulic test frames. The sea ice behavior at the large scale can now be compared in detail to its behavior under laboratory

conditions.

The application of a non-linear viscoelastic model to an *in-situ* sea ice experiment is presented. As a preliminary effort, the model fits the data quite well. Its ability to predict strain responses resulting from various loading scenarios is promising. As this was a simplified model, assuming the ice to be isothermal, the effects of the thermal gradient through the depth are not handled. Further applications of this model to the in-situ plates should incorporate a temperature dependent component.

9 REFERENCES

Abdel-Tawab, K., and Rodin, G. J., 1992, "On the Relevance of Linear Elastic Fracture Mechanics to Ice," *11th IAHR Ice Symposium, Banff, Alberta*, Vol. 3, pp. 1436-1445.

Abdel-Tawab, K., and Rodin, G. J., 1993, "Interpretation of Results of The Fracture Toughness Tests on Ice," *Ice Mechanics - 1993*, Dempsey, J. P., Bazant, J. P., Rajapakse, Y. D. S. and Sunder, S. S., ed., ASME-AMD Vol. 163, pp. 49-59.

Abdel-Tawab, K.I., 1995, "Constitutive Modeling and Fracture Analysis of Ice," *PhD Thesis*, The University of Texas at Austin.

Adamson, R. M., Dempsey, J. P, Mulmule, S. V., DeFranco, S. J., and Xie, Y., 1995, " Large-scale in-situ ice experiments, Part I: experimental aspects," ASME AMD-Vol. 207, pp. 107-128.

Adamson, R.M., Dempsey, J.P. and Mulmule, S.V., 1995, "Fracture analysis of semi-circular and semi-circular-bend geometries," *International Journal of Fracture* (in press).

Adamson, R.M., Dempsey, J.P., and Shapiro, L.H., 1996, "Core-Based Fracture (Phases III & IV) of First Year Aligned Sea Ice," *ASCE J. Cold Reg. Eng.* (submitted for review).

Adamson, R.M. and Dempsey, J.P., 1996, "A closed-loop servo-pneumatic loading system for field testing: design and results," (to be submitted).

Ashby, M. F., and Duval, P., 1985, "The Creep of Polycrystalline Ice." *Cold Regions Science and Technology*, Vol. 11, **3**, pp. 285-300.

ASTM-E399, 1981, "Standard Test Method for Plane Strain Fracture Toughness of Metalic Material." ASTM, Philadelphia.

Bazant, Z. P., and Oh, B. H., 1983, "Crack Band Theory for Fracture of Concrete." *Materiaux et Construction*, Vol. 16, **93**, pp. 155-177.

Bazant, Z. P., 1984, "Size effect in Blunt Fracture: Concrete, Rock, Metal." *ASCE Journal of Engineering Mechanics*, Vol. 110, pp. 518-535.

Bazant, Z. P., Kim, J. K., and Pfeiffer, P. A., 1986, "Nonlinear Fracture Properties From Size Effect Tests." *ASCE Journal of Structural Engineering*, Vol. 112, **2**, pp. 289-307.

Bazant, Z. P., Bai, S. P., and Gettu, R., 1993, "Fracture of Rock, Effect of Loading Rate." *Engineering Fracture Mechanics*, Vol. 45, **3**, pp. 393-398.

Bazant, Z. P., and Beissel, S., 1994, "Smeared Tip Superposition Method For Cohesive Fracture With Rate Effect and Creep." *International Journal of Fracture*, Vol. 65, pp. 277-290.

Blanchet, D., Churcher, A., Fitzpatrick, J., and Badra-Blanchet, P., 1989, "An Analysis of Observed Failure Mechanisms for Laboratory, First-Year and Multi-Year Ice", *Working Group on Ice Forces*, (Edited by G.W. Timco), Special Report 89-5, U.S. Army Cold Regions Research and Engineering Laboratory, New Hampshire.

Bueckner, H. F., 1970, "A Novel Principle for the Computation of Stress Intensity Factor." *Zeitschrift fur Angewandte Mathematik and Mechanik*, Vol. 50, pp. 529-545.

Carpinteri, A., 1982, "Notch Sensitivity in Fracture Testing of Aggregative Materials," *Engineering Fracture Mechanics*, Vol. 16, pp. 467-481.

Carpinteri, A., Chiaia, B., and Ferro, G., 1993, "Multifractal Scaling Law for the Nominal Strength Variation of Concrete." *Size Effect in Concrete Structures, Proceedings of the Japan Concrete Institute International Workshop, Sendai, Japan*, Mihashi, H., Okamura, H., and Bazant, Z. P. Ed., pp. 193-205.

Chen, A.C.T. and Lee, J., 1986, "Large-Scale Strength Tests at Slow Strain Rates," *5th OMAE Symposium*, 374–378.

Chong, K. P. and Kuruppu, M. D., 1984, "New specimen for fracture toughness determination of rock and other materials," *International Journal of Fracture*, Vol. 26, pp. R59-R62.

Cole, D.M. and Gould, L.D., 1990, "Reverse Direct-Stress Testing of Ice: Equipment and Example Results," *Cold Regions Sci. and Tech.*, 18: 295–302.

Cole, D.M., 1990, "Reversed Direct-stress Testing of Ice: Initial Experimental Results and Analysis," *Cold Regions Sci. and Tech.*, **18**, 303-321.

Cole, D. M., 1993, "The Effect of Creep on the Constitutive Behavior of Saline Ice At Low Strains," *Ice Mechanics - 1993*, Dempsey, J. P., Bazant, J. P., Rajapakse, Y. D. S. and Sunder, S. S., ed., ASME-AMD Vol. 163, pp.261-272.

Cole, D.M., Shapiro, L.H., Weeks, W., Byers, C., Dempsey, J.P., Adamson, R.M., Petrenko, V. and Gluschenkov, O.V., 1995, "Overview of recent program on mechanical properties of sea ice," *ASCE J. Cold Regions Engineering*, **9**, 219–234.

Cole, D.M. and Durell, G.D., 1995, "The effect of c-axis alignment on the constitutive behavior of sea ice at low strains," ASME AMD-Vol. 207, pp. 189-199.

Cole, D.M. and Durell, G.D., 1995, "The Cyclic Loading of Saline Ice," *Phil. Mag. A*, **72**, 209-229.

Cole, D. M., 1995, "A Model for Anelastic Straining of Saline Ice Subjected to Cyclic Loading," *Phil. Mag. A.*, **72**: 231-248.

Danilenko, V.I., 1985, "Determination of Crack Resistance (K_1c) of Freshwater Ice," *Mechanics of Solids*, Vol. 20, pp. 131-136.

DeFranco, S. J., Wei, Y., and Dempsey, J. P., 1991, "Notch Acuity Effects on Fracture Toghness of Saline Ice." *Annals of Glaciology*, Vol. 15, pp. 230-235.

DeFranco, S. J., and Dempsey, J. P., 1991, "Crack Growth Stability in Saline Ice." *Mechanice of Creep Brittle Materials -2*, Cocks, A. C. F, and Ponter, A. R. S., Eds., Elsvier Applied Science, p. 25-36.

DeFranco, S. J., and Dempsey, J. P., 1994, "Crack Propagation and Fracture Resistance In Saline Ice." *Journal of Glaciology*, Vol. 40, **136**, pp. 451-462.

Dempsey, J.P., Nigam, D. and Cole, D.M., 1988, "The Flexure and Fracture of Macrocrystalline S1 Type Freshwater Ice," *Proceedings of the 7th International OMAE Conference*, Houston, Texas, Vol. IV, pp. 39-46.

Dempsey, J.P. and Wei, Y., 1989, "Fracture Toughness K_Q, and Fractography of S1 Type Freshwater Ice," *Adavances in Fracture Research*, Edited by K. Salama, K. Ravi-Chandar, D.M.R. Taplin and P. Rama Rao, Pergamon Press, Vol. V, pp. 3421-3428.

Dempsey, J.P., 1991, "The fracture toughness of ice," *Ice-Structure Interaction*, S. J. Jones, R. F. McKenna, J. Tillotson, and I. J. Jordaan (Eds.), Springer-Verlag, Berlin Heidelberg, pp. 109–145.

Dempsey, J. P. and DeFranco, S. J., 1992, "Nonlinear Fracture Analysis of Saline Ice: Size, Rate, Temperature Effects." *IAHR 11th International Symposium on Ice*, Banff, Alberta, Vol. 3, pp. 1420-1436.

Dempsey, J.P., Wei, Y., and DeFranco, S.J., 1992, "Notch Sensitivity and Brittleness in Fracture Testing of S2 Columnar Freshwater Ice." *International Journal of Fracture* **53:** 101–120.

Dempsey, J.P., Adamson, R.M., and DeFranco, S.J., 1995, "Fracture Analysis of Base-Edge-Cracked Reverse-Tapered Plates," *International Journal of Fracture* **69:** 281-294.

Dempsey, J.P., Adamson, R.M. and Mulmule, S.V., 1995, "Large-Scale In-Situ Fracture of Ice," *Fracture Mechanics of Concrete Structures*, Proc. FRAMCOS-2, Ed. Folker H. Wittman, AEDIFICATIO Publishers, Vol. 1, 675-684.

Dempsey, J.P., 1996, "Scale effects on the fracture of ice," *Weertman Seventieth Anniversary Volume*, Ed. R.J. Arsenault.

Frocht, M.M., 1948, *Photoelasticity*, John Wiley and Sons, Inc.

Gladwell, G.M.L., 1980, *Contact Problems in the Classical Theory of Elasticity*. Sijthoff and Noordhoff.

Gow, A.J., Ueda, H.T. and Ricard, J.A., 1978, "Flexural Strength of Ice on Temperate Lakes: Comparative Tests of Large Cantilever and Simply Supported Beams," USA Cold Regions Research and Engineering Laboratory, CRREL Report 78-9.

Gow, A.J., Ueda, J.T., Govini, J.W. and Kalafut, J., 1988, "Temperature and Struc-

ture Dependence of the Flexural Strength and Modulus of Freshwater Model Ice," USA Cold Regions Research and Engineering Laboratory, CRREL Report 88-6.

Hamza, H., and Muggeridge, D. B., 1984, "An Analysis of the Viscoelastic Fracture Toughness and Crack Growth in Ice." *Cold Regions Science and Technology*, Vol. 9, pp. 249-258.

Hillerborg, A., Modeer, M., and Petersson, P. E., 1976, "Analysis of Crack Formation and Crack Growth In Concrete By Means of Fracture Mechanics and Finite Elements." *Cement and Concrete Research*, Vol. 6, pp. 773-782.

Jenq, Y. S., and Shah, S. P., 1985, "Two Parameter Fracture Model For Concrete." *ASCE Journal of Engineering Mechanics*, Vol. 111, **10**, pp. 1227-1241.

Johnson, K.L., 1985, *Contact Mechanics.* Cambridge University Press.

Karihaloo, B. L. and Nallathambi, P., 1987, "Notched Beam Test: Mode I Facture Toughness." draft report to RILEM Committee 89-FMT, Fracture Mechanics of Concrete: Test Method.

Kennedy, K.P., Blanchet, D., Prodanovic, A., Dempsey, J.P., DeFranco, S.J., Spencer, P.A. and Masterson, D., 1993, "Large-Scale Ice Fracture Experiments," *12th POAC Conference*, Vol. 2, 527–536.

Kennedy, K.P., Mamer, K.J., Dempsey, J.P., Adamson, R.M., Spencer, P.A., Masterson, D.M., 1994, "Large-scale ice Fracture Experiments: Phase 2," *IAHR 94: Proceedings of the 12th International Symposium on Ice*, Trondheim, Sweden, Vol. 1, pp 315-324.

Kim, J. K., Park, Y. D., and Eo, S. H., 1993, "Size Effect in Concrete Specimen with Dissimilar Initial Cracks," *Size Effect in Concrete Structures, Proceedings of the Japan Concrete Institute International Workshop, Sendai, Japan*, Mihashi, H., Okamura, H., and Bazant, Z. P. Ed., pp. 181-192.

Lazo, J., 1994, "Fracture of Saline Ice: Thickness, Orientation and Reversed-Direct Tension Testing," M.S. Thesis, Clarkson University

LeClair, S.L., Schapery, R.A. and Dempsey, J.P., 1996, "Tensile creep of saline

ice," Symposium on *Inelasticity and Damage in Solids Subject to Microstructural Change*, September 25-27, St. John's, Newfoundland, Canada.

LeClair, E.S., Dempsey, J.P., and Adamson, R.M., 1996, "Core-Based Fracture (Phase VI) of First Year Aligned Sea Ice," *ASCE J. Cold Reg. Eng.* (submitted for review).

Le Gac, H., and Duval, P., 1980, "Constitutive relaions for the Non-Elastic Deformation of Pollycrystalline Ice," *IUTAM Symp. on the Physics and Mechanics of Ice* Ed. Per Tryed, Springer-Verlag, pp. 51-59.

Li, V. C., and Liang, E., 1986, "Fracture Processes In Concrete and Fiber Reinforced Cementitious Composites," *ASCE Journal of Engineering Mechanics Division*, Vol. 112, pp. 566-586.

Li, Y. and Bazant, Z., P., 1993, "Size Effect in Cohesive Crack Model," Structural Engineering Report, No. 93-8/420s, Department of Civil Engineering, Northwestern University.

Lim, I. L., Johnston, I. W. and Choi, S. K., 1993, "Stress intensity factors for semi-circular specimens under three-point bending," *Engineering Fracture Mechanics*, Vol. 44, pp. 363–382.

Mulmule, S. V., and Dempsey, J. P., 1995, "Stress-Separation Curve for Saline Ice Using Fictitious Crack Model," *ASCE Journal of Engineering Mechanics* (submitted for review).

Parsons, B. L., Williams, F. M., Everard, J., and Slade, T., 1993, "Notch Sensitivity of First Year Sea Ice," *ASCE Journal of Engineering Mechanics*, Vol. 119, **7**, 1303-1313.

Parsons, B.L., Snellen, J.B., Hill, B., 1986, "Physical Modeling and the Fracture Toughness of Sea Ice," *Proceedings of the 5th International OMAE Conference*, Tokyo, Japan, Vol. 4, 358-364.

Parsons, B.L., Snellen, J.B., and Muggeridge, D.B., 1988, "The Initiation and Arrest Stress Intensity Factors of First Year Columnar Sea Ice," *Proceedings of the 9th*

IAHR Ice Symposium, Vol. 1, pp. 502-512.

Peck, L., Barton, C. C. and Gordon, R. B., 1985, "Microstructure and the Resistance of Rock to Tensile Fracture," *Journal of Geophysical Research*, Vol. 90, B13, pp. 11533-11546.

Planas, J., and Elices, M., 1991, "Nonlinear Fracture of Cohesive Materials," *International Journal of Fracture*, Vol. 51, pp. 139-157.

Quinn, R., 1987, "3-term PID Algorithm Optimizes Control Strategies (Turbo Tools 11), " *Personal Engineering and Instrumentation News*, Oct. 1987, pp. 59-64.

Rice, J. R., 1972, "Some Remarks on Elastic Crack-tip Stress Field," *International Journal of Solids and Structures*, Vol 18, pp. 751-758.

Richter-Menge, J. A., and Jones, K. F., 1993, "Tensile Strength of First Year Sea Ice," *Journal of Glaciology*, Vol. 39, **39:** 609-618.

Riedel, H., and Rice, J. R., 1980, "Tensile Cracks In Creeping Solids," Fracture Mechanics: 12^{th} Conference, ASTM STP 700, pp. 112-130.

RILEM Draft Recommendations, 1991, "Size-effect method for determining fracture energy and process zone size of concrete," *Materials and Structures*,**23:** 461-465.

Schapery, R. A., 1975, "A Theory of Crack Initiation and Growth In Viscoelastic Media. I. Theoretical Development," *International Journal of Fracture*, Vol 11, **1:** 141-159.

Schapery, R. A., 1969, "On the characterization of nonlinear viscoelastic materials," *Polymer Eng. and Sci.*, 9(4): 295-310.

Schapery, R. A., 1975, "A Theory of Crack Initiation and Growth In Viscoelastic Media. II. Approximate Method of Analysis." *International Journal of Fracture*, Vol 11, **3**, pp. 369-387.

Schapery, R. A., 1975, "A Theory of Crack Initiation and Growth In Viscoelastic Media. III. Analysis of Continuous Growth," *International Journal of Fracture*, Vol 11, **4**, pp. 549-562.

Schapery, R. A., 1993, "Viscoelastic Deformation Behavior of Ice Based On Microme-

chanical Models,"*Ice Mechanics-1993*, Dempsey, J. P., Bazant, J. P., Rajapakse, Y. D. S. and Sunder, S. S., ed., ASME-AMD Vol. 163, pp. 15-33.

Schapery, D., 1996, "Thermomechanical Constitutive Equations for Polycrystalline Ice," *IAHR 13th International Symposium on Ice*, Beijing, China, August 27-30.

Schwarz, J., Frederking, R., Gavrilo, V., Petrov, I. G., Hirayama, K. I., Mellor, M., Tryde, M., and Vaudrey, K. D., 1981, " Standardized Testing Method for Measuring Mechanical Properties of Ice," *Cold Regions Science and Technology*, Vol. 4, pp. 245-253.

Shapiro, L.H. and Hoskins, E.R., 1975, "The Use of Flatjacks for the In-Situ Determination of The Mechanical Properties of Sea Ice," *Proceedings of the* 3^{rd} *Port and Ocean Engineering Under Arctic Conditions*, pp. 427-436.

Shapiro, L.H., Metzner, R.C., and Johnson, J.B., 1981, "Fracture Toughness of Sea Ice," Report submitted to the Shell Development Company.

Shapiro, L.H. and Weeks, W.F., 1995, "Controls on the flexural strength of small plates and beams of first-year sea ice," ASME AMD-Vol. 207, pp. 179-188.

Shen, W. and Lin, S.Z., 1986, "Fracture Toughness of Bohai Bay Sea Ice," *Proc. of the 5th Int. Offshore Mechanics and Arctic Engineering Symp.*, Vol. IV., Tokyo, April 13-18, pp. 354-357.

Shyam Sunder, S., and Wu, M. S., 1990, "On the Constitutive Modeling of Transient Creep In Polycrystalline Ice," *Cold Regions Science and Technology*, Vol. 18, pp. 267-294.

Shyam Sunder, S., and Nanthikesan, S., 1992, " Fracture Process Zone Due To Transient Creep In Polycrystalline Ice," *IAHR Ice symposium, Banff, Alberta*, Vol. 2, pp. 1006-1020.

Sinha, N.K., 1992, "Creep of Sea Ice", *Proc. 11th Int. OMAE Symp.,*ASME Publ., V. 4, pp. 261-266.

Sinha, N. K., 1983, "Creep Model of Ice for Monotonically Increasing Stress," *Cold Regions Science and Technology*, Vol. 8, **1**, pp. 25-33.

Sodhi, D.S., 1986, "Flexural and Buckling Failure of Floating Ice Sheets Against Structures", *Proceedings of the 8th IAHR Symposium on Ice*, Iowa City, Vol. II, pp. 339-359.

Stehn,L., 1990, "Fracture Toughness of Sea Ice," Licentiate Thesis, Luleå University of Technology.

Timco, G.W., 1987, "Indentation and Penetration of Edge-Loaded Freshwater Ice Sheets in the Brittle Range," *ASME Journal of Offshore Mechanics and Arctic Engineering*, Vol. 109, pp. 287-294.

Timco, G.W., and Frederking, R.M.W., 1982, "Flexural Strength and Fracture Toughness of Sea Ice," *Cold Regions Science and Technology*, Vol. 8, pp. 35-41.

Urabe,N., Iwasaki, T. and Yoshitake, A., 1980, "Fracture Toughness of Sea Ice," *Cold Regions Science and Technology*, Vol. 3, pp. 29-37.

Urabe, N. and Yoshitake, A., 1981a, "Strain Rate Dependent Fracture Toughness (K_{IC}) of Pure Ice and Sea Ice," *Proceedings of the 6th IAHR Ice Symposium*, Vol. II, pp. 410-420.

Urabe, N. and Yoshitake, A., 1981b, "Fracture Toughness of Sea Ice - In-Situ Measurement and Its Application," *Proceedings of the 6th IAHR Ice Symposium*, Vol. I, pp. 356-365.

Vaudrey, K. D., and Katona, M. G., 1975, "Viscoelastic Finite Element Analysis of Sea Ice Sheets," *Third International Symposium on Ice Problems.* Frankenstein, G. E., ed., Hanover, pp. 515-525.

Walsh, P.F., 1972, "Fracture of Plain Concrete," *Indian Concrete Journal*, Vol. 46, pp. 469-470 and 476.

Weeks, W.F. and Gow, A.J., 1979, "Crystal alignment in the fast ice of arctic Alaska," CRREL Report 79-22, pp. 21.

Wei, Y., Johnston, M., Dempsey, J.P., 1995, "A Grain Multipication Mechanism for the Formation of Transition Zones in First Year Sea Ice," *Cold Regions Science and Technology*, **23**, pp. 367-375.

10 PUBLICATIONS

10.1 BOOKS

J. P. Dempsey, Z. P. Bazant, Y. D. S. Rajapakse, S. S. Sunder, *ICE MECHANICS–1993*, ASME AMD-Vol. 163.

J. P. Dempsey and Y. D. S. Rajapakse, *ICE MECHANICS–1995*, ASME AMD-Vol. 207.

SPECIAL ISSUE

Co-Editor (with Gilles Pijaudier-Cabot) of a special issue of the International Journal of Solids and Structures, a volume in honor of Zdeněk P. Bažant (in preparation).

10.2 CHAPTERS

J. P. Dempsey and S. J. DeFranco, "Laboratory and field-scale fracture of an analogue quasi-brittle material: ice," *Size Effect in Concrete Structures*, H. Mihashi, H. Okamura and Z. P. Bažant, E & FN SPON (Chapman and Hall) (1994) 151–158.

J. P. Dempsey, " Scale effects on the fracture of ice," *The Johannes Weertman Symposium*, R.J. Arsenault, D.M. Cole, T. Gross, G. Kostorz, P. Liaw, S. Parameswaran and H. Sizek Eds. (1996) 351-361.

L. I. Slepyan and J. P. Dempsey, "Radial crack dynamics with closure," *IUTAM Symposium on Nonlinear Analysis of Fracture*, J. R. Willis, Ed. (1996) (in press).

S. J. DeFranco and J. P. Dempsey, "The fracture of sea ice," *Fracture Mechanics: 25th Volume, ASTM STP 1220*, F. Erdogan, Ed., (1995) 433–447.

10.3 JOURNAL PUBLICATIONS

D. M. Cole, L. H. Shapiro, W. F. Weeks, C. Byers, J. P. Dempsey, R. M. Adamson, V. F. Petrenko & O. V. Gluschenkov, "In-situ and laboratory measurements of

the physical and mechanical properties of first-year sea ice," *ASCE Journal of Cold Regions Engineering* **9** (1995) 219–234.

J. P. Dempsey, L. I. Slepyan and I. I. Shekhtman, "Radial cracking with closure," *International Journal of Fracture* **73** (1995) 233-261.

J. P. Dempsey, "Power-logarithmic stress singularities at bi-material corners and interface cracks," *Journal of Adhesion Science and Technology* **9** # *2* (1995) 235–265.

J. P. Dempsey, R. M. Adamson and S. J. DeFranco, "Fracture analysis of base-edge-cracked reverse-tapered plates," *International Journal of Fracture* **69** (1995) 281–294.

J. P. Dempsey, S. J. DeFranco, D. Blanchet and A. Prodanovic, "Mechanisms of fracture of sea ice," *Gidroteknicheskoe Stroitel'stvo (Hydrotechnical Construction)* **No. 3** (1994) 39-42 (in Russian).

K. Ravi-Chandar, B. Adamson, J. Lazo and J. P. Dempsey, "Stress optic effect in ice," *Applied Physics Letters* **64** (1994) 1183-1185.

L. I. Slepyan, J. P. Dempsey and I. I. Shekhtman, "Asymptotic solutions for crack closure in an elastic plate under combined extension and bending," *Journal of the Mechanics and Physics of Solids* **43** (1995) 1727–1749.

L. M. Stehn, S. J. DeFranco and J. P. Dempsey, "Fracture resistance determination of freshwater ice using a chevron notched tension specimen" *International Journal of Fracture* **65** (1994) 313–328.

L. M. Stehn, S. J. DeFranco and J. P. Dempsey, "Specimen geometry effects on the fracture of warm pond (S1) ice" *ASCE Journal of Engineering Mechanics* **121** (1995) 16–25.

L. M. Stehn, S. J. DeFranco and J. P. Dempsey, "Orientation effects on the fracture of pond (S1) ice" *Engineering Fracture Mechanics* **51** (1995) 431–445.

R. M. Adamson, J. P. Dempsey and S. V. Mulmule, "Fracture analysis of semi-circular and semi-circular-bend fracture geometries," *International Journal of Fracture* **77** (1996) 213–222.

S. J. DeFranco and J. P. Dempsey, "Crack propagation and fracture resistance in saline ice" *Journal of Glaciology* **40** (1994) 451–462.

Y. Wei and J. P. Dempsey, "Creep relaxation around a crack tip in an ice crystal," *Scripta Metallurgica et Materiala* **32** # 7 (1995) 949–953.

Y. Wei, M. Johnston and J. P. Dempsey, "A grain multiplication mechanism for the formation of transition zones in first year sea ice," *Cold Regions Science and Technology* **23** (1995) 367–375.

Y. Wei, R. M. Adamson and J. P. Dempsey, "Ice/metal interfaces: fracture energy and fractography," *Journal of Materials Science* **31** (1996) 943–947.

Z. G. Zhao and J. P. Dempsey, "Planar forcing of floating ice sheets," *International Journal of Solids and Structures* **33** (1996) 19–31.

10.4 CONFERENCE PUBLICATIONS

D. M. Cole, J. P. Dempsey, R. M. Adamson, L. H. Shapiro, W. F. Weeks, C. Byers, V. Petrenko, O. V. Gluschenkov, "In-situ and laboratory measurements of the physical and mechanical properties of first-year sea ice," *ICE MECHANICS–1995*, Eds J. P. Dempsey and Y. D. S. Rajapakse, ASME AMD-Vol. 207, pp. 161–178.

J. P. Dempsey, S. J. DeFranco, D. Blanchet and A. Prodanovic, "Splitting of ice floes," *12th POAC Conference*, Vol. 1 (1993) 17–22.

J. P. Dempsey, R. M. Adamson and S. J. DeFranco, "Reverse-tapered CT testpieces," *Novel Experimental Techniques in Fracture Mechanics, Proc. 1993 ASME Winter Annual Meeting, New Orleans*, AMD-Vol. 176 (1993) 165–172.

J. P. Dempsey and S. J. DeFranco, "Laboratory and field-scale fracture of an analogue quasi-brittle material: ice," in *Proc. JCI International Workshop on Size Effect in Concrete Structures* (1993) pp. 133–140.

J. P. Dempsey, S. J. DeFranco, D. Blanchet and A. Prodanovic, "Splitting of ice floes," *1st International Conference: Development of Russian Arctic Offshore (RAO'93)*,

Ed. A. T. Shatalov, G. V. Simakov, G. V. Mirzoev (1994) 149–153.

J. P. Dempsey, R. M. Adamson and S. V. Mulmule, "Large-scale in-situ fracture of ice," *Fracture Mechanics of Concrete Structures*, Ed. F. H. Wittmann, AEDIFICATIO Publishers, Freiburg, Germany, Vol. I, pp. 675–684.

J. P. Dempsey, L. I. Slepyan and I. I. Shekhtman, "Bearing capacity or penetration of (radially) cracked ice sheets," *Proc. 13th International Conference on Port and Ocean Engineering Under Arctic Conditions*, Vol. 1, pp. 181–193.

J. P. Dempsey, R. M. Adamson and S. J. DeFranco, "Scale effects in arctic ice fracture events - Part I," *Proc. 13th International Conference on Port and Ocean Engineering Under Arctic Conditions*, Vol. 2, 76–93.

J. P. Dempsey, S. V. Mulmule and R. M. Adamson, "Scale effects in arctic ice fracture events - Part II," *Proc. 13th International Conference on Port and Ocean Engineering Under Arctic Conditions*, Vol. 2, pp. 94–103.

K. Kennedy, D. Blanchet, A. Prodanovic, J. P. Dempsey, S. J. DeFranco, P. A. Spencer and D. Masterson, "Large-scale ice fracture experiments," *12th POAC Conference*, Vol. 2 (1993) 527–536.

K. P. Kennedy, K. J. Mamer, J. P. Dempsey, R. Adamson, P. A. Spencer and D. M. Masterson, "Large-scale ice fracture experiments: Phase 2," *12th IAHR Ice Symposium* Trondheim, Norway, Vol. 1 (1994) 315–324.

K. Ravi-Chandar, B. Adamson, J. Lazo and J. P. Dempsey, "Stress-optic effects in ice," *ICE MECHANICS–1993*, Eds J. P. Dempsey, Z. P. Bazant, Y. D. S. Rajapakse, S. S. Sunder, ASME AMD-Vol. 163, pp. 113–117.

L. I. Slepyan, J. P. Dempsey and I. I. Shekhtman, "Crack closure and related problems," *ICE MECHANICS–1995*, Eds J. P. Dempsey and Y. D. S. Rajapakse, ASME AMD-Vol. 207, pp. 81–96.

L. I. Slepyan and J. P. Dempsey, "Bearing capacity of a prestressed cracked plate," *Proc. 11th ASCE Engineering Mechanics Conference*, May 19-22, 1996, Ft. Lauderdale, FL. (Edited by Y. K. Lin and T. C. Su), Vol. 2, pp. 989-992.

L. M. Stehn, S. J. DeFranco and J. P. Dempsey, "A method for determining the anisotropic fracture toughness of ice," *12th POAC Conference*, Vol. 1 (1993) 114–123.

L. M. Stehn, S. J. DeFranco and J. P. Dempsey, "Influence of specimen geometry on the fracture toughness of freshwater ice," *POLARTECH '94*, Luleå, Sweden (1994) 297–304.

R. M. Adamson, J. P. Dempsey, S. J. DeFranco and Y. Xie, " Large-scale in-situ ice fracture experiments - Part I: Experimental aspects," *ICE MECHANICS–1995*, Eds J. P. Dempsey and Y. D. S. Rajapakse, ASME AMD-Vol. 207, pp. 107–128.

R. M. Adamson and J. P. Dempsey, "Large-Scale in-situ arctic cyclic, creep-recovery and fracture measurements," 13th IAHR Ice Symposium, Beijing, China, August 27-31, 1996, Vol. I, pp. 102-109.

S. J. DeFranco and J. P. Dempsey, "Fracture process zone analysis in saline ice," *ICE MECHANICS–1993*, Eds J. P. Dempsey, Z. P. Bazant, Y. D. S. Rajapakse, S. S. Sunder, ASME AMD-Vol. 163, pp. 217–227.

S. V. Mulmule, J. P. Dempsey, R. M Adamson, " Large-scale in-situ ice fracture experiments - Part II: Modeling Aspects," *ICE MECHANICS–1995*, Eds J. P. Dempsey and Y. D. S. Rajapakse, ASME AMD-Vol. 207, pp. 129–146.

S. V. Mulmule, R. M. Adamson and J. P. Dempsey, "Nonlinear fracture theories for freshwater and sea ice," 13th IAHR Ice Symposium, Beijing, China, August 27-31, 1996, Vol. I, pp. 39-46.

Y. Wei, R. M. Adamson and J. P. Dempsey, "Fracture energy of ice/metal interfaces," in *Adhesives Engineering* Eric A. Norland and Kenneth M. Liechti, Editors, Proc. SPIE 1999 (1993) pp. 126–135.

Z. G. Zhao and J. P. Dempsey, "Planar forcing of floating ice sheets," *ICE MECHANICS–1993*, Eds J. P. Dempsey, Z. P. Bazant, Y. D. S. Rajapakse, S. S. Sunder, ASME AMD-Vol. 163, pp. 151–164.